ELSEVIER

Coupling photochemistry with haze formation in Titan's atmosphere, Part I: Model description

P.P. Lavvas[a,c], A. Coustenis[b], I.M. Vardavas[a,c],*

[a]Department of Physics, University of Crete, Vassilika Voutes, P.O. Box 2208, 71003 Heraklion, Crete, Greece
[b]Observatory of Paris at Meudon, 5 Place J. Janssen, 92195 Meudon, Cedex, France
[c]Foundation for Research and Technology Hellas (FORTH), Heraklion, Crete, Greece

Abstract

We introduce a new 1D coupled Radiative/Convective-Photochemical-Microphysical model for a planetary atmosphere and apply it to Titan. The model incorporates detailed radiation transfer calculations for the description of the shortwave and longwave fluxes which provide the vertical structure of the radiation field and temperature profile. These are used for the generation of the photochemistry inside the atmosphere from the photolysis of Titan's main constituents, nitrogen (N_2) and methane (CH_4). The resulting hydrocarbons and nitriles are used for the production of the haze precursors, whose evolution is described by the microphysical part of the model. The calculated aerosol and gas opacities are iteratively included in the radiation transfer calculations in order to investigate their effect on the resulting temperature profile and geometric albedo. The main purpose of this model is to help in the understanding of the missing link between the gas production and particle transformation in Titan's atmosphere. In this part, the basic physical mechanisms included in the model are described. The final results regarding the eddy mixing profile, the chemical composition and the role of the different haze precursors suggested in the literature are presented in Part II along with the sensitivity of the results to the molecular nitrogen photoinization scheme and the impact of galactic cosmic rays in the atmospheric chemistry.
© 2007 Elsevier Ltd. All rights reserved.

Keywords: Titan; Planetary Atmospheres; Photochemistry; Microphysics; Haze

1. Introduction

From the initial observation by Huygens (1655) and the methane detection by Kuiper (1944) to the recent Cassini/Huygens space mission, Titan has been the subject of many studies that have aimed towards understanding its climate and the important role of the haze that is formed in its atmosphere and obscures its surface from direct observations in the visible. The processes that control haze formation and its radiative properties have been the least understood to date. The recent success of the Cassini/Huygens mission has provided valuable validation data that supplement the earlier Voyager mission data and many years of ground-based observations.

The most prominent characteristic of Titan's atmosphere is the well-defined haze structure, observed since the Voyager era (Rages and Pollack, 1980). The haze is directly observed since it provides the orange color of the Titan's atmosphere in the visible images and its origin is linked to the photochemistry taking place in its atmosphere. Nitrogen and methane, the most abundant constituents in Titan's atmosphere, are photodissociated by solar ultraviolet radiation, energetic particles from Saturn's magnetosphere and galactic cosmic rays (GCR), leading to the initiation of a complex organic photochemistry, which finally produces the haze. This coupling between the photochemistry and haze formation is the subject of the present work.

*Corresponding author. Department of Physics, University of Crete, Vassilika Voutes, P.O. Box 2208, 71003 Heraklion, Crete, Greece.
E-mail address: vardavas@iesl.forth.gr (I.M. Vardavas).

The neutral photochemistry in Titan's atmosphere was investigated even before the Voyager era (Strobel, 1974; Allen et al., 1980). The Voyager mission provided data that led to the first detailed photochemical model developed by Yung et al. (1984) which described the basic photochemical schemes that control the abundance of the observed hydrocarbons and nitriles in Titan's atmosphere. Based on this early work and further analysis of Voyager data and ground-based observations, more advanced photochemical models were developed. Toublanc et al. (1995) used an elaborate Monte Carlo description for solar radiation transfer within the atmosphere to investigate the possible production of oxygen-containing species arising from an influx of water vapor at the top of the atmosphere. Lara et al. (1996) used an ablation profile for the water vapor influx, included the effects of GCR and presented a physical description of the condensation processes taking place in Titan's lower stratosphere. Lebonnois et al. (2001) investigated the seasonal variation of the composition in Titan's stratosphere using a 2-D (latitude–altitude) model. Beyond neutral species chemistry, models have included ionospheric chemistry, as in the recent work of Wilson and Atreya (2004) where the contributions of energetic electrons and photoelectrons were included.

A common approach to modelling the photochemistry has been to generate the vertical temperature distribution, from the surface to the thermosphere, using temperature vertical profiles that were synthesized by combining measurements from Voyager I (Lindal et al., 1983) and model results for the temperature structure at different altitudes (Lellouch et al., 1989; Yelle, 1991; Yelle et al., 1997). Further, in order to include the effects of the aerosols in the radiation transfer calculations, vertical profiles of haze opacity were either specified by a simple exponential decrease with altitude or in more recent work generated by microphysical models using a specified vertical haze production rate (Yung et al., 1984; Lebonnois et al., 2001; Wilson and Atreya, 2004). Using this approach, photochemical models have managed to fit most of the atmospheric species concentrations available from observations before the Cassini/Huygens mission (Coustenis et al., 1995). In the present work we develop a modelling approach that generates the thermal structure, the atmospheric composition and the haze structure, in a self-consistent manner. The haze is produced from polymer production governed by the photochemistry, which is determined by and determines both the radiation field and atmospheric temperature structure. However, we do not address the complex problem of non-LTE effects on the temperature structure in the upper atmosphere.

The microphysical models used to derive the haze vertical structure and its optical properties are usually validated against Titan's spectral geometric albedo from the ultraviolet to the near-infrared based on ground-based and space observations. As was first shown by McKay et al. (1989), the fit to the spectral geometric albedo depends mainly on three parameters; the haze particles' optical properties (refractive index, size, shape and amount), the methane profile and Titan's surface reflectivity; using different spectral domains of the above region, constraints can be set on the values of parameters controlling the haze structure.

The haze particles' refractive index is based on laboratory measurements, while the size and amount is generated by the microphysical models, assuming their shape. The shape of the haze particles in Titan's atmosphere has been the subject of debate for a long time. Photopolarimetry measurements of scattered light from the Pioneer 11 (Tomasko and Smith, 1982) and Voyager (West et al., 1983) space missions have given high polarization at ∼90° phase angle, which if the particles are spherical, constrains their size to 0.1 µm. On the other hand, high phase angle brightness measurements from Voyager (Rages et al., 1983), required particles between 0.2 and 0.5 µm with the upper limit more plausible. In order to overcome this problem, two possible solutions were suggested; one of a bimodal distribution (Courtin et al., 1991; Toon et al., 1992a,b) and the other of fractal aggregates constructed from spherical units (West and Smith, 1991; Rannou et al., 1995, 1997). Since then many microphysical models using the fractal aggregates have been published (Rannou et al., 2003 and references therein). The advantage of the fractal approach is that it provides, in general, a good fit to the geometric albedo both in the UV, visible and near-IR regions while at the same time matches the polarization data. However, fractal models have been unable to provide a good fit to the methane absorption feature at 0.62 µm in comparison with the success of the spherical particle models. The fit to the data was improved by applying a haze cut-off below 100 km, (Tomasko et al., 1997; Rannou et al., 2003) as suggested by HST measurements at that time (Young et al., 2002). A haze clearing was also included in the spherical particle models but at lower altitudes (below 30 km in McKay et al., 1989). The recent results from the DISR instrument on board the Huygens probe (Tomasco et al., 2005) show that the haze opacity extends down to the surface. Here we assume the particles to attain a spherical shape, starting from the monomer's size which corresponds to the smallest aerosol particle generated by the photochemical description. No fractal structures are considered.

In addition to the shape/size, the haze particles' refractive index is an important parameter in the model calculations. Until recently, most models used the first laboratory measurements for the refractive index of Titan haze-type analogs (tholins) made by Khare et al. (1984a), scaled by a factor which depends on the wavelength and the type of particles used; for spherical particles $\frac{4}{3}$ in the shortwave region of the geometric albedo (McKay et al., 1989), while for fractal particles 3 in the UV and 1.5 in the visible (Rannou et al., 1995). More recent measurements have shown that the optical properties of the laboratory haze analogs depend significantly on the experimental

conditions (McKay et al., 2001). Recently, Imanaka et al. (2004) have shown that the pressure under which the analogs are made defines their chemical structure and hence their radiative properties. Hence, photochemically produced particles at different altitudes in Titan's atmosphere could exhibit different optical properties.

An important simplification made in current haze microphysical models has been the adopted haze particle production rate. In most cases this is done by a symmetrical distribution (usually Gaussian) centered at some chosen altitude, usually between 350 and 600 km depending on the model, and the total column production rate varied to fit the geometric albedo. In addition, some models, calculate the radiation field but do not calculate the temperature profile that results from the model haze structure, but use synthetic temperature profiles. Recent photochemical calculations have demonstrated that vertical haze production profiles generated from the photochemistry (Lebonnois et al., 2002; Wilson and Atreya, 2003) are significantly different from the simple profiles adopted in current haze microphysical models. In the present work, we have used this fact to generate the haze production profile from the photochemistry and then use it to produce the haze vertical structure and its radiative properties. The model temperature structure then depends on the vertical haze profile. We then validate both our model temperature structure, the spectral geometric albedo and the vertical distributions of the concentrations of the chemical species against measurements. In particular, we validate our model results against available Cassini/Huygens data.

In the sections that follow we present a description of the radiative/convective-photochemical-microphysical model. We discuss the latest laboratory measurements for the haze analogs and the possible pathways suggested for haze formation. Detailed model results and validation against the latest measurements from the Cassini/Huygens mission and from earlier observations are presented in Part II of this work. There we also discuss in detail the processes that we have modelled and their role in determining Titan's atmospheric structure.

2. Model description

2.1. Model structure

In order to describe the coupling between photochemistry and haze formation in one dimension, it is necessary to have a model, which can simulate the three main processes in Titan's atmosphere. The flow chart in Fig. 1 provides a simplified view of the way this is accomplished. The Radiation sub-models perform the radiation transfer and calculate the thermal balance of the atmosphere. Hence they provide the radiation flux at each altitude of the atmosphere that controls the chemical species photodissociation rates and the vertical temperature profile. These are coupled to the chemistry sub-model that solves
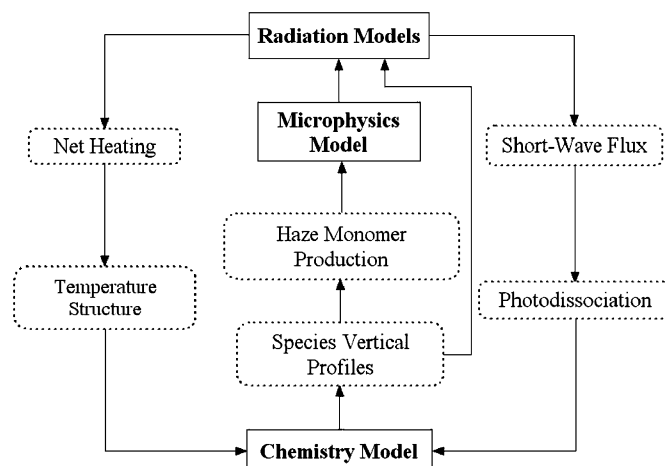

Fig. 1. Model flow chart.

Table 1
Model controlling parameters

Region	Parameter	Nominal value
Atmosphere	Eddy diffusion coefficient, K	See Part II
Haze	Charging rate, χ	$25e^-/\mu m$
	Tholin refractive index	$4/3$ for UV, VIS, and Near-IR
		$1/2$ for Thermal IR
Surface	Reflectivity	see Part II

the time-dependent continuity equation for the vertical distribution of species mixing ratios. In this sub-model, the haze pathways considered lead to the haze monomer production at each altitude. This is then used as input in the third sub-model, which describes the microphysical growth of the haze monomers. Finally the vertical distribution of chemical species concentrations and haze particle radiative properties are transferred back to the radiation sub-models.

The above solution proceeds in time until equilibrium is reached. The temporal evolution of Titan's atmosphere and haze can also be examined using different scenarios regarding Titan's past and future. In the present computations, we consider the solar flux reaching Titan to be today's. Since each process has a different characteristic time to reach equilibrium, a time integration process with varying step must be used and a fairly long total time of integration must be considered in order to take into account all the different physico-chemical processes (condensation, coagulation, photolysis, chemistry, mixing and diffusion), starting from an initial atmospheric structure. The method is described in the appendices.

The complexity of the model provides a better understanding of the processes at work, validated against different types of observations that are available, such as

composition measurements, temperature structure, geometric albedo, haze opacities, etc., since all of the above measured quantities are directly calculated by the model. In order to match these observations there are four physical quantities that need to be optimised as their values are not well known (see Table 1). These are: the eddy diffusion coefficient, K, for vertical transport of the species; the charging rate, χ, of the particles, which controls their maximum size; the scaling factors applied to the refractive index of the particles that varies their optical properties; and the surface spectral reflectivity, which mainly determines the geometric albedo inside the methane windows.

2.2. Radiative/convective sub-model (RC)

The radiative/convective (RC) sub-model is based on radiative transfer models for solar and thermal radiation (Vardavas and Carver, 1984b) that have been successfully used for the description of Earth's radiation budget and validated with 20 years of climatological data from NASA Goddard Space Flight Center (Hatzianastassiou et al., 2004, 2005; Pavlakis et al., 2004). The model calculates the temperature structure and the radiation field in 1D from the surface ($\sim$1.5 bar) up to a pressure altitude of 10^{-9} mbar ($\sim$1400 km) using a pressure grid of 300 levels. The pressure grid is preferred from an altitude grid because in this way we can avoid pressure-dependent changes in the atmospheric temperature and composition (e.g. the methane absorption coefficients in the near-IR region have a strong pressure dependence which in the case of an altitude grid would have to be calculated every time the temperature structure changes). The altitude scale of the model is derived from the pressure grid and the calculated vertical temperature profile using the hydrostatic equilibrium equation, while the atmospheric number density is calculated from the ideal-gas law taking into consideration the non-ideal correction factor (f) in the lower atmosphere suggested by Yelle et al. (1997):

$$p(f + 1) = nk_B T \tag{1}$$

with p, the pressure, n the number density, k_B the Boltzmann constant and T the temperature. The RC model comprises two detailed radiation transfer sub-models for solar radiation and Titan's thermal radiation transfer, respectively.

The solar radiation corresponds to the wavelength region 0.5 nm–10 μm and the multiple scattering radiation transfer is based on the δ-Eddington method (Joseph et al., 1976) for the calculation of the solar radiation field at each altitude. For the incoming solar flux the irradiance profile at the Earth's orbit (Woods and Rottman, 2002 for 0.5–200 nm at solar average conditions with the spectrally resolved Ly-α profile from Lemaire et al., 2005 and Gueymard, 2004 for 200 nm–10 μm) was normalized based on the ratio of the total solar irradiance of 15 Wm^{-2} for Titan and 1366 Wm^{-2} at the Earth's orbit. The spectrum is

divided into 660 wavelengths with increasing intervals towards the near-IR region.

In the visible and near-IR region methane is the dominant gaseous source of opacity. This spectral domain is divided into 325 sub-bands. The absorption coefficients of Karkoschka (1994) were used in the spectral region 0.4–1.0 μm, which is divided into 85 sub-bands. From 1.0 to 1.54 μm (28 sub-bands) the band model coefficients of Irwin et al. (2005) were used. Transmissions were calculated for different temperature, pressure and amount conditions and then convoluted to the resolution of our spectral sub-band structure and tabulated in matrices. The last were used for the derivation of the k-distribution coefficients used in the model calculations using an 8-point Gaussian-Legendre quadrature. The initial high resolution calculated transmission spectra and the ones derived by the k-distribution method were found to be in good agreement with the reference spectra from the measurements of McKellar (1989) at low temperature (77 K), as given in Sromovsky et al. (2006), and Strong et al. (1993) (moderate low temperatures but very large pathlengths, appropriate for Titan's conditions). Above 1.54 μm (212 sub-bands) the same approach was adopted using the spectroscopic parameters of Boudon et al. (2004) with Voigt line profiles. The line shapes at the far wings were constrained based on the description given by Hartmann et al. (2002) and the absorption coefficients were calculated at a resolution of 1 cm^{-1}. Rayleigh scattering is taken into consideration in the radiation transfer with cross sections for atoms and molecules given by Allen (1976):

$$\sigma_S(\text{cm}^2) = 4.577 \times 10^{-21} \frac{\delta}{\lambda^4} A \left(1 + \frac{B}{\lambda^2}\right) \tag{2}$$

with A and B constants that depend on the scattering atom or molecule, δ the depolarization factor of each scatterer and λ is the wavelength in microns. The values used in the calculations are given in Table 2 for the most important Rayleigh scatterers. In the UV region, gas opacity is provided by the major species shown in Table 3, where references for their cross sections and branching ratios can be found. The aerosol opacity is calculated with Mie theory using the Khare et al. (1984a) refractive index scaled with the corresponding control parameter and considering the haze particles to have a spherical shape. The distribution of

Table 2
Rayleigh scattering parameters

	δ	$A \times 10^{-5}$	$B \times 10^{-3}$
H_2	1.015	13.58	7.52
N_2	1.063	29.06	7.7
CH_4	1.000	44.3	–
C_2H_2	1.079	51	–
C_2H_4	1.050	50.5	–
C_2H_6	1.015	3770	–

Table 3
Photolysis reactions

Reaction			Branching ratio	Reference	
				Cross sections	Yields
Hydrocarbons					
R1	$H_2 + h\nu$	$\rightarrow$ 2 H	1	Backx et al. (1976)	Est.
R2	$CH_3 + h\nu$	$\rightarrow$ $^1CH_2 + H$	$\lambda \leqslant 165$ nm: 0; other: 1	Adachi et al. (1980)	Wilson et al. (1994)
R3		$\rightarrow$ $CH + H_2$	$\lambda \leqslant 165$ nm: 1; other: 0	Pilling et al. (1971)	Kassner and Stuhl (1994)
R4	$CH_4 + h\nu$	$\rightarrow$ $^1CH_2 + H_2$	$\lambda \leqslant$ Ly-α: 0.584; other: 0	Samson et al. (1989)	
R5		$\rightarrow$ $^1CH_2 + 2$ H	$\lambda \leqslant$ Ly-α: 0.055; other: 0	Lee et al. (2001)	Wang and Liu (1998)
R6		$\rightarrow$ $CH + H + H_2$	$\lambda \leqslant$ Ly-α: 0.070; other: 0	Hudson (1971)	Wang et al. (2000)
R7		$\rightarrow$ $CH_3 + H$	$\lambda \leqslant$ Ly-α: 0.291; other: 1	Chen and Wu (2004)	
R8	$C_2H + h\nu$	$\rightarrow$ $C_2 + H$	1	Fahr (2003)	Mebel et al. (2001)
R9	$C_2H_2 + h\nu$	$\rightarrow$ $C_2 + H_2$	0.1	Cooper et al. (1995a)	Okabe (1981)
R10		$\rightarrow$ $C_2H + H$	$\lambda < 124$ nm: 0.1; $\lambda < 150$ nm: 0.3; $\lambda < 190$ nm: 0.06; $\lambda < 225$ nm: 0.3	Smith et al. (1991) Bénilan et al. (2000) @ 173K	Okabe (1983) Seki and Okabe (1993)
R11	$C_2H_3 + h\nu$	$\rightarrow$ $C_2H_2 + H$	1	Fahr et al. (1998)	Ahmed et al. (1999)
R12	$C_2H_4 + h\nu$	$\rightarrow$ $C_2H_2 + H_2$	$\lambda < 175$ nm: 0.460; other: 0.73	Cooper et al. (1995b)	
R13		$\rightarrow$ $C_2H_2 + 2$ H	$\lambda < 175$ nm: 0.519; other: 0.27	Holland et al. (1997)	Chang et al. (1998)
R14		$\rightarrow$ $C_2H_3 + H$	$\lambda < 175$ nm: 0.021; other: 0.0	Zelikoff and Watanabe (1953)	Lee et al. (2004)
R15	$C_2H_5 + h\nu$	$\rightarrow$ $^1CH_2 + CH_3$	1	Munk et al. (1986a)	Gladstone et al. (1996)
R16	$C_2H_6 + h\nu$	$\rightarrow$ 2 CH_3	$\lambda <$ Ly-α: 0.17; Ly-α: 0.03; other: 0.0		
R17		$\rightarrow$ $CH_4 + {}^1CH_2$	$\lambda <$ Ly-α: 0.16; Ly-α: 0.26; other: 0.02	Kameta et al. (1996)	Hampson and McNesby (1965)
R18		$\rightarrow$ $C_2H_4 + 2$ H	$\lambda <$ Ly-α: 0.41; Ly-α: 0.31; other: 0.13	Lee et al. (2001)	
R19		$\rightarrow$ $C_2H_4 + H_2$	$\lambda <$ Ly-α: 0.0 ; Ly-α: 0.15; other: 0.48	Chen and Wu (2004)	Lias et al. (1970)
R20		$\rightarrow$ $C_2H_2 + 2 H_2$	$\lambda <$ Ly-α: 0.26; Ly-α: 0.25; other: 0.37		
R21	$C_3H_3 + h\nu$	$\rightarrow$ $C_3H_2 + H$	1	Fahr et al. (1997)	Jackson et al. (1991)
R22	$CH_3C_2H + h\nu$	$\rightarrow$ $C_3H_3 + H$	$\lambda \leqslant$ Ly-α: 0.0; other: 0.50	Nakayama and Watanabe (1964)	
R23		$\rightarrow$ $C_3H_2 + H_2$	$\lambda \leqslant$ Ly-α: 1.0; other: 0.39	Ho et al. (1998)	Seki and Okabe (1992)
R24		$\rightarrow$ $C_2H_2 + {}^1CH_2$	$\lambda \leqslant$ Ly-α: 0.0; other: 0.11	LISA[a] @ 183 K	Sun et al. (1999)
R25	$CH_2CCH_2 + h\nu$	$\rightarrow$ $C_3H_3 + H$	0.64	Chen et al. (2000)	Sun et al. (1999)
R26		$\rightarrow$ $C_3H_2 + H_2$	0.36	LISA[a] @ 183 K	
R27	$C_3H_6 + h\nu$	$\rightarrow$ $CH_2CCH_2 + H_2$	$\lambda < 135$ nm: 0.43; $\lambda < 155$ nm: 0.40; $\lambda < 175$ nm: 0.015; $\lambda < 195$ nm: 0.01		
R28		$\rightarrow$ $CH_3C_2H + H_2$	$\lambda < 135$ nm: 0.25; $\lambda < 155$ nm: 0.24; $\lambda < 175$ nm: 0.015; $\lambda < 195$ nm: 0.01	Koizumi et al. (1985) Fahr and Nayak (1996)	Collin (1988)[b]
R29		$\rightarrow$ $C_2H_4 + {}^1CH_2$	$\lambda < 135$ nm:0.06; $\lambda < 155$ nm: 0.04; $\lambda < 175$ nm: 0.02; $\lambda < 195$ nm: 0.0	Samson et al. (1962)	
R30		$\rightarrow$ $C_2H_3 + CH_3$	$\lambda < 135$ nm: 0.21; $\lambda < 155$ nm: 0.27; $\lambda < 175$ nm: 0.335; $\lambda < 195$ nm: 0.34		
R31		$\rightarrow$ $C_2H_2 + CH_4$	$\lambda < 135$ nm: 0.05; $\lambda < 155$ nm: 0.05; $\lambda < 175$ nm: 0.05; $\lambda < 195$ nm: 0.04		
R32		$\rightarrow$ $C_3H_5 + H$	$\lambda < 135$ nm: 0.0; $\lambda < 155$ nm: 0.0; $\lambda < 175$ nm: 0.565; $\lambda < 195$ nm: 0.60		
R33	$C_3H_8 + h\nu$	$\rightarrow$ $C_3H_6 + H_2$	$\lambda \leqslant$ Ly-α: 0.32; other: 0.67		Obi et al. (1971)
R34		$\rightarrow$ $C_2H6 + {}^1CH_2$	$\lambda \leqslant$ Ly-α: 0.10; other: 0.05	Kameta et al. (2002)	
R35		$\rightarrow$ $C_2H_4 + CH_3 + H$	$\lambda \leqslant$ Ly-α: 0.43; other: 0.17	Okabe and Becker (1963)	
R36		$\rightarrow$ $C_2H_4 + CH_4$	$\lambda \leqslant$ Ly-α: 0.15; other: 0.11		
R37	$C_4H_2 + h\nu$	$\rightarrow$ $C_4H + H$	$\lambda < 165$ nm: 0.2; else: 0		
R38		$\rightarrow$ 2 C_2H	$\lambda < 165$ nm: 0.03; $\lambda < 205$ nm: 0.01; else: 0	Okabe (1981)	
R39		$\rightarrow$ $C_2H_2 + C_2$	$\lambda < 165$ nm: 0.1; $\lambda < 205$ nm: 0.06; else: 0	Fahr and Nayak (1994)	Glicker and Okabe (1987)
R40		$\rightarrow$ C_4H_2[a]	$\lambda < 165$ nm: 0.67; $\lambda < 205$ nm:0.93; else: 1	Smith et al. (1998) at 193 K	
R41	$C_4H_4 + h\nu$	$\rightarrow$ $C_4H_2 + H_2$	0.8	Fahr and Nayak (1996)	Gladstone et al. (1996)
R42		$\rightarrow$ 2 C_2H_2	0.2		
R43	$C_4H_6 + h\nu$	$\rightarrow$ $C_4H_4 + H_2$	0.05	Fahr and Nayak (1994)	
R44		$\rightarrow$ $C_2H_4 + C_2H_2$	0.17		Bergmann and Demtröder (1968)
R45		$\rightarrow$ $CH_3 + C_3H_3$	0.40		
R46		$\rightarrow$ $C_4H_5 + H$	0.28		
R47		$\rightarrow$ 2 C_2H_3	0.10		
R48	$C_4H_8 + h\nu$	$\rightarrow$ $C_4H_6 + 2$ H	$\lambda < 135$ nm: 0.23; $\lambda < 160$ nm: 0.14; else: 0.06		
R49		$\rightarrow$ $C_3H_8 + CH_3$	$\lambda < 135$ nm: 0.12; $\lambda < 160$ nm: 0.39; else: 0.66		
R50		$\rightarrow$ $CH_3C_2H + CH_4$	$\lambda < 135$ nm: 0.03; $\lambda < 160$ nm: 0.02; else: 0.0		
R51		$\rightarrow$ $CH_2CCH_2 + CH_4$	$\lambda < 135$ nm: 0.14; $\lambda < 160$ nm: 0.10; else: 0.0	Samson et al. (1962)	Wilson and Atreya (2004)
R52		$\rightarrow$ $C_2H_5 + C_2H_3$	$\lambda < 135$ nm: 0.25; $\lambda < 160$ nm: 0.14; else: 0.04	Koizumi et al. (1985)	
R53		$\rightarrow$ 2 C_2H_4	$\lambda < 135$ nm: 0.02; $\lambda < 160$ nm: 0.04; else: 0.05		

Table 3 (*continued*)

R54		$\rightarrow$ $C_2H_2 + 2CH_3$	$\lambda < 135$ nm: 0.02; $\lambda < 160$ nm: 0.0; else: 0.04			
R55		$\rightarrow$ $C_3H_6 + {}^1CH_2$	$\lambda < 135$ nm: 0.02; $\lambda < 160$ nm: 0.02; else: 0.0			
R56	$C_4H_{10} + hv$	$\rightarrow$ $C_4H_8 + H_2$	$\lambda < 135$ nm: 0.48; other: 0.31		Obi et al. (1971)	
R57		$\rightarrow$ $C_2H_6 + C_2H_4$	$\lambda < 135$ nm: 0.15; other: 0.17	Okabe and Becker (1963)		
R58		$\rightarrow$ $C_3H_6 + CH_3 + H$	$\lambda < 135$ nm: 0.28; other: 0.41	Kameta et al. (2002)		
R59		$\rightarrow$ $C_2H_5 + C_2H_4 + H$	$\lambda < 135$ nm: 0.09; other: 0.11			
R60	$C_6H_2 + hv$	$\rightarrow$ $C_2H + C_4H$	$\lambda < 165$ nm: 0.03; other: 0.01	Kloster-Jensen et al. (1974)	$\sim C_4H_2 + hv \rightarrow 2C_2H$	
R61		$\rightarrow$ $C_6H + H$	$\lambda < 165$ nm: 0.20; other: 0.0	Shindo et al. (2005)	$\sim \rightarrow C_4H + H$	
R62	$C_6H_4 + hv$	$\rightarrow$ $C_6H_3 + H$	$\lambda < 220$ nm: 1.0; other: 0.0			
R63		$\rightarrow$ $C_6H_2 + H_2$	$\lambda < 220$ nm: 0.0; other: 0.9	Est. based on C_6H_6, Münzel and Schweig (1988)		
R64		$\rightarrow$ $C_4H_2 + C_2H_2$	$\lambda < 220$ nm: 0.0; other: 0.1			
R65	$C_6H_6 + hv$	$\rightarrow$ $C_6H_5 + H$	$\lambda < 220$ nm: 0.80; other: 0.0			
R66		$\rightarrow$ $C_6H_4 + H_2$	$\lambda < 220$ nm: 0.16; other: 0.96	Suto et al. (1992)		
R67		$\rightarrow$ $C_5H_3 + CH_3$	$\lambda < 220$ nm: 0.04; other: 0.04	Rennie et al. (1998)	Yokoyama et al. (1990)	

Nitriles

R68	$N + hv$	$\rightarrow$ $N^+ + e^-$	1	Banks and Kockarts (1973)		
R69	$N_2 + hv$	$\rightarrow$ $N(^4S) + N^+ + e^-$	$\lambda < 510$ Å: 0.10; other: 0.0			
R70		$\rightarrow$ $N(^2D) + N^+ + e^-$	$\lambda < 510$ Å: 0.90; other: 0.0	Chan et al. (1993)	Banks and Kockarts (1973)	
R71		$\rightarrow$ $N_2^+ + e^-$	510 Å $< \lambda < 796$ Å: 1.0; other: 0.0	Fennelly and Torr (1992)	Nicolas et al. (2003)	
R72		$\rightarrow$ $N(^2D) + N(^4S)$	796 Å $< \lambda < 1000$ Å: 1.0; other: 0.0			
R73	$NH_3 + hv$	$\rightarrow$ $NH_2 + H$	1	Burton et al. (1993), Chen et al. (1999)		
R74	$HCN + hv$	$\rightarrow$ $H + CN$	1	Lee (1980) and Nuth and Glicker (1982)		
R75	$CH_2NH + hv$	$\rightarrow$ $HCN + 2H$	1	Teslja et al. (2004)	Nguyen et al. (1996)	
R76	$CH_3NH_2 + hv$	$\rightarrow$ $CH_2NH + 2H$	$\lambda < 165$ nm:1.0; other: 0.55			
R77		$\rightarrow$ $HCN + H_2 + 2H$	$\lambda < 165$ nm: 0.0; other: 0.198	Hubin-Franskin et al. (2002)	Gardner and McNesby (1982)	
R78		$\rightarrow$ $CN + 2H_2$	$\lambda < 165$ nm: 0.0; other: 0.252			
R79	$C_2H_5N + hv$	$\rightarrow$ $C_2H_4 + NH$	0.38			
R80		$\rightarrow$ $CH_3 + H_2CN$	0.47	Est. as $C_2H_5NH_2$		
R81		$\rightarrow$ $C_2H_2 + NH_3$	0.03	Hubin-Franskin et al. (2002)	Scala and Salomon (1976)	
R82	$HC_3N + hv$	$\rightarrow$ $C_2H + CN$	0.3	Connors et al. (1974)	Clarke and Ferris (1995)	
R83		$\rightarrow$ $C_3N + H$	0.09	Bénilan et al. (1996)		
R84	$CH_3CN + hv$	$\rightarrow$ $CH_3 + CN$	1	Nuth and Glicker (1982); Suto et al. (1985)		
R85	$C_2H_3CN + hv$	$\rightarrow$ $C_2H_2 + HCN$	0.15			
R86		$\rightarrow$ $HC_3N + H_2$	0.59			
R87		$\rightarrow$ $C_2H_3 + CN$	0.01	Eden et al. (2003)	Derecski-Kovacs and North (1999)	
R88		$\rightarrow$ $C_2H_2CN + H$	0.25			
R89	$N_2H_4 + hv$	$\rightarrow$ $N_2H_3 + H$	1	Vaghjiani (1993, 1995)		
R90	$C_2N_2 + hv$	$\rightarrow$ $2 CN$	1	Nuth and Glicker (1982) and Connors et al. (1974) Bénilan et al. (1996) @ 193 K		
R91	$C_4N_2 + hv$	$\rightarrow$ $C_3N + CN$	1	Connors et al. (1974) and Bénilan et al. (1996) @ 233 K		

[a]LISA cross sections are taken from http://www.lisa.univ-paris12.fr/GPCOS/SCOOPweb/SCOOP.html.

[b]Assuming the total quantum yield below 155 nm to be one and the ionized products eventually yield $C_3H_4 + H_2$.

the haze particles at each altitude is provided by the microphysical part of the model discussed later.

The simulated thermal radiation corresponds to wavenumbers between 0–8200 cm^{-1} and is divided in 71 domains. From 0 to 900 cm^{-1}, where the major part of Titan's surface thermal radiation is emitted, there are 45 regions of 20 cm^{-1} width while the spectrum interval increases for higher wavenumbers. Up to ~ 700 cm^{-1} the opacity is mainly controlled by collision-induced absorption (CIA) between nitrogen, methane and hydrogen molecules. The CIA coefficients were calculated from the work of Borysow and co-workers: N_2–N_2 from Borysow and Frommhold (1986a), N_2–CH_4 from Borysow and Tang (1993), H_2–N_2 from Borysow and Frommhold (1986b),

H_2–CH_4 from Borysow and Frommhold (1986c) and CH_4–CH_4 from Borysow and Frommhold (1987). In Fig. 2 the model column opacity in the region 0–2000 cm^{-1} is shown along with the calculated thermal emission for temperatures of 94 K (characteristic of Titan's surface, Fulchignoni et al., 2005) and 180 K (characteristic of the stratopause temperature, Flasar et al., 2005). The abundances for the absorbing molecules where provided from their vertical profiles, calculated in the photochemical part of the model. The effect of the so-called Titan's thermal window (Samuelson, 1983; McKay et al., 1991) is obvious in the 400–600 cm^{-1} region where the decrease in opacity allows thermal radiation from the surface to escape to space.
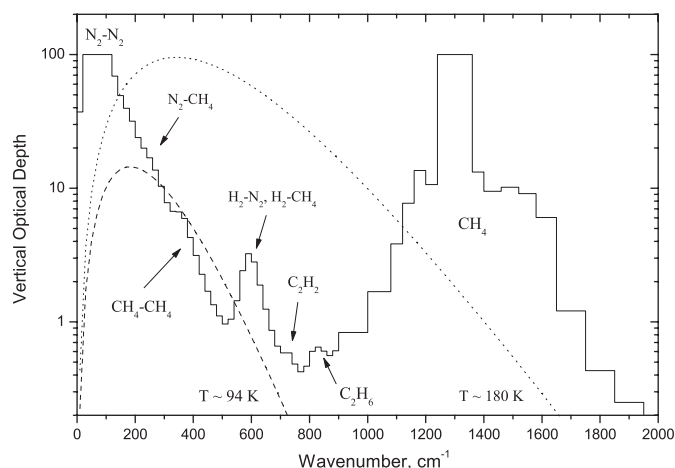
Fig. 2. Model column opacities in the thermal infrared. Up to ~700 cm^{-1} the main contribution comes from the collision induced absorption between the N$_2$/CH$_4$/H$_2$ pairs with the spectral dominance of each pair shown. At higher wavenumbers the opacity is controlled by methane, acetylene and ethane. The abundances for the absorbing species were calculated in the photochemical part of the model. The dashed and dotted lines are Planck functions (in arbitrary units) for about 94 and 180 K, respectively, representing the spectral coverage of Titan's thermal radiation.

Above 700 cm^{-1} the thermal opacity is controlled by methane, ethane and acetylene absorption. The major contribution comes from the ν_4 band of CH$_4$ which is centered at 1300 cm^{-1}. Transmissions were calculated as for the solar wavelengths using the Boudon coefficients. Opacities due to C$_2$H$_6$ and C$_2$H$_2$ contribute mainly in the region between 600 and 900 cm^{-1} and were calculated from the HITRAN database spectroscopic values. In addition to the above, opacity from the rotational lines of HCN has been included based again on the spectroscopic values given in the HITRAN database. Transmission calculations in the model were performed using the Curtis–Godson approximation. Haze opacity in the IR was calculated in the same way as for the solar region.

The model divides the atmosphere into two regions: one close to the surface where convective equilibrium defines the temperature structure and a second one above which is in radiative equilibrium. The calculation of the thermal profile is performed by balancing the total incoming and outgoing fluxes at each layer of the simulated atmosphere. In addition to the solar and thermal fluxes the model takes into consideration the conductive flux between adjacent layers. The method of solution is described in the appendix.

2.3. Photochemical sub-model (PC)

The photochemical sub-model uses the grid of the RC sub-model in order to solve the time-dependent continuity equation in 1D for the species considered. Its description is based on the Vardavas (1984) model for reactive gas flows within shock tunnels. There are 68 chemical species included in the calculations, the evolution of which is

controlled by about 520 reactions. We have performed a thorough search and used the latest to our knowledge parameters (photolysis cross sections, branching ratios and chemical reaction rates) which correspond, as closely as possible, to the low temperature conditions found in Titan's atmosphere (Tables 3 and 5). The main processes defining the vertical profile of each species in the model are: photodissociation, chemical production and loss, vertical transport, loss due to condensation, surface deposition and escape to space. A description of each process follows.

2.3.1. Photodissociation

The complex chemistry of Titan's atmosphere is initiated with the photodissociation/photoionization of molecular nitrogen and methane (in the current calculations the contributions of energetic particles are not included and ionization is considered only for N$_2$). Photons in the EUV region of the solar radiation spectrum, depending on their energy, are able to ionize and dissociate N$_2$ according to the following pathways (Banks and Kockarts, 1973; Nicolas et al., 2003):

$$
\begin{aligned}
N_2 + h\nu &\rightarrow N(^4S) + N^+ + e^- (10\%)\ \lambda < 510\ \text{Å} \\
&\rightarrow N(^2D) + N^+ + e^- (90\%)\ \lambda < 510\ \text{Å} \\
&\rightarrow N_2^+ + e^- \qquad\quad 510\ \text{Å} < \lambda < 796\ \text{Å} \\
&\rightarrow N(^2D) + N(^4S)\ 796\ \text{Å} < \lambda < 1000\ \text{Å}.
\end{aligned}
$$
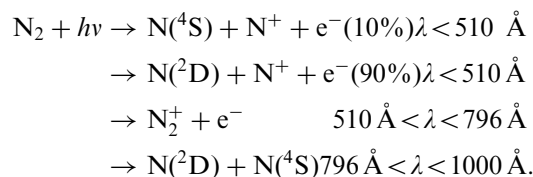
In the above, N(^{2}D) and N(^{4}S) are the first excited and ground state of atomic nitrogen while N$_2^+$ and N$^+$ are singly ionized molecular and atomic nitrogen.

The current photolysis scheme of N$_2$ is significantly different from that used in previous photochemical models. The Yung et al. (1984) model considered N$_2$ destruction by energetic electrons and galactic cosmic rays but not by high energy photons. Toublanc et al. (1995) considered only neutral dissociation production assuming excited nitrogen atoms as single products and included also an influx of N(^{2}D) and N(^{4}S) atoms for the production of atomic nitrogen by magnetospheric electrons from Saturn. Lara et al. (1996) also considered only the neutral dissociation of N$_2$ in the range 80–800 Å and assumed that excited atoms are the sole product, an approach which was adopted also by Lebonnois et al. (2001). In the latest published photochemical model, Wilson and Atreya (2004) provided a more detailed and realistic description of the N$_2$ photolysis by including the ionization, dissociative ionization and neutral dissociation pathways, in a way similar to ours. Our scheme diverges from theirs only in one point. Based on the latest measurements of Nicolas et al. (2003), the neutral nitrogen atoms released in the dissociative ionization are mainly in their excited state in contrast to the previous suggestions which favored the N(^{4}S) production. This difference has an impact on the upper atmosphere

profiles for some of the nitrile but also hydrocarbon species and is discussed in Part II.
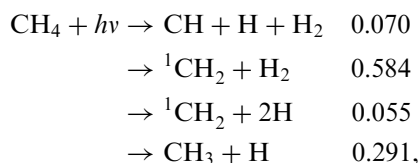
Particles in Galactic Cosmic Rays (GCR), due to their high energies penetrate to the very deep layers of the atmosphere, reaching down to the stratosphere before they encounter densities large enough to attenuate them. These rays are mainly composed of protons and alpha particles with kinetic energies in excess of 1 GeV (Capone et al., 1983). The interaction of these particles with Titan's neutral atmosphere leads to the ionization of the main species and also, depending on their initial energy, to the production of secondary energetic particles (neutrons, pions, etc.) which also contribute to the ionization (particle cascade). Since N_2 is the main component of the atmosphere, GCR act as a source of atomic nitrogen in the lower atmosphere where solar UV photons cannot reach and hence contribute to the production of nitrile species in this region. Analytical models for the description of the GCR penetration into Titan's atmosphere (Capone et al., 1983; Lellouch et al., 1994; Wilson and Atreya, 2004), have shown that the maximum deposition of the cosmic rays is situated around 100 km and that the magnitude of the N_2 destruction peaks between 10 and 20 $cm^{-3} s^{-1}$. In order to include the contribution of GCR in the model calculations we have considered a loss rate for N_2 due to this process. The shape of the loss rate was based on the work of the above authors and is presented in Fig. 3. The contribution from the cascade particles is not included. The products from the interaction of GCR with N_2 and their yields are taken from Lellouch et al. (1994):

$$N_2 + GCR \rightarrow N(^4S) + N^+ + e^-\quad 12\%$$
$$\rightarrow N_2^+ + e^-\qquad\qquad 53\%$$
$$\rightarrow N(^4S) + N(^2D)\quad 35\%.$$
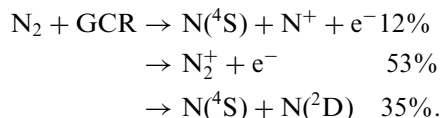
Methane is photodissociated by solar photons with $\lambda \leqslant 145$ nm. Until now the products of methane photolysis

Fig. 3. The loss rate of N_2 due to interaction with GCR. The contributions for each product pathway are also shown. Production due to the cascade particles below the peak at ~ 100 km is not included in the calculations.

have not been clarified and different production channels are proposed in the literature (Mordaunt et al., 1993; Romani, 1996; Smith and Raulin, 1999). A brief review of the up to date measurements for the methane photodissociation products and suggested photochemical schemes can be found in Romanzin et al. (2005). Wilson and Atreya (2000) investigated the impact of the different suggested pathways on the produced hydrocarbons and concluded that the choice of a quantum yield scheme affects mostly the C_3 species production in the Lyman-α region (where the major destruction of CH_4 molecules takes place) leaving the simpler C_2 species unaffected and that the Romani (1996) scheme provided an intermediate result between the other schemes. Lebonnois et al. (2001) have found similar results for the photochemical schemes of Mordaunt et al. (1993) and Smith and Raulin (1999). Recently, Wang and Liu (1998) and Wang et al. (2000) have performed the most complete up to date measurements for the methane photolysis yields at Lyman-α. By measuring the relative velocities of the atomic H produced and the relative abundances of the methyl (CH_3) and methylene ($^{1,3}CH_2$) fragments, they concluded that the major product is methylene which is released in its excited state ($^1CH_2$). We adopted these latest results for the methane photolysis in this spectral region.

In the non-Lyman CH_4 destruction, the two possible yields ($^1CH_2/CH_3$) affect, but in a smaller degree, the ethane production since CH_3 is the major precursor to C_2H_6 formation. In the current calculations we have considered only the production of methyl radicals at these wavelengths. The methane photolysis scheme used is summarized as follows:

$$CH_4 + h\nu \rightarrow CH + H + H_2\quad 0.070$$
$$\rightarrow {}^1CH_2 + H_2\qquad 0.584$$
$$\rightarrow {}^1CH_2 + 2H\qquad 0.055$$
$$\rightarrow CH_3 + H\qquad\quad 0.291,$$

where CH is the methylidyne radical. Branching ratios are given for Lyman-α. At other wavelengths the branching ratio is unity for the last pathway.

The photolysis rate, $J(s^{-1})$, for each species at altitude z is calculated by the usual formula:

$$J(z) = \int \chi_\lambda(z)\Phi_\lambda q_\lambda(z)\sigma_\lambda\, d\lambda, \qquad (3)$$

where Φ_λ is the incoming solar spectral flux, $\chi(z)$ is the enhancement factor, q_λ is the quantum yield for photodissociation and σ_λ the wavelength-dependent absorption cross section. The radiation field along with the enhancement factor at each altitude are calculated in the RC submodel. Some vertical profiles of the photolysis rates of the most important hydrocarbons and nitriles in Titan's atmosphere are shown in Fig. 4 for a solar zenith angle of $60°$.
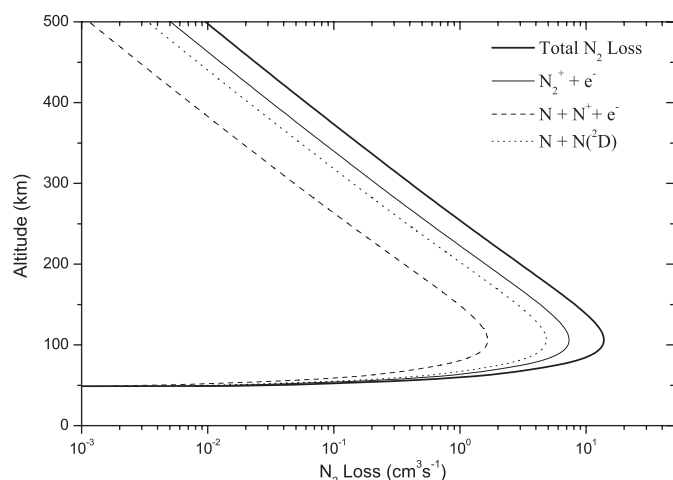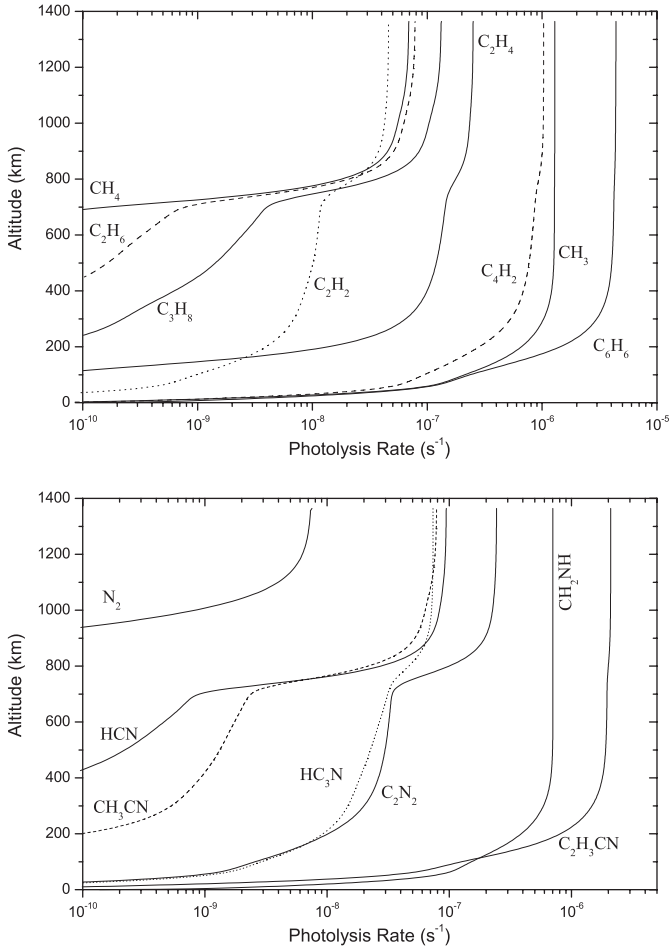
Fig. 4. Model calculated photolysis rates for the most important hydrocarbons (top panel) and nitriles (bottom panel) in Titan's atmosphere. The solar zenith angle is set to 60°. Secondary photolysis regions for some of the hydrocarbons (e.g. C_2H_2) are due to their extended absorption cross section profiles above the methane dissociation limit at 145 nm and their presence in significant amounts.

2.3.2. Vertical transport

The vertical transport of species i, is controlled by the diffusive flux, given by the expression:

$$\Phi_i = \frac{Dn}{H}\left(1 - \frac{M_i}{M} - \alpha_T \frac{H}{T}\frac{\partial T}{\partial r}\right)f_i - (D+K)n\frac{\partial f_i}{\partial r}, \qquad (4)$$

where $r = R_T + z$ with R_T being Titan's radius. D and K are the molecular and eddy diffusion coefficients, respectively, α_T the thermal diffusion coefficient, H the atmospheric scale height, M_i the molecular weight of species i, n and M the number density and the mean molecular weight of the atmosphere and f_i the mole fraction of species i.

The retrieval of the eddy mixing coefficient is discussed in Part II. For the molecular diffusion coefficients, measurements for the binary coefficients have been performed only for some of the species included in the model. These are given in the form

$$D_{ij} = A_{ij}\frac{T^s}{n}, \qquad (5)$$

Table 4
Binary and thermal diffusion coefficients used in the model calculations

Pair	$A \times 10^{17}$	s	α_T	Reference
H–N$_2$	4.87	0.698	−0.38	Banks and Kockarts (1973)
H$_2$–N$_2$	2.80	0.740	−0.38	Banks and Kockarts (1973)
N–N$_2$	0.969	0.770		Mason and Marreno (1970)
Ar–N$_2$	0.362	0.833	0.17	Mason and Marreno (1970)
CH$_4$–N$_2$	0.734	0.750		Banks and Kockarts (1973)
C$_2$H$_6$–N$_2$	0.561	0.730		Wakeham and Slater (1973)
C$_3$H$_8$–N$_2$	0.653	0.660		Wakeham and Slater (1973)
C$_4$H$_{10}$–N$_2$	0.734	0.610		Wakeham and Slater (1973)

A is given in cm^2 s^{-1}.

where A_{ij} and s are parameters that depend on the pair of diffusing species and are presented in Table 4. For the rest of the species for which no measurements were found, the diffusion coefficients were calculated using the formula (Banks and Kockarts, 1973):

$$D_{ij} = 1.52 \times 10^{18}\left(\frac{1}{M_i} + \frac{1}{M_j}\right)^{1/2}\frac{T^{1/2}}{n} \qquad (6)$$

with i corresponding to the diffusing minor species and j to the bath molecule. In order to take into account the variation of the atmospheric composition with altitude due to the changes in methane's vertical profile in the upper atmosphere, the bath gas molecular weight was replaced by the atmospheric mean molecular weight.

2.3.3. Chemistry

The derived photodissociation products, react together to give all the observed species considered in the model following the chemical reactions provided in Table 5. Although many photochemical models have been developed in the past for the simulation of Titan's neutral atmospheric composition, (Yung et al., 1984; Toublanc et al., 1995; Lara et al., 1996; Lebonnois et al., 2001; Wilson and Atreya, 2004) significant differences can be found among them regarding the rates used for some of the reactions. In the current simulations we have used the previously, well-stablished, reaction schemes for the production of most of the observed species in Titan's atmosphere and also have included new species.

The absence of measurements for the reaction rates in the temperature range 100–200 K, which is characteristic of Titan's atmosphere, has always been a problem in the photochemical models. This is more clearly shown in the last column of Table 5, where the temperature range of the measurements for each reaction used is given. Although a significant number of new measurements have been performed at low temperatures since the early photochemical models, the majority of the reaction rates used, are measured at $T \geqslant 200$ K and extrapolation to Titan's atmospheric temperatures is applied, a common approach between all photochemical models. The good agreement between the measurements and the simulated profiles for most of the species suggests that the extrapolation

Table 5
Chemical reactions

Reaction			Rate	Reference	T (K)
Hydrocarbons					
R92	$2\,H + M$	$\rightarrow H_2 + M$	$k_0 = 1.5 \times 10^{-29} T^{-1.3}$	Tsang and Hampson (1986)	77–2000
			$k_\infty = 1.0 \times 10^{-11}$	Est. from Jacobs et al. (1965)	
R93	$H + CH$	$\rightarrow H_2 + C$	$1.3 \times 10^{-10} e^{-80/T}$	Harding et al. (1993)	300–2000
R94	$H + {}^1CH_2$	$\rightarrow CH + H_2$	1.0×10^{-10}	Peeters et al. (1994)	290
R95	$H + {}^1CH_2$	$\rightarrow {}^3CH_2 + H$	2.0×10^{-10}	♯	♯
R96	$H + {}^3CH_2$	$\rightarrow CH + H_2$	$3.55 \times 10^{-11} T^{0.32}$	Fulle and Hippler (1997)	185–800
R97	$H + {}^3CH_2 + M$	$\rightarrow CH_3 + M$	$k_0 = 1.7 \times 10^{-25} T^{-1.8}$	Est. as $0.1 \times k(H + CH_3)$, Laufer et al. (1983)	
			$k_\infty = 3.54 \times 10^{-10} T^{0.32}$	Fulle and Hippler (1997)	185–800
R98	$H + CH_3$	$\rightarrow H_2 + {}^3CH_2$	$1.0 \times 10^{-10} e^{-7599/T}$	Baulch et al. (1992)	300–2500
R99	$H + CH_3 + M$	$\rightarrow CH_4 + M$	$k_0 = 1.7 \times 10^{-24} T^{-1.8}$	Baulch et al. (1994)	300–1000
			$k_\infty = 3.5 \times 10^{-10}$	♯	♯
R100	$H + CH_4$	$\rightarrow H_2 + CH_3$	$2.18 \times 10^{-20} T^3 e^{-4045/T}$	♯	♯
R101	$H + C_2H + M$	$\rightarrow C_2H_2 + M$	$k_0 = 1.26 \times 10^{-18} T^{-3.1} e^{-721/T}$	Tsang and Hampson (1986)	300–2500
			$k_\infty = 3.0 \times 10^{-10}$	♯	♯
R102	$H + C_2H_2 + M$	$\rightarrow C_2H_3 + M$	$k_0 = 3.3 \times 10^{-30} e^{-740/T}$	Baulch et al. (1992)	200–400
			$k_\infty = 1.4 \times 10^{-11} e^{-1300/T}$	♯	♯
R103	$H + C_2H_3$	$\rightarrow H_2 + C_2H_2$	$6.86 \times 10^{-11} e^{23./T}$	Monks et al. (1995)	213–298
R104	$H + C_2H_3 + M$	$\rightarrow C_2H_4 + M$	$k_0 = 5.76 \times 10^{-24} T^{-1.3}$	♯	♯
			$k_\infty = 6.45 \times 10^{-11} T^{0.2}$	Harding et al. (2005)	200–2000
R105	$H + C_2H_4$	$\rightarrow H_2 + C_2H_3$	$8.42 \times 10^{-17} T^{-1.93} e^{-6518/T}$	Knyazev et al. (1996)	200–3000
R106	$H + C_2H_4 + M$	$\rightarrow C_2H_5 + M$	$k_0 = 7.7 \times 10^{-30} e^{-380/T}$	Baulch et al. (1994)	300–800
			$k_\infty = 6.6 \times 10^{-15} T^{1.28} e^{-650/T}$	♯	200–1100
R107	$H + C_2H_5$	$\rightarrow 2\,CH_3$	1.25×10^{-10}	Sillesen et al. (1993)	298
R108	$H + C_2H_5$	$\rightarrow H_2 + C_2H_4$	3.0×10^{-12}	Tsang and Hampson (1986)	300–2500
R109	$H + C_2H_5 + M$	$\rightarrow C_2H_6 + M$	$k_0 = 5.5 \times 10^{-23} T^{-2} e^{-1040/T}$	Teng and Jones (1972)	
			$k_\infty = 1.66 \times 10^{-10}$	Sillesen et al. (1993)	298
R110	$H + C_2H_6$	$\rightarrow H_2 + C_2H_5$	$2.4 \times 10^{-15} T^{1.5} e^{-3730/T}$	Baulch et al. (1992)	300–2000
R111	$H + C_3H_2 + M$	$\rightarrow C_3H_3 + M$	$k_0 = 1.7 \times 10^{-23} T^{-1.8}$	Est. as $10 \times k_0(H + CH_3)$, Laufer et al. (1983)	
			$k_\infty = 1.0 \times 10^{-10}$	Peeters et al. (1994)	290
R112	$H + C_3H_3 + M$	$\rightarrow CH_3C_2H + M$	$k_0 = 1.7 \times 10^{-23} T^{-1.8}$	Est. as $10 \times k_0(H + CH_3)$, Laufer et al. (1983)	
			$k_\infty = 1.25 \times 10^{-10}$	Atkinson and Hudgens (1999)	295
R113	$H + C_3H_3 + M$	$\rightarrow CH_2CCH_2 + M$	$k_0 = 1.7 \times 10^{-23} T^{-1.8}$	Est. as $10 \times k_0(H + CH_3)$, Laufer et al. (1983)	
			$k_\infty = 1.25 \times 10^{-10}$	Atkinson and Hudgens (1999)	295
R114	$H + CH_2CCH_2$	$\rightarrow CH_3C_2H + H$	$1.29 \times 10^{-11} e^{-1156./T}$	Aleksandrov et al. (1980)	295–853
R115	$H + CH_2CCH_2$	$\rightarrow H_2 + C_3H_3$	$4.7 \times 10^{-16} T^{1.74} e^{-3873/T}$	Wang et al. (2000)	200–500
R116	$H + CH_2CCH_2 + M$	$\rightarrow C_3H_5 + M$	$k_0 = 8.0 \times 10^{-24} T^{-2} e^{-1225/T}$	Est. as $k_0(H + CH_3C_2H + M)$	
			$k_\infty = 9.4 \times 10^{-11} e^{-1234/T}$	Wang et al. (2000)	200–500
R117	$H + CH_3C_2H$	$\rightarrow H_2 + C_3H_3$	$4.7 \times 10^{-16} T^{1.74} e^{-3873/T}$	Wang et al. (2000)	200–500
R118	$H + CH_3C_2H + M$	$\rightarrow C_3H_5 + M$	$k_0 = 8.0 \times 10^{-24} T^{-2} e^{-1225/T}$	Yung et al. (1984)	215–363
			$k_\infty = 9.4 \times 10^{-11} e^{-1234/T}$	Wang et al. (2000)	200–500
R119	$H + C_3H_5$	$\rightarrow CH_2CCH_2 + H_2$	1.3×10^{-11}	Hanning-Lee and Pilling (1992)	291
R120	$H + C_3H_5$	$\rightarrow CH_3C_2H + H_2$	1.3×10^{-11}	♯	♯
R121	$H + C_3H_5 + M$	$\rightarrow C_3H_6 + M$	$k_0 = 1.0 \times 10^{-24}$	♯	♯
			$k_\infty = 2.54 \times 10^{-10}$	♯	♯
R122	$H + C_3H_6$	$\rightarrow C_3H_5 + H_2$	$2.87 \times 10^{-19} T^{2.5} e^{-1254/T}$	Tsang (1991)	300–2500
R123	$H + C_3H_6 + M$	$\rightarrow C_3H_7 + M$	$k_0 = 7.7 \times 10^{-29} e^{-380/T}$	Est. as $10 \times k(H + C_2H_4 + M)$, Laufer et al. (1983)	
			$k_\infty = 2.2 \times 10^{-11} e^{-1640./T}$	Tsang (1991)	300–2500
R124	$H + C_3H_7$	$\rightarrow C_3H_6 + H_2$	3.0×10^{-12}	Tsang (1988)	300–2500
R125	$H + C_3H_7 + M$	$\rightarrow C_3H_8 + M$	$k_0 = 5.5 \times 10^{-23} T^{-2} e^{-1040/T}$	Est. as $k_0(H + C_2H_5 + M)$	
			$k_\infty = 2.49 \times 10^{-10}$	Munk et al. (1986b)	298
R126	$H + C_3H_8$	$\rightarrow C_3H_7 + H_2$	$2.2 \times 10^{-18} T^{2.54} e^{-3400/T}$	♯	♯
R127	$H + C_4H + M$	$\rightarrow C_4H_2 + M$	$k_0 = 1.26 \times 10^{-18} T^{-3.1} e^{-721/T}$	Est. as $k_0(H + C_2H + M)$	
			$k_\infty = 3.0 \times 10^{-10}$	♯	
R128	$H + C_4H_2 + M$	$\rightarrow C_4H_3 + M$	$k_0 = 1.0 \times 10^{-28}$	Schwanebeck and Warnatz (1975)	298
			$k_\infty = 1.39 \times 10^{-10} e^{-1184/T}$	Nava et al. (1986)	210–423

Table 5 (*continued*)

Reaction			Rate	Reference	T (K)
R129	$H + C_4H_3$	$\rightarrow C_4H_2 + H_2$	3.0×10^{-11}	Wang and Frenklach (1997)	300–2500
R130	$H + C_4H_3$	$\rightarrow 2\,C_2H_2$	1.0×10^{-11}	♯	♯
R131	$H + C_4H_3 + M$	$\rightarrow C_4H_4 + M$	$k_0 = 5.76 \times 10^{-24} T^{-1.3}$	Est. as $k_0(H + C_2H_3 + M)$	
			$k_\infty = 8.55 \times 10^{-10} e^{-403/T}$	Duràn et al. (1988)	700–1300
R132	$H + C_4H_4 + M$	$\rightarrow C_4H_5 + M$	$k_0 = 1.0 \times 10^{-28}$	Est. as $k_0(H + C_4H_2 + M)$	
			$k_\infty = 3.3 \times 10^{-12}$	Schwanebeck and Warnatz (1975)	298
R133	$H + C_4H_5$	$\rightarrow C_4H_4 + H_2$	$6.86 \times 10^{-11} e^{23/T}$	Est. as $k(H + C_2H_3)$	
R134	$H + C_4H_5 + M$	$\rightarrow C_4H_6 + M$	$k_0 = 5.5 \times 10^{-23} T^{-2} e^{-1040/T}$	Est. as $k_0(H + C_2H_5 + M)$	
			$k_\infty = 1.0 \times 10^{-10}$	Gladstone et al. (1996)	Est.
R135	$H + C_4H_6$	$\rightarrow C_4H_5 + H_2$	$1.05 \times 10^{-13} T^{0.7} e^{-3019/T}$	Weissman and Benson (1988)	300–1500
R136	$H + C_5H_3$	$\rightarrow C_2H_2 + C_3H_2$	1.0×10^{-11}	Est. as $k(H + C_4H_3)$	
R137	$H + C_6H + M$	$\rightarrow C_6H_2 + M$	$k_0 = 1.26 \times 10^{-18} T^{-3.1} e^{-721/T}$	Est. as $k(H + C_2H + M)$	
			$k_\infty = 3.0 \times 10^{-10}$	♯	
R138	$H + C_6H_2 + M$	$\rightarrow C_6H_3 + M$	$k_0 = 1.0 \times 10^{-28}$	Est. as $k(H + C_4H_2 + M)$	
			$k_\infty = 1.39 \times 10^{-10} e^{-1184}$	♯	
R139	$H + C_6H_3$	$\rightarrow C_6H_2 + H_2$	3.0×10^{-11}	Wang and Frenklach (1997)	300–2500
R140	$H + C_6H_3$	$\rightarrow C_4H_2 + C_2H_2$	1.0×10^{-11}	♯	♯
R141	$H + C_6H_3 + M$	$\rightarrow C_6H_4 + M$	$k_0 = 5.76 \times 10^{-24} T^{-1.3}$	Est. as $k_0(H + C_4H_3 + M)$	
			$k_\infty = 8.55 \times 10^{-10} e^{-403/T}$	♯	
R142	$H + C_6H_4$	$\rightarrow C_6H_3 + H_2$	$1.1 \times 10^{-17} T^{2.53} e^{-4648/T}$	Wang and Frenklach (1997)	300–2500
R143	$H + C_6H_4 + M$	$\rightarrow C_6H_5 + M$	$k_0 = 1.96 \times 10^{33} T^{-18.35} e^{-6694/T}$	Wang and Frenklach (1994)	400–2500
			$k_\infty = 1.06 \times 10^{-14} T^{1.11} e^{-705/T}$	♯	300–2500
R144	$H + C_6H_5$	$\rightarrow C_4H_4 + C_2H_2$	$3.16 \times 10^{-5} T^{-1.6} e^{-1117/T}$	Wang and Frenklach (1997)	300–2500
R145	$H + C_6H_5 + M$	$\rightarrow C_6H_6 + M$	$k_0 = 1.82 \times 10^{28} T^{-16.3} e^{-3521/T}$	♯	♯
			$k_\infty = 3.65 \times 10^{-10}$	Ackermann et al. (1990)	300
R146	$H + C_6H_6$	$\rightarrow C_6H_5 + H_2$	$4.15 \times 10^{-10} e^{-8057/T}$	Wang and Frenklach (1997)	300–2500
R147	$H_2 + C + M$	$\rightarrow {}^3CH_2 + M$	$k_0 = 6.89 \times 10^{-32}$	Husain and Young (1975)	300
			$k_\infty = 2.06 \times 10^{-11} e^{-57/T}$	Harding et al. (1993)	300–2000
R148	$H_2 + CH + M$	$\rightarrow CH_3 + M$	$k_0 = 4.7 \times 10^{-26} T^{-1.6}$	Brownsword et al. (1997)	53–744
			$k_\infty = 2.52 \times 10^{-10} T^{-0.08}$	♯	♯
R149	$H_2 + CH$	$\rightarrow {}^3CH_2 + H$	$3.10 \times 10^{-10} e^{-1650/T}$	♯	♯
R150	$H_2 + {}^1CH_2$	$\rightarrow {}^3CH_2 + H_2$	1.26×10^{-11}	Langford et al. (1983)	298
R151	$H_2 + {}^1CH_2$	$\rightarrow CH_3 + H$	9.24×10^{-11}	♯	♯
R152	$H_2 + {}^3CH_2$	$\rightarrow CH_3 + H$	5.0×10^{-15}	Tsang and Hampson (1986)	300–2500
R153	$H_2 + CH_3$	$\rightarrow CH_4 + H$	$1.14 \times 10^{-20} T^{2.74} e^{-4740/T}$	Baulch et al. (1992)	300–2500
R154	$H_2 + C_2$	$\rightarrow C_2H + H$	$1.77 \times 10^{-10} e^{-1470/T}$	Pitts et al. (1982)	300–500
R155	$H_2 + C_2H$	$\rightarrow C_2H_2 + H$	$1.20 \times 10^{-11} e^{-998/T}$	Opansky and Leone (1996b)	150–359
R156	$H_2 + C_2H_3$	$\rightarrow C_2H_4 + H$	$1.57 \times 10^{-20} T^{2.56} e^{-2529/T}$	Knyazev et al. (1996)	200–3000
R157	$H_2 + C_2H_5$	$\rightarrow C_2H_6 + H$	$5.11 \times 10^{-24} T^{3.6} e^{-4253/T}$	Tsang and Hampson (1986)	300–2500
R158	$H_2 + C_3H_5$	$\rightarrow C_3H_6 + H$	$1.80 \times 10^{-19} T^{2.38} e^{-9557/T}$	Tsang (1991)	300–2500
R159	$H_2 + C_3H_7$	$\rightarrow C_3H_8 + H$	$3.0 \times 10^{-21} T^{2.84} e^{-4600/T}$	Tsang (1988)	300–2500
R160	$H_2 + C_4H$	$\rightarrow C_4H_2 + H$	$1.20 \times 10^{-11} e^{-998/T}$	Est. as $k(H_2 + C_2H)$	
R161	$H_2 + C_4H_5$	$\rightarrow C_4H_6 + H$	$6.61 \times 10^{-15} T^{0.5} e^{-1862/T}$	Weissman and Benson (1988)	300–1500
R162	$H_2 + C_6H$	$\rightarrow C_6H_2 + H$	$1.20 \times 10^{-11} e^{-998/T}$	Est. as $k(H_2 + C_2H)$	
R163	$H_2 + C_6H_5$	$\rightarrow C_6H_6 + H$	$9.48 \times 10^{-20} T^{2.43} e^{-3159/T}$	Mebel et al. (1997)	300–5000
R164	$2\,C + M$	$\rightarrow C_2 + M$	$k_0 = 4.97 \times 10^{-27} T^{-1.6}$	Slack (1976)	5000–6000
			$k_\infty = 2.16 \times 10^{-11}$	Martinotti et al. (1968)	298
R165	$C + CH_4$	$\rightarrow C_2H_4$	2.0×10^{-15}	Husain and Kirsch (1971)	300
R166	$C + C_2H_2$	$\rightarrow C_3H_2$	$k_0 = 1.0 \times 10^{-30}$	Moses et al. (2005)	Est.
			$k_\infty = 5.75 \times 10^{-10} T^{-0.12}$	Chastaing et al. (2001)	15–295
R167	$C + C_2H_4$	$\rightarrow C_3H_3 + H$	$5.61 \times 10^{-10} T^{-0.11}$	♯	♯
R168	$C + CH_3C_2H$	$\rightarrow C_4H_3 + H$	$5.05 \times 10^{-10} T^{-0.11}$	♯	♯
R169	$C + CH_2CCH_2$	$\rightarrow C_4H_3 + H$	$3.71 \times 10^{-10} T^{-0.01}$	♯	♯
R170	$C + C_3H_6$	$\rightarrow C_4H_5 + H$	$4.57 \times 10^{-10} T^{-0.08}$	Chastaing et al. (1998)	♯
R171	$C + C_4H_6$	$\rightarrow$ Products	1.1×10^{-9}	Husain and Ioannou (1997)	300
R172	$C + C_4H_8$	$\rightarrow$ Products	4.3×10^{-10}	Haider and Husain (1993)	300
R173	$2\,CH$	$\rightarrow C_2H_2$	1.99×10^{-10}	Braun et al. (1967)	298

Table 5 (*continued*)

Reaction			Rate	Reference	T (K)
R174	$CH + CH_4$	$\rightarrow C_2H_4 + H$	$3.96 \times 10^{-8} T^{-1.04} e^{-36.1/T}$	Canosa et al. (1997)	23–295
R175	$CH + C_2H_2$	$\rightarrow C_3H_2 + H$	$1.59 \times 10^{-9} T^{-0.23} e^{-16/T}$	♯	♯
R176	$CH + C_2H_4$	$\rightarrow CH_3C_2H + H$	$3.87 \times 10^{-9} T^{-0.55} e^{-29.6/T}$	♯	♯
R177	$CH + C_2H_4$	$\rightarrow CH_2CCH_2 + H$	$3.87 \times 10^{-9} T^{-0.55} e^{-29.6/T}$	♯	♯
R178	$CH + C_2H_6$	$\rightarrow C_3H_6 + H$	$1.9 \times 10^{-8} T^{-0.86} e^{-53.2/T}$	♯	♯
R179	$CH + C_2H_6$	$\rightarrow C_2H_4 + CH_3$	$1.9 \times 10^{-8} T^{-0.86} e^{-53.2/T}$	♯	♯
R180	$CH + CH_3C_2H$	$\rightarrow C_4H_4 + H$	4.6×10^{-10}	Butler et al. (1981)	298
R181	$CH + C_3H_6$	$\rightarrow C_4H_6 + H$	$5.3 \times 10^{-11} e^{528/T}$	Est. from Zabarnick et al. (1988)	295–668
R182	$CH + C_3H_8$	$\rightarrow C_3H_6 + CH_3$	$1.9 \times 10^{-10} e^{242/T}$	Baulch et al. (1992)	300–700
R183	$CH + C_4H_4$	$\rightarrow Products + H$	$1.59 \times 10^{-9} T^{-0.23} e^{-16/T}$	Est. as $k(CH + C_2H_2)$	
R184	$CH + C_4H_8$	$\rightarrow Products$	$8.78 \times 10^{-9} T^{-0.53} e^{-33.5/T}$	Canosa et al. (1997)	23–295
R185	$CH + C_4H_{10}$	$\rightarrow C_4H_8 + CH_3$	$4.4 \times 10^{-10} e^{28/T}$	Baulch et al. (1992)	250–700
R186	$2\ ^1CH_2$	$\rightarrow C_2H_2 + 2\ H$	5.0×10^{-11}	Tsang and Hampson (1986)	300–2500
R187	$^1CH_2 + {}^3CH_2$	$\rightarrow C_2H_2 + 2\ H$	3.0×10^{-11}	♯	♯
R188	$^1CH_2 + CH_3$	$\rightarrow C_2H_4 + H$	3.0×10^{-11}	♯	♯
R189	$^1CH_2 + CH_4$	$\rightarrow 2\ CH_3$	5.9×10^{-11}	Böhland et al. (1985a)	
R190	$^1CH_2 + CH_4$	$\rightarrow {}^3CH_2 + CH_4$	1.2×10^{-11}	♯	♯
R191	$^1CH_2 + C_2H$	$\rightarrow C_2H_2 + CH$	3.0×10^{-11}	Tsang and Hampson (1986)	300–2500
R192	$^1CH_2 + C_2H_2$	$\rightarrow {}^3CH_2 + C_2H_2$	9.2×10^{-11}	Blitz et al. (2000)	205
R193	$^1CH_2 + C_2H_2$	$\rightarrow C_3H_3 + H$	3.27×10^{-10}	♯	♯
R194	$^1CH_2 + C_2H_3$	$\rightarrow C_2H_2 + CH_3$	3.0×10^{-11}	Tsang and Hampson (1986)	
R195	$^1CH_2 + C_2H_4$	$\rightarrow {}^3CH_2 + C_2H_4$	2.3×10^{-11}	Baulch et al. (1992)	300–3000
R196	$^1CH_2 + C_2H_4 + M$	$\rightarrow C_3H_6 + M$	$k_0 = 1.5 \times 10^{-18} T^{-3} e^{-300/T}$	Moses et al. (2005)	Est.
			$k_\infty = 1.5 \times 10^{-10}$	Baulch et al. (1992)	300–3000
R197	$^1CH_2 + C_2H_5$	$\rightarrow C_2H_4 + CH_3$	1.5×10^{-11}	Tsang and Hampson (1986)	300–2500
R198	$^1CH_2 + C_2H_5$	$\rightarrow C_3H_6 + H$	1.5×10^{-11}	♯	♯
R199	$^1CH_2 + C_2H_6$	$\rightarrow {}^3CH_2 + C_2H_6$	3.6×10^{-11}	Baulch et al. (1992)	300–3000
R200	$^1CH_2 + C_2H_6$	$\rightarrow C_2H_5 + CH_3$	5.9×10^{-11}	Est. as $k(^1CH_2 + CH_4)$	
R201	$^1CH_2 + C_3H_3$	$\rightarrow C_4H_4 + H$	3.3×10^{-10}	Est. as $k(^1CH_2 + C_3H_5)$	
R202	$^1CH_2 + CH_3C_2H$	$\rightarrow C_4H_5 + H$	5.0×10^{-11}	Est. based on other $^1CH_2$ reactions	
R203	$^1CH_2 + CH_2CCH_2$	$\rightarrow C_4H_5 + H$	5.0×10^{-11}	♯	
R204	$^1CH_2 + C_3H_5$	$\rightarrow C_4H_6 + H$	3.3×10^{-10}	Tsang (1991)	300–2500
R205	$^1CH_2 + C_3H_5$	$\rightarrow C_2H_4 + C_2H_3$	6.67×10^{-11}	♯	♯
R206	$^1CH_2 + C_3H_6$	$\rightarrow {}^3CH_2 + C_3H_6$	5.0×10^{-11}	♯	♯
R207	$^1CH_2 + C_3H_6$	$\rightarrow C_3H_5 + CH_3$	8.7×10^{-11}	♯	♯
R208	$^1CH_2 + C_3H_6 + M$	$\rightarrow C_4H_8 + M$	$k_0 = 1.5 \times 10^{-18} T^{-3} e^{-300/T}$	Est. as $k_0(^1CH_2 + C_2H_4)$	
			$k_\infty = 8.1 \times 10^{-11}$	Tsang (1991)	300–2500
R209	$^1CH_2 + C_3H_7$	$\rightarrow C_2H_5 + C_2H_4$	4.29×10^{-11}	Tsang (1988)	300–2500
R210	$^1CH_2 + C_3H_7$	$\rightarrow C_3H_6 + CH_3$	1.71×10^{-11}	♯	♯
R211	$^1CH_2 + C_3H_8$	$\rightarrow 2\ C_2H_5$	1.6×10^{-10}	♯	♯
R212	$^1CH_2 + C_4H_4$	$\rightarrow Product + H$	3.27×10^{-10}	Est. as $k(^1CH_2 + C_2H_2)$	
R213	$^1CH_2 + C_4H_8 + M$	$\rightarrow Product + M$	$k_0 = 1.5 \times 10^{-18} T^{-3} e^{-300/T}$	Est. as $k_0(^1CH_2 + C_2H_4)$	
			$k_\infty = 8.1 \times 10^{-11}$	Est. as $k_\infty(^1CH_2 + C_2H_4)$	
R214	$^1CH_2 + C_4H_{10}$	$\rightarrow C_2H_5 + C_3H_7$	1.6×10^{-10}	Est. as $k(^1CH_2 + C_3H_8)$	
R215	$^1CH_2 + N_2$	$\rightarrow {}^3CH_2 + N_2$	1.0×10^{-11}	Baulch et al. (1992)	300–3000
R216	$2\ ^3CH_2$	$\rightarrow C_2H_2 + 2\ H$	$1.8 \times 10^{-10} e^{-400/T}$	♯	♯
R217	$2\ ^3CH_2$	$\rightarrow C_2H_2 + H_2$	$2.0 \times 10^{-11} e^{-400/T}$	♯	♯
R218	$^3CH_2 + CH_3$	$\rightarrow C_2H_4 + H$	7.0×10^{-11}	♯	♯
R219	$^3CH_2 + CH_4$	$\rightarrow 2\ CH_3$	$7.13 \times 10^{-12} e^{-5052/T}$	Böhland et al. (1985b)	296–707
R220	$^3CH_2 + C_2H$	$\rightarrow C_2H_2 + CH$	3.0×10^{-11}	Tsang and Hampson (1986)	300–2500
R221	$^3CH_2 + C_2H_2$	$\rightarrow C_3H_3 + H$	$2.0 \times 10^{-11} e^{-3330/T}$	♯	♯
R222	$^3CH_2 + C_2H_3$	$\rightarrow C_2H_2 + CH_3$	3.0×10^{-11}	Tsang and Hampson (1986)	300–2500
R223	$^3CH_2 + C_2H_4$	$\rightarrow C_3H_5 + H$	$5.31 \times 10^{-12} e^{-2658/T}$	Kraus et al. (1993)	296–728
R224	$^3CH_2 + C_2H_5$	$\rightarrow C_2H_4 + CH_3$	3.0×10^{-11}	Tsang and Hampson (1986)	300–2500
R225	$^3CH_2 + C_2H_6$	$\rightarrow C_2H_5 + CH_3$	$1.07 \times 10^{-11} e^{-3981/T}$	Böhland et al. (1985b)	296–707
R226	$^3CH_2 + C_3H_3$	$\rightarrow C_4H_4 + H$	5.0×10^{-11}	Est. as $k(^3CH_2 + C_3H_5)$	

Table 5 (*continued*)

Reaction			Rate	Reference	T (K)
R227	$^3CH_2 + CH_3C_2H$	$\rightarrow C_4H_5 + H$	5.0×10^{-11}	Est. based on other $^3CH_2$ reactions	
R228	$^3CH_2 + CH_2CCH_2$	$\rightarrow C_4H_5 + H$	5.0×10^{-11}	♯	
R229	$^3CH_2 + C_3H_5$	$\rightarrow C_4H_6 + H$	5.0×10^{-11}	Tsang (1991)	300–2500
R230	$^3CH_2 + C_3H_6$	$\rightarrow C_3H_5 + CH_3$	$1.2 \times 10^{-12}e^{-3120/T}$	♯	♯
R231	$^3CH_2 + C_3H_7$	$\rightarrow C_3H_6 + CH_3$	3.0×10^{-12}	Tsang (1988)	300–2500
R232	$^3CH_2 + C_3H_7$	$\rightarrow C_2H_4 + C_2H_5$	3.0×10^{-11}	♯	♯
R233	$^3CH_2 + C_3H_8$	$\rightarrow C_3H_7 + CH_3$	$1.5 \times 10^{-24}T^{3.65}e^{-3600/T}$	♯	♯
R234	$^3CH_2 + C_4H_2$	$\rightarrow C_4H + CH_3$	$2.16 \times 10^{-11}e^{-2165/T}$	Böland et al. (1988)	296–700
R235	$^3CH_2 + C_4H_6$	$\rightarrow CH_3C_2H + C_2H_4$	$6.14 \times 10^{-12}e^{-1732/T}$	Kraus et al. (1993)	296–728
R236	$^3CH_2 + C_4H_{10}$	$\rightarrow$ Products $+ CH_3$	8.1×10^{-12}	Halberstadt and Crump (1973)	304
R237	$2 CH_3$	$\rightarrow C_2H_5 + H$	$8.28 \times 10^{-12}T^{0.1}e^{-5335/T}$	Stewart et al. (1989)	200–2500
R238	$2 CH_3 + M$	$\rightarrow C_2H_6 + M$	$k_0 = 2.822 \times 10^{-3}T^{-8.749}e^{-985.4/T}$	See text, Part II	
			$k_\infty = 9.3132 \times 10^{-11}e^{-1.519 \times 10^{-3} \times T}$	Cody et al. (2003)	155–906
R239	$CH_3 + C_2H$	$\rightarrow C_3H_3 + H$	4.0×10^{-11}	Tsang and Hampson (1986)	300–2500
R240	$CH_3 + C_2H_2$	$\rightarrow CH_3C_2H + H$	$3.18 \times 10^{-20}T^{2.42}e^{-6488/T}$	Diau and Lin (1994)	300–3000
R241	$CH_3 + C_2H_2 + M$	$\rightarrow C_3H_5 + M$	$k_0 = 3.3 \times 10^{-30}e^{-740/T}$	Est. as $k_0(H + C_2H_2 + M)$	
			$k_\infty = 1.0 \times 10^{-12}e^{-3880/T}$	Tsang and Hampson (1986)	300–2500
R242	$CH_3 + C_2H_3$	$\rightarrow C_2H_2 + CH_4$	3.4×10^{-11}	Fahr et al. (1991)	298
R243	$CH_3 + C_2H_3 + M$	$\rightarrow C_3H_6 + M$	$k_0 = 2.822 \times 10^{-3}T^{-8.749}e^{-985.4/T}$	Est. as $10 \times k_0(2 CH_3 + M)$, Laufer et al. (1983)	
			$k_\infty = 1.2 \times 10^{-10}$	Fahr et al. (1991)	298
R244	$CH_3 + C_2H_4$	$\rightarrow C_2H_3 + CH_4$	$1.1 \times 10^{-23}T^{3.7}e^{-4780/T}$	Tsang and Hampson (1986)	300–2500
R245	$CH_3 + C_2H_4 + M$	$\rightarrow C_3H_7 + M$	$k_0 = 7.7 \times 10^{-30}e^{-380/T}$	Est. as $k_0(H + C_2H_4 + M)$	
			$k_\infty = 3.5 \times 10^{-13}e^{-3700/T}$	Baulch et al. (1992)	300–600
R246	$CH_3 + C_2H_5$	$\rightarrow C_2H_4 + CH_4$	$5.04 \times 10^{-14}T^{0.41}e^{429/T}$	Zhu et al. (2004)	200–600
R247	$CH_3 + C_2H_5 + M$	$\rightarrow C_3H_8 + M$	$k_0 = 2.822 \times 10^{-3}T^{-8.749}e^{-985.4/T}$	Est. as $k_0(2 CH_3 + M)$	
			$k_\infty = 2.41 \times 10^{-10}T^{-0.34}e^{259/T}$	Zhu et al. (2004)	200–600
R248	$CH_3 + C_2H_6$	$\rightarrow C_2H_5 + CH_4$	$2.5 \times 10^{-31}T^6e^{-3043/T}$	Baulch et al. (1992)	300–1500
R249	$CH_3 + C_3H_3 + M$	$\rightarrow C_4H_6 + M$	$k_0 = 2.822 \times 10^{-3}T^{-8.749}e^{-985.4/T}$	Est. as $k_0(2 CH_3 + M)$	
			$k_\infty = 6.8 \times 10^{-11}e^{131/T}$	Knyazev and Slagle (2001b)	300–800
R250	$CH_3 + CH_3C_2H$	$\rightarrow C_2H_6 + C_2H$	$8.32 \times 10^{-13}e^{-4428/T}$	Kerr and Parsonage (1972)	379–465
R251	$CH_3 + CH_2CCH_2$	$\rightarrow C_2H_5 + C_2H_2$	$3.32 \times 10^{-13}e^{-4076/T}$	♯	♯
R252	$CH_3 + C_3H_5$	$\rightarrow CH_2CCH_2 + CH_4$	$5.0 \times 10^{-12}T^{-0.32}e^{66/T}$	Tsang (1991)	300–2500
R253	$CH_3 + C_3H_5 + M$	$\rightarrow C_4H_8 + M$	$k_0 = 2.822 \times 10^{-3}T^{-8.749}e^{-985.4/T}$	Est. as $k_0(2 CH_3 + M)$	
			$k_\infty = 1.55 \times 10^{-9}T^{-0.54}e^{117/T}$	Knyazev and Slagle (2001a)	300–800
R254	$CH_3 + C_3H_6$	$\rightarrow C_3H_5 + CH_4$	$2.66 \times 10^{-13}e^{-4440/T}$	Kinsman and Roscoe (1994)	300–580
R255	$CH_3 + C_3H_6$	$\rightarrow$ Products	$k_0 = 7.7 \times 10^{-30}e^{-380/T}$	Est. as $k_0(H + C_2H_4 + M)$	
			$k_\infty = 1.19 \times 10^{-13}e^{-3260/T}$	Kinsman and Roscoe (1994)	300–580
R256	$CH_3 + C_3H_7$	$\rightarrow C_3H_6 + CH_4$	$1.9 \times 10^{-11}T^{-0.32}$	Tsang (1988)	300–2500
R257	$CH_3 + C_3H_7 + M$	$\rightarrow C_4H_{10} + M$	$k_0 = 2.822 \times 10^{-3}T^{-8.749}e^{-985.4/T}$	Est. as $k_0(2 CH_3 + M)$	
			$k_\infty = 3.06 \times 10^{-11}e^{387/T}$	Knyazev and Slagle (2001b)	297–600
R258	$CH_3 + C_3H_8$	$\rightarrow C_3H_7 + CH_4$	$1.5 \times 10^{-24}T^{3.65}e^{-3600/T}$	Tsang (1988)	300–2500
R259	$CH_3 + C_4H_4$	$\rightarrow C_4H_3 + CH_4$	$6.61 \times 10^{-13}e^{-2502/T}$	Scherzer et al. (1985)	553–593
R260	$CH_3 + C_4H_6$	$\rightarrow$ Products	$k_0 = 3.3 \times 10^{-30}e^{-740/T}$	Est. as $k_0(H + C_2H_2 + M)$	
			$k_\infty = 1.35 \times 10^{-13}e^{-2063/T}$	Kerr and Parsonage (1972)	353–453
R261	$CH_3 + C_4H_8$	$\rightarrow$ Products	$1.69 \times 10^{-13}e^{-3620/T}$	♯	♯
R262	$CH_3 + C_4H_{10}$	$\rightarrow$ Products $+ CH_4$	$6.64 \times 10^{-13}e^{-4840/T}$	Warnatz (1984)	300–1000
R263	$CH_3 + C_5H_3$	$\rightarrow 2 C_3H_3$	4.0×10^{-11}	Est. Moses et al. (2005)	
R264	$CH_3 + C_5H_3 + M$	$\rightarrow C_6H_6 + M$	$k_0 = 2.822 \times 10^{-3}T^{-8.749}e^{-985.4/T}$	Est. as $k_0(2 CH_3 + M)$	
			$k_\infty = 3.06 \times 10^{-11}e^{387/T}$	Est. as $k_\infty(CH_3 + C_3H_7 + M)$	
R265	$CH_3 + C_6H_4$	$\rightarrow C_6H_3 + CH_4$	$6.61 \times 10^{-13}e^{-2502/T}$	Est. as $k(CH_3 + C_4H_4)$	
R266	$CH_4 + C_2$	$\rightarrow C_2H + CH_3$	$5.05 \times 10^{-11}e^{-297/T}$	Pitts et al. (1982)	300–600
R267	$CH_4 + C_2H$	$\rightarrow C_2H_2 + CH_3$	$1.2 \times 10^{-11}e^{-491/T}$	Opansky and Leone (1996a)	154–359
R268	$CH_4 + C_2H_3$	$\rightarrow C_2H_4 + CH_3$	$2.4 \times 10^{-24}T^{4.02}e^{-2754/T}$	Tsang and Hampson (1986)	300–2500
R269	$CH_4 + C_2H_5$	$\rightarrow C_2H_6 + CH_3$	$1.43 \times 10^{-25}T^{4.14}e^{-6322/T}$	♯	♯
R270	$CH_4 + C_3H_7$	$\rightarrow C_3H_8 + CH_3$	$4.0 \times 10^{-26}T^{4.02}e^{-5473/T}$	Tsang (1988)	300–2500
R271	$CH_4 + C_4H$	$\rightarrow C_4H_2 + CH_3$	$1.2 \times 10^{-11}e^{-491/T}$	Est. as $k(CH_4 + C_2H)$	
R272	$CH_4 + C_6H$	$\rightarrow C_6H_2 + CH_3$	$1.2 \times 10^{-11}e^{-491/T}$	♯	

Table 5 (*continued*)

Reaction			Rate	Reference	T (K)
R273	$CH_4 + C_6H_5$	$\rightarrow C_6H_6 + CH_3$	$3.32 \times 10^{-11}e^{-4328/T}$	Heckmann et al. (1996)	560–1410
R274	$C_2 + C_2H_2$	$\rightarrow 2\ C_2H$	4.3×10^{-10}	Reisler et al. (1980)	300
R275	$C_2 + C_2H_4$	$\rightarrow C_4H_3 + H$	3.26×10^{-10}	♯, Balucani et al. (2001)	♯
R276	$C_2 + C_2H_6$	$\rightarrow C_2H + C_2H_5$	3.0×10^{-10}	♯, Est.	♯
R277	$C_2 + CH_3C_2H$	$\rightarrow C_2H + C_3H_3$	4.74×10^{-10}	♯	♯
R278	$C_2 + CH_2CCH_2$	$\rightarrow C_2H + C_3H_3$	4.74×10^{-10}	♯	♯
R279	$C_2 + C_3H_8$	$\rightarrow C_2H + C_3H_7$	3.3×10^{-10}	♯	♯
R280	$C_2 + C_4H_{10}$	$\rightarrow C_2H + Products$	3.19×10^{-10}	Huang et al. (2004)	298
R281	$C_2 + C_6H_6$	$\rightarrow C_2H + C_6H_5$	5.2×10^{-10}	Reisler et al. (1980)	300
R282	$2\ C_2H$	$\rightarrow C_2H_2 + C_2$	3.0×10^{-12}	Tsang and Hampson (1986)	300–2500
R283	$C_2H + C_2H_2$	$\rightarrow C_4H_2 + H$	1.3×10^{-10}	Vakhtin et al. (2001a)	103
R284	$C_2H + C_2H_3$	$\rightarrow 2\ C_2H_2$	1.6×10^{-12}	Tsang and Hampson (1986)	300–2500
R285	$C_2H + C_2H_4$	$\rightarrow C_4H_4 + H$	1.4×10^{-10}	Vakhtin et al. (2001b)	103
R286	$C_2H + C_2H_5$	$\rightarrow C_2H_2 + C_2H_4$	3.0×10^{-12}	Tsang and Hampson (1986)	300–2500
R287	$C_2H + C_2H_5$	$\rightarrow C_3H_3 + CH_3$	3.0×10^{-11}	♯	♯
R288	$C_2H + C_2H_6$	$\rightarrow C_2H_2 + C_2H_5$	$5.1 \times 10^{-11}e^{-76/T}$	Murhpy et al. (2003)	96–800
R289	$C_2H + CH_3C_2H$	$\rightarrow C_4H_2 + CH_3$	$1.6 \times 10^{-10}e^{71/T}$	Hoobler and Leone (1999)	155–298
R290	$C_2H + CH_2CCH_2$	$\rightarrow C_2H_2 + C_3H_3$	$1.3 \times 10^{-10}e^{103/T}$	♯	♯
R291	$C_2H + C_3H_5$	$\rightarrow CH_2CCH_2 + C_2H_2$	1.2×10^{-11}	Tsang (1991)	300–2500
R292	$C_2H + C_3H_6$	$\rightarrow Products + H$	2.4×10^{-10}	Vakhtin et al. (2001b)	103
R293	$C_2H + C_3H_7$	$\rightarrow C_3H_3 + C_2H_5$	2.0×10^{-11}	Tsang (1988)	300–2500
R294	$C_2H + C_3H_7$	$\rightarrow C_3H_6 + C_2H_2$	1.0×10^{-11}	♯	♯
R295	$C_2H + C_3H_8$	$\rightarrow C_3H_7 + C_2H_2$	$9.8 \times 10^{-11}e^{-71/T}$	Murhpy et al. (2003)	96–297
R296	$C_2H + C_4H_2$	$\rightarrow C_6H_2 + H$	1.3×10^{-10}	Est. as $k(C_2H + C_2H_2)$	
R297	$C_2H + C_4H_6$	$\rightarrow C_6H_6 + H$	3.1×10^{-10}	Nizamov and Leone (2004)	104–296
R298	$C_2H + C_4H_8$	$\rightarrow Products$	2.6×10^{-10}	Laufer and Fahr (2004)	296
R299	$C_2H + C_4H_{10}$	$\rightarrow Products + C_2H_2$	$8.3 \times 10^{-11}e^{-112/T}$	Hoobler et al. (1997)	176–297
R300	$C_2H_2 + C_2H_3$	$\rightarrow C_4H_4 + H$	$3.32 \times 10^{-12}e^{-2516/T}$	Fahr and Stein (1989)	298–1330
R301	$C_2H_2 + C_2H_3 + M$	$\rightarrow C_4H_5 + M$	$k_0 = 1.54 \times 10^{-14}T^{-5.84}e^{-2364/T}$	Wang and Frenklach (1994)	500–2500
			$k_\infty = 4.16 \times 10^{-19}T^{1.9}e^{-1058/T}$	Weissman and Benson (1988)	300–1500
R302	$C_2H_2 + C_2H_5 + M$	$\rightarrow Products + M$	$k_0 = 3.3 \times 10^{-30}e^{-740/T}$	Est. as $k_0(H + C_2H_2)$	
			$k_\infty = 8.32 \times 10^{-14}e^{-3520/T}$	Kerr and Parsonage (1972)	373–473
R303	$C_2H_2 + C_3H_5 + M$	$\rightarrow Products + M$	$k_0 = 3.3 \times 10^{-30}e^{-740/T}$	Est. as $k_0(H + C_2H_2)$	
			$k_\infty = 5.3 \times 10^{-14}e^{-3500/T}$	Tsang (1991)	300 –2500
R304	$C_2H_2 + C_3H_7$	$\rightarrow C_2H_4 + C_3H_5$	$1.2 \times 10^{-12}e^{-4531/T}$	Tsang (1988)	300–2500
R305	$C_2H_2 + C_4H$	$\rightarrow C_6H_2 + H$	1.3×10^{-10}	Est. as $k(C_2H + C_2H_2)$	
R306	$C_2H_2 + {}^*C_4H_2$	$\rightarrow C_6H_2 + 2\ H$	3.5×10^{-13}	Seki et al. (1986) Est. as $k({}^*C_2H_2 + C_2H_2)$	
R307	$C_2H_2 + C_4H_3 + M$	$\rightarrow C_6H_5 + M$	$k_0 = 3.3 \times 10^{-30}e^{-740/T}$	Est. as $k_0(H + C_2H_2)$	
			$k_\infty = 5.53T^{-3.89}e^{-4635/T}$	Westmoreland et al. (1989)	400–1600
R308	$C_2H_2 + C_4H_5$	$\rightarrow C_6H_6 + H$	$3.16 \times 10^{-17}T^{1.47}e^{-2471/T}$	♯	♯
R309	$C_2H_2 + C_4H_5 + M$	$\rightarrow C_6H_7 + M$	$k_0 = 1.24 \times 10^{-21}T^{-3.28}e^{-5130/T}$	Wang and Frenklach (1994)	600–2500
		$\rightarrow C_6H_6 + H$	$k_\infty = 4.2 \times 10^{-19}T^{1.8}e^{-602/T}$	Weissman and Benson (1988)	300–1500
R310	$2\ C_2H_3$	$\rightarrow C_2H_2 + C_2H_4$	3.5×10^{-11}	Laufer and Fahr (2004)	298
R311	$2\ C_2H_3 + M$	$\rightarrow C_4H_6 + M$	$k_0 = 2.822 \times 10^{-3}T^{-8.749}e^{-985.4/T}$	Est. as $k_0(2\ CH_3 + M)$	
			$k_\infty = 9.5 \times 10^{-11}$	Laufer and Fahr (2004))	298
R312	$C_2H_3 + C_2H_4$	$\rightarrow C_4H_6 + H$	$8.3 \times 10^{-13}e^{-3676/T}$	Tsang and Hampson (1986)	300–2500
R313	$C_2H_3 + C_2H_5$	$\rightarrow C_2H_2 + C_2H_6$	8.0×10^{-13}	♯	♯
R314	$C_2H_3 + C_2H_5$	$\rightarrow 2\ C_2H_4$	8.0×10^{-13}	♯	♯
R315	$C_2H_3 + C_2H_5 + M$	$\rightarrow C_4H_8 + M$	$k_0 = 2.822 \times 10^{-3}T^{-8.749}e^{-985.4/T}$	Est. as $k_0(2\ CH_3 + M)$	
			$k_\infty = 6.5 \times 10^{-11}$	Laufer and Fahr (2004)	298
R316	$C_2H_3 + C_2H_6$	$\rightarrow C_2H_4 + C_2H_5$	$9.98 \times 10^{-22}T^{3.3}e^{-5285/T}$	Tsang and Hampson (1986)	300–2500
R317	$C_2H_3 + C_3H_3$	$\rightarrow CH_3C_2H + C_2H_2$	8.0×10^{-12}	Est. as $k(C_2H_3 + C_3H_5)$, Vuitton et al. (2006b)	
R318	$C_2H_3 + C_3H_3$	$\rightarrow Products$	$k_0 = 2.822 \times 10^{-3}T^{-8.749}e^{-985.4/T}$	Est. as $k_0(2\ CH_3 + M)$	
			$k_\infty = 8.0 \times 10^{-11}$	Est. as $k(C_2H_3 + C_3H_5)$, Vuitton et al. (2006b)	
R319	$C_2H_3 + C_3H_5$	$\rightarrow CH_2CCH_2 + C_2H_4$	4.0×10^{-12}	Tsang (1991)	300–2500
R320	$C_2H_3 + C_3H_5$	$\rightarrow C_3H_6 + C_2H_2$	8.0×10^{-12}	♯	♯
R321	$C_2H_3 + C_3H_5$	$\rightarrow Products$	$k_0 = 2.822 \times 10^{-3}T^{-8.749}e^{-985.4/T}$	Est. as $k_0(2\ CH_3 + M)$	

Table 5 (*continued*)

Reaction			Rate	Reference	T (K)
			$k_\infty = 8.0 \times 10^{-11}$	Tsang (1991)	300–2500
R322	$C_2H_3 + C_3H_6$	$\rightarrow C_4H_6 + CH_3$	$1.2 \times 10^{-12}e^{-2520/T}$	‡	‡
R323	$C_2H_3 + C_3H_6$	$\rightarrow C_3H_5 + C_2H_4$	$3.68 \times 10^{-24}T^{3.5}e^{-2356/T}$	‡	‡
R324	$C_2H_3 + C_3H_6$	$\rightarrow$ Products + H	$1.2 \times 10^{-12}e^{-3240/T}$	‡	‡
R325	$C_2H_3 + C_3H_7$	$\rightarrow C_3H_6 + C_2H_4$	2.0×10^{-12}	Tsang (1988)	300–2500
R326	$C_2H_3 + C_3H_7$	$\rightarrow C_3H_8 + C_2H_2$	2.0×10^{-12}	‡	‡
R327	$C_2H_3 + C_3H_7 + M$	$\rightarrow$ Adduct + M	$k_0 = 2.822 \times 10^{-3}T^{-8.749}e^{-985.4/T}$	Est. as $k_0(2\ CH_3 + M)$	
			$k_\infty = 1.6 \times 10^{-11}$	Tsang (1988)	300–2500
R328	$C_2H_3 + C_3H_8$	$\rightarrow C_3H_7 + C_2H_4$	$1.0 \times 10^{-21}T^{3.3}e^{-5285/T}$	‡	‡
R329	$C_2H_3 + C_4H_3$	$\rightarrow C_2H_4 + C_4H_2$	1.75×10^{-12}	Est. as $k(2C_2H_3)$	
R330	$C_2H_3 + C_4H_3$	$\rightarrow C_2H_2 + C_2H_4$	1.75×10^{-12}	‡	
R331	$C_2H_3 + C_4H_3 + M$	$\rightarrow C_6H_6 + M$	$k_0 = 1.646 \times 10^{-3}T^{-8.749}e^{-985.4/T}$	‡	
			$k_\infty = 9.5 \times 10^{-11}$	‡	
R332	$C_2H_3 + C_4H_4$	$\rightarrow C_6H_6 + H$	$1.23 \times 10^{-5}T^{-0.66}e^{4235/T}$	Wang and Frenklach (1997)	400–1600
R333	$C_2H_3 + C_4H_5$	$\rightarrow C_6H_6 + H_2$	$3.05 \times 10^{-37}T^{7.07}e^{1817/T}$	Westmoreland et al. (1989)	400–1600
R334	$C_2H_3 + C_4H_6 + M$	$\rightarrow$ Adduct + M	$k_0 = 2.822 \times 10^{-3}T^{-8.749}e^{-985.4/T}$	Est. as $k_0(2\ CH_3 + M)$	
			$k_\infty = 2.45 \times 10^{-12}T^{-0.17}e^{-1630/T}$	Westmoreland et al. (1989)	400–1600
R335	$C_2H_3 + C_4H_{10}$	$\rightarrow C_2H_4 + $ Product	$2.25 \times 10^{-24}T^{3.65}e^{-2600/T}$	Est. from Tsang (1990)	300–2500
R336	$C_2H_4 + C_2H_5$	$\rightarrow C_2H_6 + C_2H_3$	$1.0 \times 10^{-21}T^{3.13}e^{-9063/T}$	Tsang and Hampson (1986)	300–2500
R337	$C_2H_4 + C_2H_5 + M$	$\rightarrow$ Product + M	$k_0 = 7.7 \times 10^{-30}e^{-380/T}$	Est. as $k_0(H + C_2H_4 + M)$	
			$k_\infty = 6.6 \times 10^{-21}T^{2.44}e^{-2700/T}$	Knyazev and Slagle (1996)	298–1500
R338	$C_2H_4 + C_3H_5$	$\rightarrow$ Products + H	$1.0 \times 10^{-14}e^{-5776/T}$	Tsang (1991)	300–2500
R339	$C_2H_4 + C_3H_7 + M$	$\rightarrow$ Adduct + M	$k_0 = 7.7 \times 10^{-30}e^{-380/T}$	Est. as $k_0(H + C_2H_4 + M)$	
			$k_\infty = 3.24 \times 10^{-14}e^{-3070/T}$	Kerr and Parsonage (1972)	375–503
R340	$C_2H_4 + C_4H$	$\rightarrow C_4H_2 + C_2H_3$	1.4×10^{-10}	Est. as $k(C_2H + C_2H_4)$	
R341	$C_2H_4 + {}^*C_4H_2$	$\rightarrow C_6H_4 + H_2$	3.87×10^{-13}	Zwier and Allen (1996)	Relative to R306
R342	$C_2H_4 + {}^*C_4H_2$	$\rightarrow C_6H_5 + H$	1.03×10^{-13}	‡	‡
R343	$C_2H_4 + C_6H$	$\rightarrow C_6H_2 + C_2H_3$	1.4×10^{-10}	Est. as $k(C_2H + C_2H_4)$	
R344	$2\ C_2H_5$	$\rightarrow C_2H_6 + C_2H_4$	2.4×10^{-12}	Baulch et al. (1992)	300–1200
R345	$2\ C_2H_5 + M$	$\rightarrow C_4H_{10} + M$	$k_0 = 6.59 \times 10^{-6}T^{-6.39}e^{-301/T}$	Laufer et al. (1983)	100–300
			$k_\infty = 1.26 \times 10^{-11}e^{-96/T}$	Teng and Jones (1972)	303–603
R346	$C_2H_5 + C_3H_3$	$\rightarrow CH_3C_2H + C_2H_4$	$4.3 \times 10^{-12}e^{66/T}$	Est. as $k(C_2H_5 + C_3H_5)$, Vuitton et al. (2006b)	
R347	$C_2H_5 + C_3H_3 + M$	$\rightarrow$ Products + M	$k_0 = 2.822 \times 10^{-3}T^{-8.749}e^{-985.4/T}$	Est. as $k(2\ CH_3 + M)$	
			$k_\infty = 9.24 \times 10^{-11}$	Est. as $k(C_2H_5 + C_3H_5)$, Vuitton et al. (2006b)	
R348	$C_2H_5 + C_3H_5$	$\rightarrow CH_2CCH_2 + C_2H_6$	$1.6 \times 10^{-12}e^{66/T}$	Tsang (1991)	300–2500
R349	$C_2H_5 + C_3H_5$	$\rightarrow C_3H_6 + C_2H_4$	$4.3 \times 10^{-12}e^{66/T}$	‡	‡
R350	$C_2H_5 + C_3H_5 + M$	$\rightarrow$ Products + M	$k_0 = 2.822 \times 10^{-3}T^{-8.749}e^{-985.4/T}$	Est. as $k(2\ CH_3 + M)$	
			$k_\infty = 9.24 \times 10^{-11}$	Garland and Bayes (1990)	300
R351	$C_2H_5 + C_3H_6$	$\rightarrow C_2H_6 + C_3H_5$	$3.7 \times 10^{-24}T^{3.50}e^{-3340/T}$	Tsang (1991)	300–2500
R352	$C_2H_5 + C_3H_6 + M$	$\rightarrow$ Products + M	$k_0 = 7.7 \times 10^{-30}e^{-380/T}$	Est. as $k_0(H + C_2H_4 + M)$	
			$k_\infty = 1.69 \times 10^{-13}e^{-3620/T}$	Tsang (1991)	300–2500
R353	$C_2H_5 + C_3H_7$	$\rightarrow C_3H_6 + C_2H_6$	2.4×10^{-12}	Tsang (1988)	300–2500
R354	$C_2H_5 + C_3H_7$	$\rightarrow C_3H_8 + C_2H_4$	1.9×10^{-12}	‡	‡
R355	$C_2H_5 + C_3H_7$	$\rightarrow$ Products	$k_0 = 6.59 \times 10^{-6}T^{-6.39}e^{-301/T}$	Est. as $k_0(2\ C_2H_5 + M)$	
			$k_\infty = 3.3 \times 10^{-11}$	Tsang (1988)	300–2500
R356	$C_2H_5 + C_3H_8$	$\rightarrow C_2H_6 + C_3H_7$	$1.5 \times 10^{-24}T^{3.65}e^{-4600/T}$	‡	‡
R357	$C_2H_5 + C_4H_3$	$\rightarrow C_4H_2 + C_2H_6$	8.0×10^{-13}	Est. as $k(C_2H_3 + C_2H_5)$	
R358	$C_2H_5 + C_4H_3$	$\rightarrow C_4H_4 + C_2H_4$	8.0×10^{-13}	‡	
R359	$C_2H_5 + C_4H_3 + M$	$\rightarrow C_4H_8 + M$	$k_0 = 2.822 \times 10^{-3}T^{-8.749}e^{-985.4/T}$	Est. as $k_0(2\ CH_3 + M)$	
			$k_\infty = 6.5 \times 10^{-11}$	Est. as $k_\infty(C_2H_3 + C_2H_5 + M)$	
R360	$C_2H_5 + C_4H_4 + M$	$\rightarrow$ Products + M	$k_0 = 2.822 \times 10^{-3}T^{-8.749}e^{-985.4/T}$	Est. as $k_0(2\ CH_3 + M)$	
			$k_\infty = 6.8 \times 10^{-11}e^{-131/T}$	Est. as $k_\infty(CH_3 + C_3H_3 + M)$	
R361	$C_2H_5 + C_4H_8 + M$	$\rightarrow$ Products + M	$k_0 = 7.7 \times 10^{-30}e^{-380/T}$	Est. as $k_0(H + C_2H_4 + M)$	
			$k_\infty = 1.69 \times 10^{-13}e^{-3620/T}$	Est. as $k_\infty(C_2H_5 + C_3H_6 + M)$	
R362	$C_2H_5 + C_4H_{10}$	$\rightarrow C_2H_6 + $ Products	$1.5 \times 10^{-24}T^{3.65}e^{-4600/T}$	Est. as $k(C_2H_5 + C_3H_8)$	
R363	$C_2H_6 + C_3H_5$	$\rightarrow C_3H_6 + C_2H_5$	$3.9 \times 10^{-22}T^{3.30}e^{-9986/T}$	Tsang (1991)	300–2500

Table 5 (*continued*)

Reaction			Rate	Reference	T (K)
R364	$C_2H_6 + C_3H_7$	$\rightarrow C_3H_8 + C_2H_5$	$4.2 \times 10^{-25} T^{3.82} e^{-4550/T}$	Tsang (1988)	300–2500
R365	$C_2H_6 + C_4H$	$\rightarrow C_4H_2 + C_2H_5$	$5.1 \times 10^{-11} e^{-76/T}$	Est. as $k(C_2H + C_2H_6)$	
R366	$C_2H_6 + C_6H$	$\rightarrow C_6H_2 + C_2H_5$	$5.1 \times 10^{-11} e^{-76/T}$	Est. as $k(C_2H + C_2H_6)$	
R367	$2\,C_3H_3 + M$	$\rightarrow C_6H_6 + M$	$k_0 = 6.0 \times 10^{-28} e^{1680/T}$	Moses et al. (2000)	Est.
			$k_\infty = 1.2 \times 10^{-10}$	Morter et al. (1994)	298
R368	$C_3H_3 + C_3H_5$	$\rightarrow 2\,CH_2CCH_2$	$1.4 \times 10^{-13} e^{132/T}$	Est. as $k(2\,C_3H_5)$	
R369	$C_3H_3 + C_3H_5 + M$	$\rightarrow$ Product + M	$k_0 = 1.65 \times 10^{-4} T^{-8.75} e^{-985.4/T}$	♯	
			$k_\infty = 1.7 \times 10^{-11} e^{132/T}$	♯	
R370	$CH_3C_2H + {}^*C_4H_2$	$\rightarrow C_6H_2 + CH_3 + H$	2.43×10^{-13}	Zwier and Allen (1996)	Relative to R306
R371	$CH_3C_2H + {}^*C_4H_2$	$\rightarrow$ Products + H_2	1.67×10^{-13}	♯	♯
R372	$CH_3C_2H + {}^*C_4H_2$	$\rightarrow$ Products + C_2H_2	2.58×10^{-13}	♯	♯
R373	$CH_3C_2H + {}^*C_4H_2$	$\rightarrow$ Products + C_2H_3	9.12×10^{-14}	♯	♯
R374	$2\,C_3H_5$	$\rightarrow CH_2CCH_2 + C_3H_6$	$1.4 \times 10^{-13} e^{132/T}$	Tsang (1991)	300–2500
R375	$2\,C_3H_5 + M$	$\rightarrow$ Products + M	$k_0 = 2.822 \times 10^{-3} T^{-8.749} e^{-985.4/T}$	Est. as $k_0(2\,CH_3 + M)$	
			$k_\infty = 1.69 \times 10^{-11} e^{131/T}$	Tsang (1991)	300–2500
R376	$C_3H_5 + C_3H_6$	$\rightarrow$ Products + H	$1.0 \times 10^{-14} e^{-5776/T}$	♯	♯
R377	$C_3H_5 + C_3H_7$	$\rightarrow 2\,C_3H_6$	$2.4 \times 10^{-12} e^{66/T}$	♯	♯
R378	$C_3H_5 + C_3H_7$	$\rightarrow CH_2CCH_2 + C_3H_8$	$1.2 \times 10^{-12} e^{66/T}$	♯	♯
R379	$C_3H_5 + C_3H_7 + M$	$\rightarrow$ Product + M	$k_0 = 2.822 \times 10^{-3} T^{-8.749} e^{-985.4/T}$	Est. as $k_0(2\,CH_3 + M)$	
			$k_\infty = 3.4 \times 10^{-11} e^{66/T}$	Tsang (1991)	300–2500
R380	$C_3H_5 + C_3H_8$	$\rightarrow C_3H_6 + C_3H_7$	$3.9 \times 10^{-22} T^{3.3} e^{-9986/T}$	♯	♯
R381	$C_3H_6 + C_3H_7$	$\rightarrow C_3H_8 + C_3H_5$	$3.7 \times 10^{-24} T^{3.5} e^{-3340/T}$	♯	♯
R382	$C_3H_6 + {}^*C_4H_2$	$\rightarrow C_6H_4 + CH_3 + H$	3.94×10^{-13}	Zwier and Allen (1996)	Relative to R306
R383	$C_3H_6 + {}^*C_4H_2$	$\rightarrow$ Products + H_2	1.71×10^{-13}	♯	♯
R384	$C_3H_6 + {}^*C_4H_2$	$\rightarrow$ Products + C_2H_2	2.4×10^{-13}	♯	♯
R385	$C_3H_6 + {}^*C_4H_2$	$\rightarrow$ Products + C_2H_3	5.1×10^{-14}	♯	♯
R386	$2\,C_3H_7$	$\rightarrow C_3H_8 + C_3H_6$	2.8×10^{-12}	Tsang (1988)	300–2500
R387	$2\,C_3H_7 + M$	$\rightarrow$ Product + M	$k_0 = 2.822 \times 10^{-3} T^{-8.749} e^{-985.4/T}$	Est. as $k_0(2\,CH_3 + M)$	
			$k_\infty = 1.7 \times 10^{-11}$	Tsang (1988)	300–2500
R388	${}^*C_4H_2$	$\rightarrow C_4H_2$	10	Vuitton et al. (2003)	11–40
R389	${}^*C_4H_2 + N_2$	$\rightarrow C_4H_2 + N_2$	1.4×10^{-15}	Zwier and Allen (1996)	Relative to R306
R390	${}^*C_4H_2 + C_4H_2$	$\rightarrow C_6H_2 + C_2H_2$	8.58×10^{-13}	♯	♯
R391	${}^*C_4H_2 + C_4H_2$	$\rightarrow$ Products + 2H	1.59×10^{-12}	♯	♯
R392	${}^*C_4H_2 + C_4H_6$	$\rightarrow C_6H_6 + C_2H_2$	1.48×10^{-12}	Arrington et al. (1998)	Relative to R306
R393	${}^*C_4H_2 + C_4H_6$	$\rightarrow$ Products + 2 H	1.48×10^{-12}	♯	♯
R394	$2\,C_4H_4 + M$	$\rightarrow$ Product + M	$k_0 = 2.822 \times 10^{-3} T^{-8.749} e^{-985.4/T}$	Est. as $k_0(2\,CH_3 + M)$	
			$k_\infty = 7.25 \times 10^{-14} e^{-9261/T}$	Lungard and Heicklen (1984)	573–723
Nitriles					
R395	$N_2^+ + e^-$	$\rightarrow 2\,N$	$3.5 \times 10^{-7} (300/T_e)^{0.5}$	Keller et al. (1992)	$T_e \sim$ 1200 K
R396	$N_2^+ + N$	$\rightarrow N^+ + N_2$	1.0×10^{-11}	McEwan and Phillips (1975)	Upper Limit
R397	$N_2^+ + CH_4$	$\rightarrow CH_3 + N_2 + H + e^-$	1.0×10^{-9}	Est. based on Keller et al. (1992)	
R398	$N^+ + e^-$	$\rightarrow N$	$3.5 \times 10^{-12} (300/T_e)^{0.7}$	Keller et al. (1992)	$T_e \sim$ 1200 K
R399	$N^+ + NH$	$\rightarrow N_2^+ + H$	3.7×10^{-10}	♯	♯
R400	$N^+ + CH_4$	$\rightarrow CH_3 + NH + e^-$	5.0×10^{-10}	Est. based on Keller et al. (1992)	
R401	$N^+ + CH_4$	$\rightarrow H_2CN + H_2 + e^-$	5.0×10^{-10}	♯	
R402	$N(^2D)$	$\rightarrow N$	2.3×10^{-5}	Okabe (1978)	
R403	$N(^2D) + e^-$	$\rightarrow N + e^-$	$6.0 \times 10^{-10} (300/T_e)^{-0.5}$	Frederick and Rusch (1977)	$T_e \sim$ 1200 K
R404	$N(^2D) + NH_3$	$\rightarrow NH + NH_2$	5.0×10^{-11}	Herron (1999)	298
R405	$N(^2D) + N_2$	$\rightarrow N + N_2$	1.7×10^{-14}	♯	♯
R406	$N(^2D) + H_2$	$\rightarrow NH + H$	$4.2 \times 10^{-11} e^{-880/T}$	♯	200–300
R407	$N(^2D) + CH_4$	$\rightarrow NH + CH_3$	$9.6 \times 10^{-12} e^{-750/T}$	♯	232–292
R408	$N(^2D) + CH_4$	$\rightarrow CH_2NH + H$	$3.84 \times 10^{-11} e^{-750/T}$	♯	232–292
R409	$N(^2D) + C_2H_2$	$\rightarrow CHCN + H$	$1.6 \times 10^{-10} e^{-270/T}$	♯	220–300
R410	$N(^2D) + C_2H_4$	$\rightarrow CH_3CN + H$	$2.3 \times 10^{-10} e^{-503/T}$	Sato et al. (1999)	225–292
R411	$N(^2D) + C_2H_6$	$\rightarrow C_2H_5N$	1.9×10^{-11}	Herron (1999)	298

Table 5 (*continued*)

Reaction			Rate	Reference	T (K)
R412	$N(^2D) + CH_3C_2H$	$\rightarrow C_2H_3CN + H$	$1.6 \times 10^{-10}e^{-270/T}$	Est. as $k(N(^2D) + C_2H_2)$	
R413	$N(^2D) + C_3H_6$	$\rightarrow$ Product + H	$2.3 \times 10^{-10}e^{-503/T}$	Est. as $k(N(^2D) + C_2H_4)$	
R414	$N(^2D) + C_3H_8$	$\rightarrow$ Product + H	2.9×10^{-11}	Herron (1999)	298
R415	$N(^2D) + C_4H_2$	$\rightarrow$ Product + H	$1.6 \times 10^{-10}e^{-270/T}$	Est. as $k(N(^2D) + C_2H_2)$	
R416	$N(^2D) + C_4H_8$	$\rightarrow$ Product + H	$2.3 \times 10^{-10}e^{-503/T}$	Est. as $k(N(^2D) + C_2H_4)$	
R417	$N(^2D) + C_4H_{10}$	$\rightarrow$ Product + H	3.1×10^{-11}	Herron (1999)	298
R418	$N(^2D) + CH_2NH$	$\rightarrow$ Products	$2.3 \times 10^{-10}e^{-503/T}$	Est. as $k(N(^2D) + C_2H_4)$	
R419	$2 N + M$	$\rightarrow N_2 + M$	$k_0 = 1.78 \times 10^{-33}e^{483/T}$	Clyne and Stedman (1967)	90–611
			$k_\infty = 5.0 \times 10^{-16}$	Takahashi and Miyazaki (1977)	298
R420	$N + H + M$	$\rightarrow NH + M$	$k_0 = 5.0 \times 10^{-32}$	Brown (1973)	♯
R421	$N + H_2 + M$	$\rightarrow NH_2 + M$	$k_0 = 1.0 \times 10^{-36}$	Petrishchev and YuSapozhkov (1981)	♯
			$k_\infty = 1.94 \times 10^{-20}$	Aleksandrov et al. (1994)	♯
R422	$N + C + M$	$\rightarrow CN + M$	$k_0 = 9.41 \times 10^{-33}$	Kley et al. (1974)	♯
R423	$N + CH$	$\rightarrow CN + H$	$2.67 \times 10^{-10}T^{-0.09}$	Brownsword et al. (1996)	216–584
R424	$N + CH_3$	$\rightarrow H_2CN + H$	5.76×10^{-11}	♯	♯
R425	$N + CH_3$	$\rightarrow HCN + H_2$	5.76×10^{-12}	Marston et al. (1989)	200
R426	$N + C_2H_3$	$\rightarrow CH_3CN$	3.1×10^{-12}	Payne et al. (1996)	298
R427	$N + C_2H_3$	$\rightarrow C_2H_2 + NH$	1.23×10^{-11}	♯	♯
R428	$N + C_2H_3$	$\rightarrow$ Products	6.16×10^{-11}	♯	♯
R429	$N + C_2H_4$	$\rightarrow HCN + CH_3$	$3.32 \times 10^{-14}e^{-352/T}$	Kerr and Parsonage (1972)	291–600
R430	$N + C_2H_5$	$\rightarrow C_2H_4 + NH$	7.1×10^{-11}	Stief et al. (1995)	298
R431	$N + C_2H_5$	$\rightarrow H_2CN + CH_3$	3.9×10^{-11}	♯	♯
R432	$N + C_2H_6$	$\rightarrow C_2H_5N + H$	4.0×10^{-16}	Aleksandrov et al. (1990)	253
R433	$N + CH_3C_2H$	$\rightarrow CHCN + CH_3$	$1.15 \times 10^{-13}e^{-745/T}$	Kerr and Parsonage (1972)	320–550
R434	$N + C_3H_6$	$\rightarrow C_2H_4 + HCN + H$	$1.94 \times 10^{-13}e^{-654/T}$	♯	338–697
R435	$N + C_3H_8$	$\rightarrow C_2H_6 + HCN + H$	$3.39 \times 10^{-13}e^{-2561/T}$	Onyszchuk et al. (1953)	336–523
R436	$N + C_4H_6$	$\rightarrow CH_3C_2H + HCN + H$	$3.09 \times 10^{-13}e^{-926/T}$	Kerr and Parsonage (1972)	320–550
R437	$N + C_4H_8$	$\rightarrow$ Products	$2.57 \times 10^{-13}e^{-659/T}$	♯	♯
R438	$N + C_4H_{10}$	$\rightarrow C_3H_8 + HCN + H$	$2.97 \times 10^{-14}e^{-1812/T}$	Back and Winkler (1954)	348–523
R439	$N + NH$	$\rightarrow N_2 + H$	2.49×10^{-11}	Hack et al. (1994)	298
R440	$N + NH_2$	$\rightarrow 2 NH$	1.15×10^{-10}	Dransfeld and Wagner (1987)	♯
R441	$N + CN$	$\rightarrow N_2 + C$	$3.24 \times 10^{-13}e^{-1771/T}$	Atakan and Wolfrum (1992)	298–534
R442	$N + H_2CN$	$\rightarrow HCN + NH$	$1.0 \times 10^{-10}e^{-200/T}$	Nesbitt et al. (1990)	200–363
R443	$N + CH_2NH$	$\rightarrow H_2CN + NH$	$3.32 \times 10^{-14}e^{-352/T}$	Est. as $k(N + C_2H_4)$	
R444	$N + C_2N$	$\rightarrow 2 CN$	1.0×10^{-10}	Whyte and Phillips (1983)	300
R445	$N + CHCN$	$\rightarrow C_2N_2 + H$	1.0×10^{-12}	Yung (1987)	
R446	$NH + H$	$\rightarrow N + H_2$	$3.12 \times 10^{-12}T^{1.55}e^{-103.2/T}$	Adam et al. (2005)	300–2000
R447	$2 NH$	$\rightarrow NH_2 + N$	$9.9 \times 10^{-22}T^{2.89}e^{1021.5/T}$	Zu et al. (1997)	297
R448	$2 NH + M$	$\rightarrow N_2 + 2 H + M$	$k_0 = 1.0 \times 10^{-33}$	Yung et al. (1984)	Est.
			$k_\infty = 3.49 \times 10^{-12}$	Nicholas et al. (1986)	298
R449	$NH + CH_3$	$\rightarrow CH_2NH + H$	1.0×10^{-11}	Est.	
R450	$NH + CH_4$	$\rightarrow NH_2 + CH_3$	2.11×10^{-24}	Xu et al. (1999)	300
R451	$NH + C_2H_2$	$\rightarrow CHCN + H_2$	$2.01 \times 10^{-9}T^{-1.07}$	Mullen and Smith (2005)	53–188
R452	$NH + C_2H_4$	$\rightarrow CH_3CN + H_2$	$1.15 \times 10^{-9}T^{-1.09}$	♯	♯
R453	$NH + C_2H_6$	$\rightarrow NH_2 + C_2H_5$	1.41×10^{-23}	Xu et al. (1999)	300
R454	$NH + C_3H_6$	$\rightarrow$ Products	$6.24 \times 10^{-9}T^{-1.27}$	Mullen and Smith (2005)	53–188
R455	$NH + C_4H_2$	$\rightarrow$ Products	$8.24 \times 10^{-9}T^{-1.23}$	♯	♯
R456	$NH + NH_3 + M$	$\rightarrow N_2H_4 + M$	$k_0 = 5.02 \times 10^{-35}$	Zetzsch and Stuhl (1981)	298
			$k_\infty = 1.08 \times 10^{-12}e^{820/T}$	Mantei and Bair (1968)	300–345
R457	$NH_2 + H + M$	$\rightarrow NH_3 + M$	$k_0 = 3.0 \times 10^{-30}$	Schofield (1973)	298
			$k_\infty = 2.66 \times 10^{-11}$	Pagsberg et al. (1979)	348
R458	$NH_2 + H_2$	$\rightarrow NH_3 + H$	$4.89 \times 10^{-25}T^{3.89}e^{-1399/T}$	Garrett et al. (1990)	200–2400
R459	$NH_2 + CH_4$	$\rightarrow NH_3 + CH_3$	$5.11 \times 10^{-23}T^{3.59}e^{-4540/T}$	Mebel and Lin (1999)	300–2000
R460	$2 NH_2$	$\rightarrow NH_3 + NH$	$2.26 \times 10^{-21}T^{2.79}e^{-664/T}$	Xu et al. (1998)	300–1800
R461	$2 NH_2 + M$	$\rightarrow N_2H_4 + M$	$k_0 = 8.97 \times 10^{-20}T^{-3.9}$	Fagerstrom et al. (1995)	200–400
			$k_\infty = 2.5 \times 10^{-11}T^{0.27}$	♯	♯

Table 5 (*continued*)

Reaction			Rate	Reference	T (K)
R462	$NH_2 + CH_3 + M$	$\rightarrow CH_3NH_2 + M$	$k_0 = 6.0 \times 10^{-18} T^{-3.85}$	Jodkowski et al. (1995)	200–400
			$k_\infty = 1.2 \times 10^{-11} T^{0.42}$	♯	
R463	$NH_3 + H$	$\rightarrow NH_2 + H_2$	$1.14 \times 10^{-23} T^{3.87} e^{-3920/T}$	Garrett et al. (1990)	200–2400
R464	$NH_3 + CH$	$\rightarrow CH_2NH + H$	$4.11 \times 10^{-9} T^{-0.56} e^{-3/T}$	Bocherel et al. (1996)	23–296
R465	$NH_3 + CN$	$\rightarrow NH_2 + HCN$	$1.83 \times 10^{-8} T^{-1.14}$	Sims et al. (1994)	25–295
R466	$N_2 + CH + M$	$\rightarrow Product + M$	$k_0 = 3.86 \times 10^{-25} T^{-2.6}$	Fulle and Hippler (1996)	200–715
			$k_\infty = 9.65 \times 10^{-11} T^{-0.15}$	♯	
R467	$N_2H_3 + H$	$\rightarrow 2 NH_2$	2.66×10^{-12}	von Gehring et al. (1971)	300
R468	$2 N_2H_3$	$\rightarrow N_2H_4 + N_2 + H_2$	1.84×10^{-11}	Stief (1970)	298
R469	$2 N_2H_3$	$\rightarrow 2 NH_3 + N_2$	4.98×10^{-12}	Schiavello and Volpi (1962)	423
R470	$N_2H_4 + H$	$\rightarrow N_2H_3 + H_2$	$1.17 \times 10^{-11} e^{-1260/T}$	Vaghjiani (1995)	222–657
R471	$CN + H + M$	$\rightarrow HCN + M$	$k_0 = 2.39 \times 10^{-24} T^{-2.2} e^{-569/T}$	Tsang (1992)	500–2500
			$k_\infty = 2.99 \times 10^{-9} T^{-0.5}$	♯	♯
R472	$CN + H_2$	$\rightarrow HCN + H$	$2.23 \times 10^{-21} T^{3.31} e^{-756/T}$	Sun et al. (1990)	209–740
R473	$CN + CH_4$	$\rightarrow HCN + CH_3$	$5.73 \times 10^{-12} e^{-674/T}$	Sims et al. (1993)	160–298
R474	$CN + C_2H_2$	$\rightarrow HC_3N + H$	$5.26 \times 10^{-9} T^{-0.52} e^{-20/T}$	♯, Huang et al. (1999)	25–298
R475	$CN + C_2H_4$	$\rightarrow C_2H_3CN + H$	$1.36 \times 10^{-8} T^{-0.69} e^{-30/T}$	♯, Balucani et al. (2000)	♯
R476	$CN + C_2H_6$	$\rightarrow HCN + C_2H_5$	$5.91 \times 10^{-12} T^{0.22} e^{58/T}$	♯	♯
R477	$CN + CH_3C_2H$	$\rightarrow Products + H$	4.1×10^{-10}	Carty et al. (2001)	15–298
R478	$CN + CH_2CCH_2$	$\rightarrow Products + H$	4.1×10^{-10}	♯	♯
R479	$CN + C_3H_6$	$\rightarrow Products + H$	$1.73 \times 10^{-10} e^{101/T}$	Sims et al. (1993)	160–298
R480	$CN + C_3H_8$	$\rightarrow HCN + C_3H_7$	$3.58 \times 10^{-15} T^{1.14} e^{284/T}$	Hess et al. (1989)	298–736
R481	$CN + C_4H_2$	$\rightarrow Products + H$	4.2×10^{-10}	Seki et al. (1996)	298
R482	$CN + C_4H_4$	$\rightarrow Products + H$	$1.07 \times 10^{-7} T^{-0.82} e^{-228/T}$	Yang et al. (1992b)	174–740
R483	$CN + C_4H_6$	$\rightarrow Products + H$	$2.57 \times 10^{-10} e^{-171/T}$	Butterfield et al. (1993)	297–740
R484	$CN + C_6H_6$	$\rightarrow Products + H$	2.82×10^{-10}	Balucani et al. (1999)	297–740
R485	$2 CN + M$	$\rightarrow C_2N_2 + M$	$k_0 = 9.41 \times 10^{-23} T^{-2.61}$	Tsang (1992)	500–2500
			$k_\infty = 9.4 \times 10^{-12}$	♯	♯
R486	$CN + HCN$	$\rightarrow C_2N_2 + H$	$2.5 \times 10^{-17} T^{1.71} e^{-770/T}$	Yang et al. (1992a)	297–740
R487	$CN + CH_2NH$	$\rightarrow HCN + H_2CN$	$6.71 \times 10^{-11} e^{-412/T}$	Est. as $k(CN + CH_2O)$, Chang and Wang (1994)	
R488	$CN + CH_3CN$	$\rightarrow C_2N_2 + CH_3$	$6.46 \times 10^{-11} e^{-1190/T}$	Zabarnick and Lin (1989)	296–578
R489	$CN + HC_3N$	$\rightarrow C_4N_2 + H$	1.7×10^{-11}	Halpern et al. (1989)	298
R490	$CN + C_4N_2$	$\rightarrow C_2N_2 + C_3N$	$k_0 = 9.41 \times 10^{-23} T^{-2.61}$	Est. as $k_0(2 CN + M)$	
			$k_\infty = 5.4 \times 10^{-13}$	Seki et al. (1996)	298
			$k = k_\infty - k(p)$		
R491	$HCN + H + M$	$\rightarrow H_2CN + M$	$k_0 = 4.4 \times 10^{-24} T^{-2.73} e^{-3860/T}$	Tsang and Herron (1991)	300–2500
			$k_\infty = 5.5 \times 10^{-11} e^{-2438/T}$	♯	♯
R492	$HCN + CH$	$\rightarrow CHCN + H$	$5.0 \times 10^{-11} e^{498/T}$	Zabarnick and in	296–674
R493	$HCN + C_2H$	$\rightarrow HC_3N + H$	$5.26 \times 10^{-12} e^{-770/T}$	Hoobler and Leone (1997)	297–360
R494	$HCN + C_2H_3$	$\rightarrow C_2H_3CN + H$	$1.1 \times 10^{-12} e^{-900/T}$	Monks et al. (1993)	298
R495	$HCN + C_3N$	$\rightarrow C_4N_2 + H$	3.0×10^{-11}	Petrie and Osamura (2004)	298
R496	$H_2CN + H$	$\rightarrow HCN + H_2$	7.0×10^{-11}	Nesbitt et al. (1990)	lower limit, 298
R497	$2 H_2CN + M$	$\rightarrow Product + M$	$k_0 = 9.41 \times 10^{-23} T^{-2.61}$	Est. as $k_0(2 CN + M)$	
			$k_\infty = 2.57 \times 10^{-12}$	Nizamov and Dagdigian (2003)	
R498	$2 H_2CN$	$\rightarrow HCN + CH_2NH$	5.13×10^{-12}	Horne and Norrish (1970)	
R499	$CH_2NH + H$	$\rightarrow H_2 + H_2CN$	4.0×10^{-14}	Est. as $k(H + CH_2O)$, Dobe et al. (1994)	
R500	$CH_2NH + C_2H$	$\rightarrow Products + H$	1.4×10^{-10}	Est. as $k(C_2H_4 + C_2H)$	
R501	$C_2N + CH_4$	$\rightarrow CHCN + CH_3$	6.0×10^{-14}	Zhu et al. (2003)	298
R502	$C_2N + C_2H_6$	$\rightarrow CHCN + C_2H_5$	2.9×10^{-12}	♯	♯
R503	$C_2N + C_3H_8$	$\rightarrow CHCN + C_3H_7$	1.9×10^{-11}	♯	♯
R504	$C_2N + C_4H_{10}$	$\rightarrow CHCN + Products$	4.2×10^{-11}	♯	♯
R505	$2 CHCN$	$\rightarrow C_4N_4 + H_2$	5.0×10^{-11}	Yung (1987)	Est.
R506	$CH_3CN + H$	$\rightarrow HCN + CH_3$	$3.39 \times 10^{-12} e^{-3950/T}$	Jamieson et al. (1970)	313–780
R507	$CH_3CN + H$	$\rightarrow CN + CH_4$	$1.66 \times 10^{-13} e^{-1500/T}$	♯	♯

Table 5 (*continued*)

Reaction			Rate	Reference	T (K)
R508	$CH_3CN + C_2H$	$\rightarrow HC_3N + CH_3$	$1.79 \times 10^{-11}e^{-770/T}$	Hoobler and Leone (1997)	262–360
R509	$C_3N + H + M$	$\rightarrow HC_3N + M$	$k_0 = 1.26 \times 10^{-18}T^{-3.1}e^{-721/T}$	Est. as $k_0(H + C_2H + M)$	
			$k_\infty = 3.0 \times 10^{-10}$	‡	
R510	$C_3N + H_2$	$\rightarrow HC_3N + H$	$1.2 \times 10^{-11}e^{-998/T}$	Est. as $k(C_2H + H_2)$	
R511	$C_3N + CH_4$	$\rightarrow HC_3N + CH_3$	$1.11 \times 10^{-10}e^{-998/T}$	Clarke and Ferris (1995)	Relative to R510
R512	$C_3N + C_2H_2$	$\rightarrow Products + H$	1.3×10^{-10}	Est. as $k(C_2H + C_2H_2)$	
R513	$C_3N + C_2H_4$	$\rightarrow Products + H$	1.4×10^{-10}	Est. as $k(C_2H + C_2H_4)$	
R514	$C_3N + C_2H_6$	$\rightarrow HC_3N + C_2H_5$	$7.56 \times 10^{-10}e^{-998/T}$	Clarke and Ferris (1995)	Relative to R510
R515	$C_3N + C_3H_8$	$\rightarrow HC_3N + C_3H_7$	$7.56 \times 10^{-10}e^{-998/T}$	Est. as $k(C_3N + C_2H_6)$	
R516	$C_3N + C_4H_2$	$\rightarrow Products + H$	1.3×10^{-10}	Est. as $k(C_2H + C_4H_2)$	
R517	$C_3N + C_4H_{10}$	$\rightarrow HC_3N + Products$	$7.56 \times 10^{-10}e^{-998/T}$	Est. as $k(C_3N + C_2H_6)$	
R518	$HC_3N + H + M$	$\rightarrow H_2C_3N + M$	$k_0 = 1.0 \times 10^{-27}e^{-740/T}$	Est. based on Parker et al. (2004)	
			$k_\infty = 1.1 \times 10^{-12}e^{-500/T}$	Parker et al. (2004)	200–298
R519	$HC_3N + CH_3 + M$	$\rightarrow Product + M$	$k_0 = 3.3 \times 10^{-28}e^{-740/T}$	Est. as $k(CH_3 + C_2H_2)$	
			$k_\infty = 1.1 \times 10^{-12}e^{-3880/T}$	‡	
R520	$H_2C_3N + H$	$\rightarrow C_2H_2 + HCN$	$6.86 \times 10^{-11}e^{23/T}$	Est. as $k(H + C_2H_3)$	
R521	$C_2H_3CN + C_2$	$\rightarrow C_2H_3 + C_3N$	4.4×10^{-10}	Reisler et al. (1980)	300
R522	$C_2H_3CN + C_2H_5$	$\rightarrow Products$	$1.02 \times 10^{-13}e^{-1710/T}$	Kerr and Parsonage (1972)	323–454
R523	$C_2N_2 + C$	$\rightarrow C_2N + CN$	3.0×10^{-11}	Whyte and Phillips (1983)	300
R524	$C_4N_2 + C_2H$	$\rightarrow Products + CN$	1.3×10^{-10}	Est. as $k(C_2H + C_2H_2)$	

procedure applied is adequate. Nevertheless, the high accuracy measurements provided by the Cassini/Huygens mission require the use of accurate and realistic laboratory measurements which will constrain better the photochemistry and allow a safer interpretation of the haze production processes. A short description of the main pathways which lead to the formation of the most important hydrocarbons and nitriles in Titan's atmosphere is given here, while a discussion for some of the reaction rates used is given in Paper II along with the model results.

2.4. Hydrocarbons

The most abundant hydrocarbon found in Titan's atmosphere after methane, is ethane (C_2H_6) which is mainly produced in the collisional addition of two methyl radicals:

$$2\ CH_3 + M \rightarrow C_2H_6 + M.$$
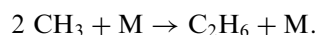
The chemical destruction of methane molecules by the methylene radicals enhances the production of methyl radicals and hence the total ethane production:

$$^1CH_2 + CH_4 \rightarrow 2\ CH_3.$$

Because ethane's absorption cross section falls in the same wavelength region as that of methane, its photolysis is constrained by the high amounts of the latter. Hence its destruction is mainly due to chemical reactions with radicals, from which the most important are with excited methylene:
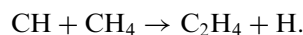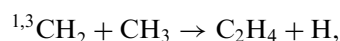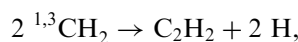
$$^1CH_2 + C_2H_6 \rightarrow CH_3 + C_2H_5$$
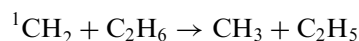
and ethynyl (C_2H) that is produced in the photolysis of acetylene (C_2H_2):

$$C_2H_2 + hv \rightarrow C_2H + H,$$
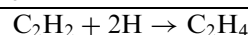
$$C_2H + C_2H_6 \rightarrow C_2H_2 + C_2H_5.$$
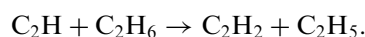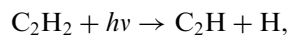
Acetylene and ethylene (C_2H_4) are the next most abundant hydrocarbons after ethane and their formation is initiated in the upper atmosphere directly from the products of methane photolysis:

$$2\ ^{1,3}CH_2 \rightarrow C_2H_2 + 2\ H,$$

$$^{1,3}CH_2 + CH_3 \rightarrow C_2H_4 + H,$$

$$CH + CH_4 \rightarrow C_2H_4 + H.$$

Destruction of ethylene through photolysis, acts as the major source of acetylene in the upper atmosphere:

$$C_2H_4 + hv \rightarrow C_2H_2 + 2H/H_2$$
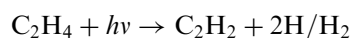
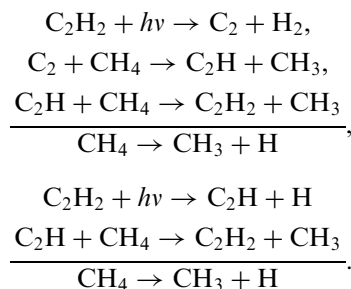while in the lower atmosphere acetylene recycles back to ethylene through the vinyl radical (C_2H_3) according to the following scheme:

$$\begin{array}{c} C_2H_2 + H + M \rightarrow C_2H_3 + M \\ \underline{C_2H_3 + H + M \rightarrow C_2H_4 + M} \\ C_2H_2 + 2H \rightarrow C_2H_4 \end{array}.$$

The main loss of acetylene in the upper atmosphere is from reaction with methylene which leads to the formation of propargyl radicals (C_3H_3):

$$^1CH_2 + C_2H_2 \rightarrow C_3H_3 + H$$
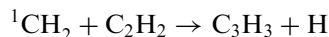
while in the lower atmosphere the main loss is due to photolysis. Acetylene's cross section extends well beyond methane's dissociation limit, up to $\sim$230 nm and due to its high concentration, it is the main absorber in this part of the spectrum (along with the haze). This means that its photolysis rate retains high values even down to the stratosphere (Fig. 4). Hence there is a significant production of the radicals formed (C_2 and C_2H) in acetylene's photolysis in this region, which, as in the case of ethane discussed above, lead to the catalytic destruction of saturated hydrocarbons through hydrogen abstraction. The effect of this mechanism has its highest impact on methane due to its high concentration in Titan's atmosphere:

$$\frac{\begin{array}{l} C_2H_2 + hv \rightarrow C_2 + H_2, \\ C_2 + CH_4 \rightarrow C_2H + CH_3, \\ C_2H + CH_4 \rightarrow C_2H_2 + CH_3 \end{array}}{CH_4 \rightarrow CH_3 + H},$$

$$\frac{\begin{array}{l} C_2H_2 + hv \rightarrow C_2H + H \\ C_2H + CH_4 \rightarrow C_2H_2 + CH_3 \end{array}}{CH_4 \rightarrow CH_3 + H}.$$

As was shown by previous photochemical models, the overall destruction of methane is dominated by its catalytic destruction by radicals with the above two schemes along with the loss due to excited methylene radicals, having the strongest contribution. The photolysis of methane corresponds only to $\sim$10% of the total loss, based on our calculations, but is of course the driving force for the initialization of the photochemistry. The three molecules described above (C_2H_6, C_2H_4, C_2H_2) along with molecular hydrogen correspond to the most abundant hydrocarbons observed in Titan's atmosphere since the Voyager missions (Coustenis et al., 1989 and references therein). From these, more complex species are produced leading finally to the formation of the haze precursors.

Methylacetylene (CH_3C_2H) and its isomer, allene (CH_2CCH_2), are formed initially in the upper atmosphere through the reaction of CH with ethylene:

$$CH + C_2H_4 \rightarrow (CH_2CCH_2, CH_3C_2H) + H$$
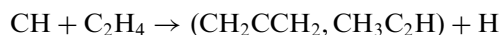
while the isomerization between the two species is balanced through:

$$H + CH_2CCH_2 \rightarrow CH_3C_2H + H.$$
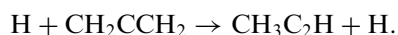
Similarly, propylene (C_3H_6) is produced in the upper atmosphere from ethane with the replacement of H by CH:

$$CH + C_2H_6 \rightarrow C_3H_6 + H$$
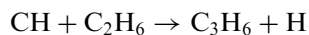
while in the lower atmosphere where the C_2H_3 population is significant, there is a secondary production through the collisional addition of CH_3:
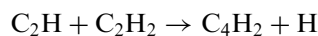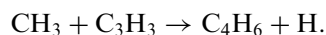
$$CH_3 + C_2H_3 + M \rightarrow C_3H_6 + M.$$

In the same way, propane (C_3H_8) is formed in the collisional addition of methyl to ethyl radicals (C_2H_5):
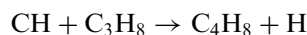
$$CH_3 + C_2H_5 + M \rightarrow C_3H_8 + M.$$

The production of four-C hydrocarbons, starts with the first step of acetylene's polymerization through ethyl radical addition, giving diacetylene (C_4H_2):

$$C_2H + C_2H_2 \rightarrow C_4H_2 + H$$

while the 1,3-butadiene (C_4H_6) is formed by

$$CH_3 + C_3H_3 \rightarrow C_4H_6 + H.$$

1-butene (C_4H_8) is formed in the upper atmosphere through the CH replacement of H in propane:

$$CH + C_3H_8 \rightarrow C_4H_8 + H$$

and in the lower atmosphere through the collisional addition of C_2H_3 with C_2H_5:

$$C_2H_3 + C_2H_5 + M \rightarrow C_4H_8 + M.$$

The different isomers of the last species have not been included in the calculations and we consider that they are finally isomerized to their stable structures considered above. The loss of these species is dominated by their photolysis which recycles them back to their precursors, constraining in this way their net production to small values.

Due to the lack of data regarding the reaction rates and photolysis properties of five-C species, the only one included is C_5H_3, since it is a direct product of benzene (C_6H_6) photolysis. The latter has been included in the photochemical model, based on the work of Wilson et al. (2003) and Lebonnois (2005) which have investigated its possible formation pathways in Titan's atmosphere. We did not include any linear isomers of benzene in the calculations since we consider that they will finally isomerize to their cyclic forms as was suggested by Lebonnois (2005), but also because the reaction rates of benzene formation correspond to high temperatures and the extrapolation of different measurements to Titan's conditions could lead to significantly different profiles. Hence, since the production is not well defined we believe that the inclusion of more complicated schemes would not provide any safer estimation of the final benzene profile. The main production pathway is the addition of two propargyl radicals under high pressure:

$$2\,C_3H_3 + M \rightarrow C_6H_6 + M.$$
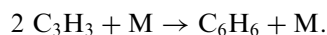
A secondary contribution comes from

$$C_2H_2 + C_4H_5 + M \rightarrow C_6H_7 + M \rightarrow C_6H_6 + H,$$

where the produced C_6H_7 is considered to provide eventually benzene (Lebonnois, 2005). Finally a small contribution originates from the hydrogen addition on the

phenyl radical (C_6H_5):

$$H + C_6H_5 + M \rightarrow C_6H_6 + M$$

with the chemical formation of the last based on diacetylene (there is also a strong production of phenyl from the photolysis of benzene but this does not contribute to the net production):

$$H + C_4H_2 + M \rightarrow C_4H_3 + M$$
$$C_2H_2 + C_4H_3 + M \rightarrow C_6H_5 + M.$$

2.5. Nitriles

The basis of the nitrile chemistry is the hydrogen cyanide molecule (HCN) which is formed directly by the reaction of atomic nitrogen with the methyl radical produced in methane photolysis:

$$N + CH_3 \rightarrow HCN + H_2.$$
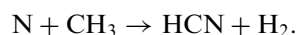
This pathway is not the dominant one since the H_2CN radical, also produced in the above reaction, reacts readily with atomic hydrogen to give HCN with an overall rate which is bigger that the previous one:

$$N + CH_3 \rightarrow H_2CN + H$$
$$\underline{H_2CN + H \rightarrow HCN + H_2}$$
$$N + CH_3 \rightarrow HCN + H_2.$$
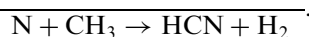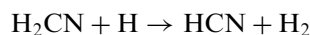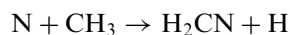
Since the majority of nitrogen atoms is produced in the upper atmosphere, the production of HCN has a maximum in this region. The photolysis of HCN leads to the production of cyano radicals (CN):

$$HCN + hv \rightarrow CN + H$$
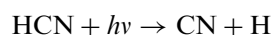
which have a double role in atmospheric chemistry. Like C_2H radicals, they enhance the catalytic destruction of molecular hydrogen and saturated hydrocarbons through the hydrogen abstraction mechanism:

$$CN + H_2 \rightarrow HCN + H$$
$$CN + CH_4 \rightarrow HCN + CH_3$$
$$CN + C_2H_6 \rightarrow HCN + C_2H_5$$
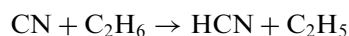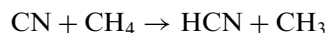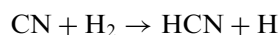
leaving a free radical and a HCN molecule, but also lead to the production of other nitrile species in reaction with unsaturated hydrocarbons through the abstraction/addition mechanism. In the last, a hydrogen atom is abstracted from the unsaturated hydrocarbon and the CN radical is added in its place. Typical examples are the formation of cyanoacetylene (HC_3N) and acrylonitrile (C_2H_3CN):

$$CN + C_2H_2 \rightarrow HC_3N + H$$
$$CN + C_2H_4 \rightarrow C_2H_3CN + H.$$
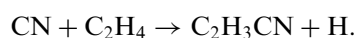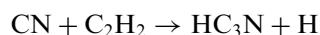
Even though the latest was not observed in Titan's atmosphere before the Cassini/Huygens mission, it was believed to be formed and taken into consideration in all previous photochemical models which included nitrile

chemistry in their reactions. Only recently, the analysis of the ionospheric composition by the ion neutral mass spectrometer (INMS) on the Cassini spacecraft has verified the presence of this species in the upper atmosphere along with other nitrile species (Vuitton et al., 2006a). Another pathway for the production of acrylonitrile, included in previous models, is the one suggested by Monks et al. (1993):

$$HCN + C_2H_3 \rightarrow C_2H_3CN + H$$
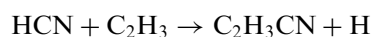
who measured the rate for this reaction and found it to be efficient at room temperature. Since C_2H_3 formation has a strong pressure dependance, the contribution of the last reaction on the overall C_2H_3CN production will become significant in the lower atmosphere where the pressure is high. The main loss for acrylonitrile is due to photolysis which is also an important source of cyanoacetylene, since this pathway has a significant branching ratio (59% based on Derecskei-Kovacs and North, 1999):

$$C_2H_3CN + hv \rightarrow HC_3N + H_2.$$
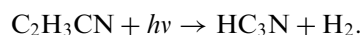
The production of HC_3N is balanced by its destruction by photolysis but also by its chemical recycling through the cyanovinyl radical (H_2C_3N):

$$HC_3N + H + M \rightarrow H_2C_3N + M$$
$$\underline{H + H_2C_3N \rightarrow C_2H_2 + HCN}$$
$$HC_3N + 2H \rightarrow C_2H_2 + HCN.$$
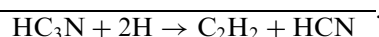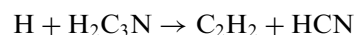
Excited nitrogen atoms produced in the upper atmosphere from the photoionization of N_2, lead to the production of other nitriles and amines. Reaction with methane has two possible products, imidogen (NH) and methyleneimine (CH_2NH) (Herron, 1999):

$$N(^2D) + CH_4 \rightarrow \quad NH + CH_3 (20\%)$$
$$\rightarrow CH_2NH + H (80\%).$$
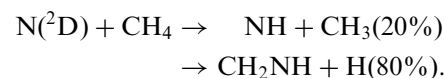
Self-reaction of two NH radicals leads to the production of an amino radical (NH_2) which is also formed in the collisional addition of N with H_2:

$$2\,NH \rightarrow NH_2 + N,$$

$$N + H_2 + M \rightarrow NH_2 + M.$$
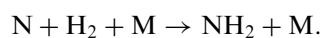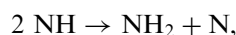
NH_2 in reaction with H yields ammonia (NH_3):

$$NH_2 + H + M \rightarrow NH_3 + M.$$

Although the production of ammonia is believed to be related to the ion chemistry (Wilson and Atreya, 2004), recent results (Ge et al., 2006) have shown that in the low temperature conditions found in Titan's atmosphere, this might not be the case. We have included ammonia, in the model, in order to investigate the extent of neutral chemistry contribution in its total production. Another possible pathway for the production of ammonia could be from the photolysis of ethyleneimine (C_2H_5N), a possible product of the reaction of $N(^2D)$ with ethane

$$N(^2D) + C_2H_6 \rightarrow C_2H_5N + H.$$
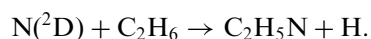
The total rate of this reaction has been measured (Herron, 1999) but the possible products are not well defined. Nevertheless, we have included it in our model in order to investigate the maximum contribution it could have to the final ammonia abundance.

Recently, Redondo et al. (2006) investigated theoretically the possible products of the $NH + CH_3$ reaction and found that the production of CH_2NH is energetically favored over other products

$$NH + CH_3 \rightarrow CH_2NH + H.$$
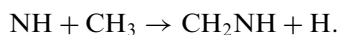
The reaction of methyl radical with the amino radical leads to the formation of methylamine (CH_3NH_2):

$$NH_2 + CH_3 + M \rightarrow CH_3NH_2 + M$$
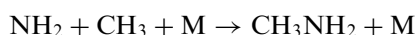
which when photolyzed, also produces CH_2NH (Gardner and McNesby, 1982):

$$CH_3NH_2 + h\nu \rightarrow CH_2NH + 2\,H.$$
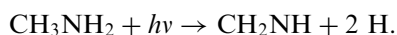
The photolysis of CH_2NH eventually produces HCN, but due to the lack of measurements for its absorption cross section and also the absence of chemical reaction rates, it was not included in photochemical models. Both ammonia and methyleneimine have also been detected by INMS (Vuitton et al., 2006a), hence we have decided to investigate their vertical profiles in Titan's atmosphere based on the available laboratory measurements and theoretical suggestions about their reactivity.

Finally, reaction of excited nitrogen atoms with ethylene and acetylene leads to the production of acetonitrile (CH_3CN) and the CHCN radical, respectively:

$$N(^2D) + C_2H_4 \rightarrow CH_3CN + H$$
$$N(^2D) + C_2H_2 \rightarrow CHCN + H$$
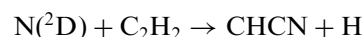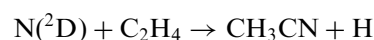
while the production of the latter is dominated in the same region by the CH replacement of H in HCN:

$$CH + HCN \rightarrow CHCN + H.$$
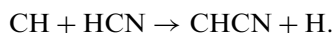
Yung (1987) suggested that the CHCN radical could be the basis for the production of cyanogen (C_2N_2) and dicyanoacetylene (C_4N_2):

$$N + CHCN \rightarrow C_2N_2 + H$$
$$CHCN + CHCN \rightarrow C_4N_2 + H_2$$

which have been detected in the gas and solid phase, respectively, on Titan's North pole from the Voyager observations (Coustenis et al., 1991; Samuelson et al., 1997). The latter is included in photochemical models as it is believed to be a possible precursor of haze formation. Finally, another possible path for dicyanoacetylene is the one suggested by Petrie and Osamura (2004) based on quantum chemical calculations:

$$HCN + C_3N \rightarrow C_4N_2 + H$$

while Halpern et al. (1989) measured the rate for reaction:

$$CN + HC_3N \rightarrow products$$

which is believed to yield $C_4N_2 + H$. Both these two last processes have a minor contribution to the overall dicyanoacetylene production based on our calculations.

2.5.1. Condensation

For most of the hydrocarbons and nitriles found in the lower stratosphere–troposphere of Titan, their saturation vapor pressure for the prevailing temperature conditions is smaller than their partial pressure allowed by photochemistry (Sagan and Thompson, 1984). This means that their saturation ratio, S, exceeds unity and that these species can condense. Under such conditions and provided that the atmosphere contains enough number of nucleation sites on the surface of which condensation proceeds readily (heterogeneous nucleation), the nucleation rate reaches very high values that lead to rapid loss of the condensing species (Pruppacher and Klett, 1978). In order to take into consideration the effects of this process in the final vertical profiles of the calculated species, a loss rate is included of the form

$$L = -A_c(S-1)\frac{\exp(-0.5/\ln(S+1)^2)}{\ln(S+1)^2}, \quad S > 1, \qquad (7)$$

where A_c is constant in units of s^{-1}. The last part of the expression resembles the dependence of the heterogeneous nucleation rate of spherical nuclei on the saturation ratio, while the $(S-1)$ term forces the calculated volume mixing ratio to converge close to the saturated value. As can be seen in Fig. 5, the above expression provides increasing loss rates with increasing saturation ratios. Also shown for comparison, is a loss rate of the form $\sim -(S-1)/S$ which is similar to the ones used in previous photochemical models (Yung et al., 1984). This expression must provide a smooth transition between the condensing and non-condensing regions which is necessary in order to avoid the oscillation of the simulation between the two. Typical
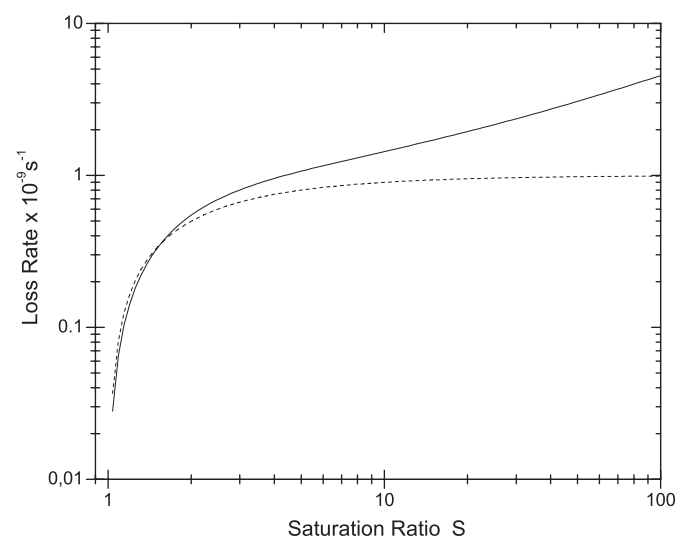

Fig. 5. Loss rate for condensing species as a function of their saturation ratio from the function used in this work (solid line) and used in previous photochemical models (dashed line).

values used for A_c are of the order $(0.1-1) \times 10^{-7}\,s^{-1}$. For the calculation of the saturation vapor pressure curves for each condensing species we used the data from Vargaftik (1975) and the NIST web database (http://webbok.nist.gov/chemistry/).

2.5.2. Methane profile

The Cassini/Huygens measurements for the methane stratospheric mixing ratio were $1.41 \pm 0.05\%$ from GCMS (Niemann et al., 2005) and $1.6 \pm 0.5\%$ from CIRS (Flasar et al., 2005). The two results are compatible within error bars. Below 32 km GCMS has measured an increase in the mixing ratio down to about 8 km, below which altitude the mixing ratio was constant at 4.9% until the surface. The DISR measurements have given a similar value of $5 \pm 1\%$ for the methane mixing ratio close to the surface (Tomasco et al., 2005). Although the Huygens results, corresponding to its landing site, have smaller uncertainties, we use the measured profile with a surface value of 5% and allow the profile to decrease to 1.6% at 32 km following the slope of its saturation vapor pressure (Fig. 6). We choose this stratospheric value because higher stratospheric values are also favored from the extrapolation of the INMS high atmosphere measurements for the stratospheric mixing ratio, using a diffusion model that gave values between 2% and 2.4% (Yelle et al., 2006). Above that level the methane mixing ratio is calculated as for all other species in the model. N_2 was fixed to 95% and ^{40}Ar at 4.32×10^{-5} at the surface. No other species concentration is fixed at the surface or anywhere else in the simulated atmosphere.

2.6. Microphysical sub-model (MP)

The third part of the model describes the evolution of the photochemically produced haze monomers to the haze particles in Titan's atmosphere. The monomers here correspond to the smaller aerosol particles derived initially from the photoc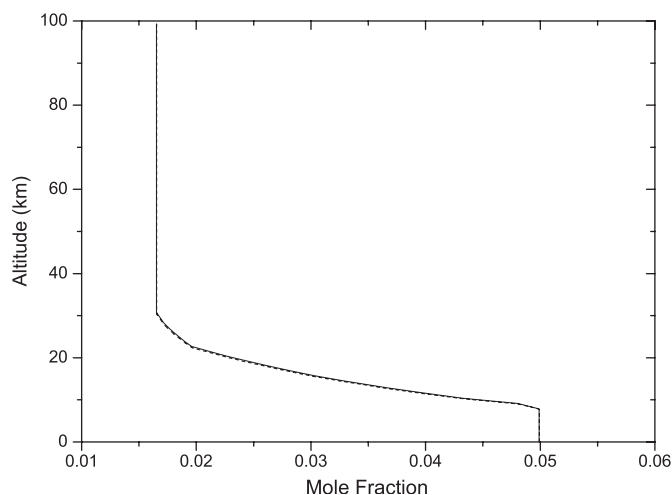hemical pathways. The MP sub-model uses the same pressure grid as the RC and PC models and solves the time-dependent continuity equation for particle coagulation in one dimension, generating the populations of different size particles at each altitude (pressure) level. It considers that the particles coagulate following the Brownian (random collisions between particles) and gravitational (scavenging due to different settling velocities of different size particles) kernels, with the latter having a negligible contribution compared to the former. In addition, the effects of atmospheric eddy mixing and particle charge in the derived vertical distributions are taken into consideration.

In order to simulate the coagulation of particles with a limited number of different sizes, the spectrum of volumes is divided into a number of bins, describing particles with certain size limits. The volume spectrum division used, results from the doubling of each previous volume bin. In this volume grid there are 35 size bins, covering the range between the monomer size $(7.25\,Å)$ and a maximum radius of $\sim 2\,\mu m$. Larger size values are not allowed due to the electrostatic repulsion between the particles, which is controlled through the charging rate, χ. With this division, high resolution is achieved for the resulting particle size distributions. This is important for the spectral variation of the resulting haze opacity used in the RC model, since the contribution of each size bin in the opacity of each layer is included independently. The method of solution along with the parameterizations used are described in the appendix.

The significant difference between the current simulation and all previous ones, regarding the microphysical evolution of an initial monomer population, is in the way these initial monomers are produced and how they are distributed over the vertical extent of Titan's atmosphere. As discussed in the introduction, previous microphysical models (McKay et al., 1989; Toon et al., 1992a,b; Tomasko et al., 1997; Rannou et al., 2003) treat the column production rate of haze monomers as a free parameter which they scale in order to get a good fit to the observed data (geometric albedo, temperature). The range of values was deduced to be of $(0.5-2) \times 10^{-14}\,gm\,cm^{-2}\,s^{-1}$ depending on the type of particles considered (spheres or fractals) (McKay et al., 2001). In previous works, the vertical distribution of the production rate was given a symmetric form (usually Gaussian) centered at the production altitude that was arbitrarily set from 350 up to $\sim 600\,km$ amongst different models. In the current work, these two parameters are directly determined by the photochemical description of haze production. The pathways used control the production rate of the haze monomers at each altitude and depend directly on the correct description of the total photochemical evolution of the atmospheric species. This of course makes the fit to the observed data more constrained since there are less free parameters that can be optimised to get a good match and at the same time provides a direct validation for the assumptions made for the gas–particle transformation and also the efficiency of

Fig. 6. Methane profile in the troposphere and lower stratosphere used in the model calculations.

this transformation as a possible sink for some of the atmospheric gases.

As discussed in the introduction, the shape of the haze particles in Titan's atmosphere is not well constrained. The fractal approach although favored due to its ability to explain the polarization measurements, has also some difficulties. Under this more detailed description of haze formation, we have adopted the simpler spherical particle approach.

3. Haze formation pathways

3.1. Laboratory measurements

Based on the idea that the haze particles were of photochemical origin in Titan's atmosphere, many laboratory experiments were and are still carried out to simulate haze production. The main idea of the simulation is usually to irradiate a specific mixture of nitrogen, methane and possibly other hydrocarbons (in amounts equivalent to those present in the atmosphere of Titan) with energy sources analogous to those in Titan (UV radiation, magnetospheric electrons and protons, cosmic rays). The energy sources usually chosen are electric discharge, cold plasma discharge and UV radiation. The results of such experiments were the production of complex organic solids, called tholins (Sagan and Khare, 1979).

The most well-stablished laboratory simulation of tholins was the one made by Khare et al. (1984a) using a mixture of $90\% N_2 - 10\% CH_4$ with a DC electrical discharge. They provided the first measurements of the complex refractive index of haze particles that exhibited the correct wavelength dependence of the imaginary part (absorption), necessary to fit the geometric albedo. As was shown by Rages and Pollack (1980), haze is the main absorber in the UV region responsible for the sharp decrease of the geometric albedo below $0.6\,\mu m$ and the slope of the geometric albedo is directly correlated with the slope of the imaginary part of the refractive index in this region. All radiation transfer models published so far use the above refractive index values scaled by a (wavelength-dependent) factor to achieve the best possible fit to the geometric albedo.

Other simulations for the production of haze analogs had as the primary mixture photochemical products of an $N_2 - CH_4$ atmosphere. Bar-Nun et al. (1988) used acetylene (C_2H_2), ethylene (C_2H_4) and hydrogen cyanide (HCN) in Ar while Scattergood et al. (1992) used C_2H_2 and C_2H_4 in N_2, HCN in He and also mixtures of them in different amounts. They both got spherical particles, which were sticky and hence formed clusters giving in this way credit to the suggestion of West and Smith (1991) of non-spherical final particles in Titan's atmosphere. The disadvantage of these simulations was that they did not correspond to mixtures found in Titan's atmosphere.

With the interest in Titan's organic chemistry increasing, laboratory researchers tried to simulate better the condi-

tions prevailing in Titan's atmosphere. Coll et al. in a series of publications (1995, 1998, 1999), pointed out the significance of low temperature conditions in the experiments, close to those in Titan's atmosphere, and the possible contamination of previous simulations by terrestrial gases; many of the species formed in the reactor vessels were found to be unstable at standard room temperature and the solid products were of low stability in the presence of O_2 and H_2O. McKay (1996) investigated the effect of different initial methane amounts in the mixture on the optical properties of the particles produced. He concluded that increasing the methane content of the mixture, produces tholins which are darker in the UV and violet compared to the visible and near-IR. Clarke and Ferris (1997) studied the possible formation of haze analogs from cyanoacetylene (HC_3N) and cyanoacetylene–acetylene copolymers. They concluded that HC_3N is much more reactive in polymerization than HCN and that the optical properties of the produced HC_3N/C_2H_2 copolymers matched those of Titan's haze properties better than the pure polymers. Khare et al. (2002) studied the time evolution of laboratory tholins and observed the formation of aromatic rings almost immediately after the glow discharge in their initial mixture. Ramirez et al. (2002) used a N_2/CH_4 mixture closer to the one in Titan's atmosphere and without the possible effects of terrestrial contamination and found that the refractive index of their tholins exhibited a wavelength variation similar to that of Khare et al. (1984a), but of smaller absolute value. Tran et al. (2003) used mixtures of $CH_4, H_2, C_2H_2, C_2H_4$ and HC_3N in N_2, and produced haze analogs using as an energy source direct UV light. They also retrieved a similar slope for the imaginary part of the refractive index with wavelength, as previous investigators, but its absolute value varied depending on the composition of the mixture and the conditions of the experiment.

Many methods have been used for the chemical analysis and elemental composition of the produced tholin particles (Khare et al., 1984b; Ehrenfreund et al., 1995; McKay, 1996; Coll et al., 1999; Khare et al., 2002; Tran et al., 2003). Their structure was found to be a complex mixture of hydrocarbon and nitriles including aromatic compounds and polycyclic aromatic hydrocarbons (PAH), but the results between different experiments were not always similar. The parameters commonly used for the elemental composition of the particles are their C/N and C/H ratios. These are important not only because they provide an estimate of the bulk mass of the haze particles, but also an estimate of the role of the haze particles as a possible sink for atmospheric gases. Again, as for the optical properties, the derived ratios depend on the experimental conditions and the energy sources used: C/N ratios were found to range from 0.75 (McDonald et al., 1994) to 17.6 (Tran et al., 2003) and C/H ratios between 0.6 (Khare et al., 1984a) and 1.6 (Clarke and Ferris, 1997).

Motivated by the different results between the published simulations, Imanaka et al. (2004) performed a systematic

study, with experiments covering a wide range of pressures that represent different altitude regions in Titan's atmosphere. They found that the pressure is a critical parameter in the chemical and hence optical properties of the derived analogs, with nitrogen being more efficiently incorporated in the particles at low deposition pressures (increasing C/N ratio with increasing pressure). In addition, the presence of aromatic compounds and nitrogen-containing polycyclic aromatic compounds (N-PACs) was found to increase with decreasing pressure, making in this way the derived tholins more absorbing in the UV/Visible region due to the delocalized π electrons of these structures. These conclusions explained the differences observed between the earlier experiments and proved that the haze particles found in Titan's atmosphere could have different properties at different pressures, as was suggested in the past (Chassefiere and Cabane, 1995).

3.2. In situ measurements and other observations

The ACP instrument on board the Huygens probe, provided the first results regarding the chemical composition of the haze particles in Titan's atmosphere (Israël et al., 2005). The pyrolysis of the refractory core of the particles, provided evidence for the presence of HCN and NH_3 in their structural form, although the results were preliminary and as stated by the authors, the poor resolution of the mass spectrometer did not allow for a clear verification of the above conclusions. If correct, they suggest that there is a strong incorporation of nitrogen in the haze particles which could act as a significant sink for this atmospheric component. In addition to the above, the two different altitude sample collections have shown that the aerosol composition is homogeneous below 130 km, which suggests that the production region must be situated above this altitude.

In view of the low temperature conditions prevailing in the interstellar medium, and the formation of complex organic structures in it, possible pathways in which haze could be formed in Titan's atmosphere can be suggested. The presence of polyaromatics (PAH) in the interstellar clouds has been known for long time (Allamandola et al., 1989), while recently Hudgins et al. (2005) have found N-PACs to be also abundant in the universe and produced around dying stars. These are considered to be much more important than simple PAHs due to their connection with the chemistry of life. Chlorophyll for example is such a compound. Although it was believed that the formation of these complexes was related to ion chemistry, recent results (Ricca et al., 2001) suggest that they are produced by neutral radical reactions which proceed even at the very low temperatures found in these regions of the universe. Similar mechanisms could also lead to the production of haze in Titan's atmosphere.

3.3. Formation pathways

Based on the laboratory measurements certain possible pathways for the transformation of gases to particles have

been suggested (Lebonnois et al., 2002; Wilson and Atreya, 2003) but remain to be tested with regard to the formation of the haze from the photochemistry. In the present work we shall use the suggested pathways to generate the vertical haze structure from the photochemistry, and validate this (in Part II) by comparing the model vertical temperature structure, spectral geometric albedo and vertical species distributions against measurements.

The reactions used along with their rates are given in Table 6. The particles are believed to form from the chemical growth of certain polymer structures. Allen et al. (1980) suggested that a possible mechanism for the production of these polymers could be the photolysis of acetylene, leading to polyyne ($C_{2n+2}H_2$) formation. The first step of this process, as was described in the previous section, is the production of diacetylene from the reaction of ethyl radical with acetylene. The process continues giving higher order polyacetylenes (C_6H_2, C_8H_2, etc.):

$$C_{2n}H_2 + C_2H \rightarrow C_{2n+2}H_2 + H.$$
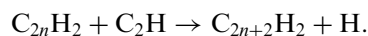
In addition to the above, the photolysis of the polyynes formed leads to the production of polyyne radicals (C_4H, C_6H, C_8H) which also enhance the polymerization. On the other hand, the production of polyynes is constrained by the acetylenic recycling of the C_2H and other polyyne radicals through reactions with the saturated hydrocarbons in the atmosphere from which the main contribution comes from methane:

$$C_2H + CH_4 \rightarrow C_2H_2 + CH_3.$$
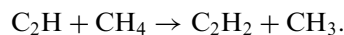
Due to the high number densities of the saturated species, this recycling is very efficient and the contribution of increasing order polyynes will have a decreasing effect on the total haze production (Wilson and Atreya, 2003). According to laboratory measurements (Opansky and Leone, 1996a; Chastaing et al., 1998; Vakhtin et al., 2001a), the reaction of the ethyl radical with acetylene proceeds readily even at very low temperatures. Since the reaction rates for the higher order polyyne radicals have not been measured at low temperatures, we estimated them from their equivalent reactions with the C_2H radical. We consider all reactions leading to the formation of hydrocarbons with more than ten carbon atoms to lead to the formation of haze. Based on this, the reactions used in the model as haze pathways in Titan's atmosphere from this process, are:

$$C_4H + C_6H_2 \rightarrow polymer,$$
$$C_6H + C_4H_2 \rightarrow polymer,$$
$$C_6H + C_6H_2 \rightarrow polymer.$$
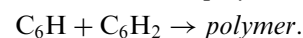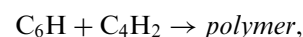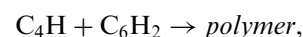
Similar to polyynes, cyanopolyynes are also possible haze precursors. These are formed in the same way as polyynes but with the ethynyl radical replaced by its isoelectronic nitrile equivalent, the cyanogen, CN. The process is initiated with the reaction of the CN radical with unsaturated hydrocarbons and nitriles giving cyanoacetylene, acrylonitrile and dicyanoacetylene, as described in the

Table 6
Reactions used for the gas to particle transformation

Reaction				ε	Rate	Reference	T (K)
Polyynes							
R525	$C_4H + C_6H_2$	$\rightarrow$	*Polymer*	17.9	1.3×10^{-10}	Est. as $k(C_2H + C_2H_2)$	
R526	$C_6H + C_4H_2$	$\rightarrow$	*Polymer*	17.5	1.3×10^{-10}	Est. as $k(C_2H + C_2H_2)$	
R527	$C_6H + C_6H_2$	$\rightarrow$	*Polymer*	11.7	1.3×10^{-10}	Est. as $k(C_2H + C_2H_2)$	
Aromatics							
R528	$C_6H_5 + C_2H_2$	$\rightarrow$	*Polymer*	34.5	$k_0 = 4.96 \times 10^{-19} T^{-4.08} e^{403/T}$	Wang and Frenklach (1994)	500–2500
					$k_\infty = 6.64 \times 10^{-17} T^{1.56} e^{-1912/T}$	‖	300–2500
R529	$C_6H_5 + C_6H_6$	$\rightarrow$	*Polymer*	11	$1.6 \times 10^{-12} e^{-2168/T}$	Park et al. (1999)	298–1330
R530	$C_6H_5 + HC_3N$	$\rightarrow$	*Polymer*	17.1	$k_0 = 4.96 \times 10^{-19} T^{-4.08} e^{403/T}$	Est. as $k(C_2H_2 + C_6H_5)$	
					$k_\infty = 6.64 \times 10^{-17} T^{1.56} e^{-1912/T}$	‖	
Pure Nitriles							
R531	$H_2CN + HCN$	$\rightarrow$	*Polymer*	35	$1.1 \times 10^{-12} e^{-900/T}$	Est. as $k(C_2H_3 + HCN)$	
R532	$H_2CN + CH_2NH$	$\rightarrow$	*Polymer*	33.7	$1.1 \times 10^{-12} e^{-900/T}$	Est. as $k(C_2H_3 + HCN)$	
R533	$CN + C_2H_3CN$	$\rightarrow$	*Polymer*	35.4	$3.02 \times 10^{-11} e^{103.6/T}$	Butterfield et al. (1993)	297–528
R534	$CN + C_2N_2$	$\rightarrow$	*Polymer*	35.5	$2.2 \times 10^{-21} T^{2.7} e^{-325/T}$	Yang et al. (1992a)	300–740
R535	$CN + C_4N_2$	$\rightarrow$	*Polymer*	35.5	5.4×10^{-13}	Seki et al. (1996)	300
Copolymers							
R536	$C_4H + HC_3N$	$\rightarrow$	*Polymer*	18.4	$8.6 \times 10^{-16} T^{1.80} e^{474/T}$	Est. as $k(C_2H + C_2H_2)$	
R537	$C_3N + C_4H_2$	$\rightarrow$	*Polymer*	18	$8.6 \times 10^{-16} T^{1.80} e^{474/T}$	Est. as $k(C_2H + C_2H_2)$	
R538	$C_4H_3 + HC_3N + M$	$\rightarrow$	*Polymer*	17.6	$k_0 = 3.3 \times 10^{-30} e^{-740/T}$	Est. as $k_0(H + C_2H_2 + M)$	
					$k_\infty = 5.53 T^{-3.89} e^{-4635/T}$	Est. as $k(C_2H_2 + C_4H_3)$, Wang and Frenklach (1994)	

chemistry section. The polymerization is considered to proceed with further addition of the CN radical on the produced polyynes and nitriles. In the model calculations, the reaction used is

$$CN + C_6H_2 \rightarrow polymer.$$
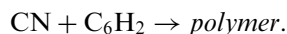
The above pathways lead to the production of polymers which due to their structural form, are characterized by large C/N and C/H ratios, which are not supported by the laboratory results. This suggests that if indeed the haze in Titan's atmosphere is similar to the analogs produced in the laboratories, these polymers must have a small contribution to the total haze production.

Polymers of HCN could lead to C/N ratios closer to those observed in the laboratory. In these, the polymerization starts with the production of an $(HCN)_2$ dimer and subsequent addition of HCN molecules leads to poly-HCN structures (Rettig et al., 1992). Even though HCN structures were defined in the haze analogs produced (Coll et al., 1999), the optical properties of pure poly-HCN structures do not exhibit the correct wavelength dependence inferred from Titan's geometric albedo (Khare et al., 1994) and hence they are not expected to have a major contribution to bulk haze production. Thompson and Sagan (1989) suggested the possible formation of hetero-polymeric structures from the addition of R–CN structures and CN radicals on nitriles. In order to take into consideration the R–CN type process, the following pathway was suggested:

$$H_2CN + HCN \rightarrow polymer.$$

The rate for this reaction has not been measured and in previous works it was estimated with the rate of the $C_2H_3 + HCN$ reaction (Monks et al., 1993), due to the similarity observed for the rates of reaction between H_2CN and C_2H_3 with H and N. Wilson and Atreya (2003) suggested that the measured rate, is strongly overestimated based on their calculated vertical profiles for C_2H_3CN and HC_3N, which were above the observed values. In addition, using the measured rate for the $H_2CN + HCN$ reaction, led to large haze production in the lower atmosphere, which was above the magnitude defined by microphysical models. Hence they estimated the rate of the latter reaction to be 1000 times smaller than that of Monks et al. (1993).

This requirement for a lower rate could possibly originate from the presence of the CN radical on the two reactants. Seki and Okabe (1993) have measured the rates for the reaction of CN radicals with diacetylene and dicyanoacetylene and reported the first to be about 500 times faster than the second, while Butterfield et al. (1993) found that the rate of reaction between CN and acrylonitrile is significantly smaller that the rate for reaction with ethylene. This decrease in the rate of CN reaction between hydrocarbons and their equivalent H/CN replaced nitriles is attributed to a significant electron withdrawing effect of the cyanogen group. It could be possible that the same process reduces the rate of the $H_2CN + HCN$ reaction relative to its C_2H_3 equivalent.

In the calculations presented in Part II, we have performed a sensitivity test of the model results for different values of the above reaction rate. Our results

suggest that the chemical loss of atmospheric molecules in the growth of the polymer structures described here, to the monomer size beyond which microphysics takes over, has an important role in the total haze production. The way this loss is included in the model calculations is described in the following section.

Pathways based on the CN addition process on nitrile species are described by

$$CN + C_2N_2 \rightarrow polymer,$$
$$CN + C_4N_2 \rightarrow polymer,$$
$$CN + C_2H_3CN \rightarrow polymer.$$
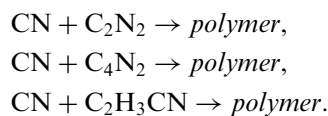
The rates for the last two reactions have been measured, as discussed above, while the rate for the CN reaction with cyanogen was measured by Yang et al. (1992b). Although these measurements were performed at temperature conditions higher than in Titan's atmosphere, the radical character of the reactions with the small negative temperature dependence suggests that these reactions can take place at very low temperatures with rates close to the above.

Clarke and Ferris (1997) suggested a pathway for HC_3N/C_2H_2 copolymer mixtures. HC_3N was found to be much more reactive in polymerization than HCN and that the copolymers formed could exhibit the necessary wavelength dependence, something which the pure polymers of either case did not do. For this case the reactions used are

$$C_4H_2 + C_3N \rightarrow polymer,$$
$$HC_3N + C_4H \rightarrow polymer.$$
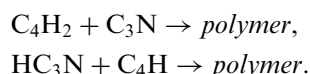
The rates for these reactions are also not measured, however, based on the relative rates of abstraction between C_2H and C_3N radicals with hydrocarbons (Clarke and Ferris, 1995), they can be estimated with their C_2H equivalent. Lebonnois et al. (2002) have included also a possible pathway based on

$$HC_3N + C_4H_3 \rightarrow polymer.$$
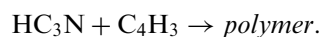
This is a pressure-dependent reaction and we have used the rate expression of Wang and Frenklach (1994).

Pathways including aromatic hydrocarbons have also been suggested. PAHs are well known to exist in the low temperatures of the interstellar medium (Allamandola et al., 1989) in significant amounts. Since benzene, C_6H_6, the simplest aromatic hydrocarbon, has been detected on Titan (Coustenis et al., 2003, 2007), PAH could also be a possible pathway for haze formation. The production of PAHs is considered to proceed through the reaction of benzene molecules with acetylene (Bauschlicher and Ricca, 2000):

$$C_2H_2 + C_6H_5 \rightarrow polymer.$$
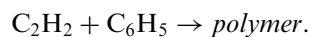
The rate for this reaction has been measured but, as in the case of benzene formation, the measurements were performed at high temperatures. Yu et al. (1994) measured

the rate in the temperature range 297–523 K, while Wang and Frenklach (1994) performed theoretical simulations for the rate in the range 300–2500 K. Both studies suggest that the overall reaction rate is pressure-independent while the products (either stabilized adduct which leads to the formation of PAHs or dissociation of the initially vibrationally excited adduct) have a strong temperature and pressure dependance, with the adduct becoming increasingly more important as the pressure increases and the temperature decreases. Another pathway considered in previous works is the one of the direct addition of phenyl radical on a benzene molecule:

$$C_6H_5 + C_6H_6 \rightarrow polymer$$
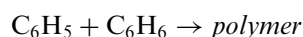
with the rate for this reaction measured by Park et al. (1999).

For the case of the N-PACs, Ricca et al. (2001) investigated the possible incorporation of nitrogen atoms in the PAH structures. Considering reactions between C_6H_5, HCN and C_2H_2 they found that the formation of a second ring with a nitrogen atom in the skeleton through radical reactions, is strongly prohibited by high energy barriers unless the aromatic molecules are vibrationally excited. Yet once such a ring is formed, the presence of the nitrogen atom promotes the formation of the next ring. On the other hand reactions with cyanoacetylene and acetylene which lead to the formation of rings with CN as a side group, have barriers which are very close to those for the case of pure PAHs and hence can proceed in Titan's low temperatures. We have thus included the following reaction as a possible pathway in the model:

$$HC_3N + C_6H_5 \rightarrow polymers$$

and estimated the rate with that of acetylene reaction with phenyl.

Finally, we have included another pathway with methyleneimine based on the suggestions of Redondo et al. (2006). $CH_2 = NH$ is a suitable compound for polymerization and could be a precursor for haze production. The same component was also found in the low pressure tholins produced in the Imanaka et al. (2004) experiments. The growth of this polymer could be initiated by the addition of the H_2CN radical, as for the case of the HCN polymerization:

$$H_2CN + CH_2 = NH \rightarrow polymer.$$
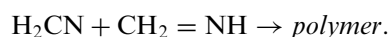
Some of the above pathways have been used in photochemical models in order to test their validity (Lebonnois et al., 2002; Wilson and Atreya, 2003). Even though their results showed that the suggested reactions lead to column haze production rates which are close to those needed by microphysical models for the reproduction of the geometric albedo, the effects of the derived haze production rates on the radiation field and the temperature structure were not tested, but done in the present work.

3.4. Monomer size

The above pathways describe the production and chemical growth of the haze precursors by means of polymerization. This growth is considered to proceed until the precursors reach a specific size beyond which the chemical growth ceases and the laws of microphysics control their evolution. This is the monomer stage in our work. It should be made clear that the monomers in this work do not correspond to the monomers used in other microphysical models of fractal-type particles where the monomers define the transition region between spherical growth of particles and fractal growth (Rannou et al., 2003). In the present work, the monomers correspond to the lower size limit of haze particles from which all others are produced through coagulation. The size of the monomers was set to 7.35 Å. This choice was based on laboratory results which showed that nucleation of polymers to particles starts at masses between 600 and 2000 amu depending on the chemical composition of the particles and the environment in which they nucleate (Dimitrov and Bar-Nun, 2002; Richter and Howard, 2000). Taking as a typical value the mass for the monomers to be of the order of 1000 amu and considering the mass density of the particles to have the typical value of 1 gm/cm^3 (an assumption used in all microphysical models) we obtain the above radius for the spherical monomers.

3.5. Chemical loss to haze

The impact of haze formation on the chemical loss of species is also an important issue for atmospheric composition. The production of haze monomers discussed above, does not include the chemical growth of the polymers but only the production of an initial dimer. From the monomer point of view this is realistic because the chemical growth of these dimers provides the final monomer population. The chemical addition of molecules to these structures will only change their size and not their number density. Yet, for the atmospheric composition there is a sink for the gas molecules lost during the chemical growth of the dimers that has to be taken into account. We have estimated this loss, based on the assumed mass of the haze monomers and that the chemical growth of the dimers for each suggested pathway is based on the smallest mass molecule. That is, the growth of the initially formed dimers proceeds with the addition of the smallest of the two molecules that form it. Under this condition the chemical loss for atmospheric gases can be estimated from:

$$\frac{\partial n_i}{\partial t} = -\varepsilon_i Pr_i, \tag{8}$$

where n_i is the number density of the gas molecule which is lost during the chemical growth of the dimer described through pathway i, Pr_i is the production rate of dimers for this pathway and ε_i is the number of molecules that have to be added on the dimer in order to reach the mass of the

monomer. The ε factors are presented in Table 6 for each pathway. Their values range between 11 and 35.5, which means that the total chemical loss is significantly larger than the loss due to the dimer formation.

4. Conclusions

In this Part I of our present work we have given a detailed description of the radiative/convective-photochemical-microphysical model developed to study the complex photochemistry in Titan's atmosphere that leads to the formation of the haze vertical structure, and through its radiative properties to the control of the vertical temperature structure and the radiation field, which in turn control the photochemistry and the vertical species mixing ratios. We thus generate all vertical structures in a self-consistent manner. The model allows us to study the important processes by which Titan's haze is formed and its subsequent effects on the photochemistry from which it was formed. In Part II of this work we give detailed model results and validate these against measurements from the Cassini/Huygens mission and from previous ground-based and other space measurements. The validation is performed for the vertical temperature structure, spectral geometric albedo, and vertical profiles of species concentrations. We also perform sensitivity analyses for model processes for which the associated data are not well known.

Appendix A. Thermal structure

The calculation of the temperature structure is based on the Vardavas and Carver (1984b) radiative/convective model developed for the Earth's atmosphere. The modelled atmosphere is separated in two regions. One close to the surface which is in convective equilibrium (CE) and one above, which is in radiative equilibrium (RE). In the first region (CE), the temperature structure is controlled by the

atmospheric lapse rate, Γ. For the Earth's atmosphere the convective region of the atmosphere corresponds to the troposphere. Yet for Titan, although we use the observed temperature minimum at ~ 40 km to define the position of the tropopause, the troposphere—when defined as the region of convective equilibrium—corresponds to a small layer with width of only a few km above the surface. This was initially derived from Voyager measurements of the vertical temperature profile (Lindal et al., 1983; Eshleman et al., 1983) and also by model results (McKay et al., 1989). The slope of the temperature profile from the observed temperature structure derived by HASI (Fulchignoni et al., 2005) in the lower atmosphere is very close to the expected dry adiabatic lapse rate:

$$\Gamma = -\frac{g(r)}{c_p} \tag{A.1}$$

with $g(r)$ the acceleration due to gravity at radial distance r and c_p is the atmospheric specific heat capacity. Hence, in the model calculations we have adopted the dry adiabatic lapse rate as given by this expression for the calculation of the temperature structure inside the convective region. The average value for this parameter, based on our model results is 1.26 K/km. We note that the lapse rate is not constant but has a small variability due to the temperature and altitude dependence of the heat capacity and gravity, respectively.

In the rest of the atmosphere along with the value at the surface, the temperature is controlled by the balance between the absorption of solar and the emission of thermal radiation. In addition to the above, the conduction between adjacent layers has been included in the energy balance. For each atmospheric layer in the RE region, the flux balance is described at the top and base of each layer by

$$\Delta F_{IR} = \Delta F_{\odot} + \Delta F_C, \tag{A.2}$$

where for each process, ΔF corresponds to $F_{i+1} - F_i$ with F_i the net outgoing flux at the base of each layer i and F_{i+1} the net outgoing flux at the top of the layer. The conductive flux is given by the expression:

$$F_C = -K\frac{dT}{dz} = \frac{g(r)Mp}{R}\frac{K}{T}\frac{dT}{dp}, \tag{A.3}$$

where K is the atmospheric conduction coefficient, M the atmospheric mean molecular weight, p the pressure and T the temperature, and R is the universal gas constant. The conduction coefficient can be written in the form $K = \alpha T^\beta$ with $\alpha = 56$ and $\beta = 0.69$ for N_2 (Banks and Kockarts, 1973).

The thermal flux into each layer k can be written as the sum over each spectral domain i

$$F_k = \sum_i F_{i,k} \tag{A.4}$$

with the contribution of each domain being

$$F_{i,k} = \pi\varepsilon_g B_i(T_g)t(z_k,0) + \int_0^\infty \pi B_i(T_{z_j})\frac{dt(z_k,z_j)}{dz}dz_j, \tag{A.5}$$

where T_g is the surface temperature, ε_g is the surface emissivity, B_i corresponds to the average value of the Planck function over the spectral domain i multiplied by the width of the domain, $t(z_k,z_i)$ is the atmospheric transmission between layers j and k. The solar flux is calculated based on the delta-Eddington method (Joseph et al., 1976). This method allows for the calculation of the fluxes at each point of the pressure grid knowing the asymmetry factor, single scattering albedo and extinction optical depth of each atmospheric layer.

The calculation of the vertical temperature structure can be easily performed with the Newton–Raphson method as described in Vardavas and Carver (1984a). The position of the transition region between convective and radiative equilibrium is determined for the lowest altitude where the condition (Vardavas and Carver, 1984a; Ramanathan and Coakley, 1978; Manabe and Wetherland, 1967):

$$\left(\frac{dT}{dz}\right)_{boundary} \geqslant -\Gamma \tag{A.6}$$

is valid. The vertical temperature structure of the modelled atmosphere, is calculated for each time step of photochemical and microphysical evolution, in order to include feedbacks from chemical composition and haze opacity changes on the temperature structure and the radiation field, and vice versa.

Appendix B. Photochemistry

The model solves the time dependent continuity equation in 1D for spherical geometry

$$\frac{\partial n_i}{\partial t} = -\frac{1}{r^2}\frac{\partial(r^2\Phi_i)}{\partial r} + P_i - L_i \tag{B.1}$$

for each species i at each altitude z with $r = R_T + z$, R_T being Titan's radius. In the above, n_i is the number density of species i, Φ_i is the vertical flux and P_i and L_i describe production (photochemistry) and loss (photochemistry, condensation, surface deposition) processes, respectively. If the continuity equation is solved in cartesian geometry, the resulting mixing ratios in the lower atmosphere can be under-estimated by a factor of about 3, for species whose vertical profile depends significantly on the transportation processes. Using the hydrostatic equilibrium approximation in order to transform B.1 to a pressure dependent form, the flux divergence term takes the form

$$-\frac{1}{r^2}\frac{\partial(r^2\Phi_{i,k})}{\partial r} = \frac{p}{H}\frac{\partial\Phi_{i,k}}{\partial p} - \frac{2}{r}\Phi_{i,k}, \tag{B.2}$$

where k refers to the pressure level and H is the atmospheric pressure scale height. In the same way, the

vertical flux can be written in a compact form as

$$\Phi_{i,k} = C_1(p,T)f_{i,k} + C_2(p,T)\frac{\partial f_{i,k}}{\partial p} \qquad (B.3)$$

with (see Eq. (4))

$$C_1(p,T) = \frac{Dp}{k_B TH}\left(1 - \frac{M_i}{M} + \alpha_T \frac{p}{T}\frac{\partial T}{\partial p}\right)$$

$$C_2(p,T) = (D+K)\frac{p^2}{k_B TH}. \qquad (B.4)$$

Under this form, (B.2) can be expressed as

$$-\frac{1}{r^2}\frac{\partial(r^2\Phi_{i,k})}{\partial r}$$

$$= D_1(p,T)f_{i,k} + D_2(p,T)\frac{\partial f_{i,k}}{\partial p} + D_3(p,T)\frac{\partial^2 f_{i,k}}{\partial p^2} \qquad (B.5)$$

with

$$D_1(p,T) = \frac{p}{H}\frac{\partial C_1}{\partial p} - \frac{2}{r}C_1,$$

$$D_2(p,T) = \frac{p}{H}\left(C_1 + \frac{\partial C_2}{\partial p}\right) - \frac{2}{r}C_2,$$

$$D_3(p,T) = \frac{p}{H}C_2. \qquad (B.6)$$

On the other hand, the time derivative of the number density of each species can be written as

$$\frac{\partial n_{i,k}}{\partial t} = \frac{\partial(nf_{i,k})}{\partial t}$$

$$= n\frac{\partial f_{i,k}}{\partial t} + B(p,T)f_{i,k}, \quad B(p,T) = -\frac{p}{k_B T^2}\frac{\partial T}{\partial t}. \qquad (B.7)$$

Substituting the above in (B.3), the continuity equation can be written as

$$\frac{\partial f_{i,k}}{\partial t} + a_k f_{i,k} + b_k\frac{\partial f_{i,k}}{\partial p} + c_k\frac{\partial^2 f_{i,k}}{\partial p^2} = u_{i,k} - v_{i,k}, \qquad (B.8)$$

where

$$a_k = \frac{1}{n_k}(B(p,T) + D_1(p,T)),$$

$$b_k = \frac{D_2(p,T)}{n_k}, \quad c_k = \frac{D_3(p,T)}{n_k},$$

$$u_{ik} = P_{i,k}/n_k, \quad v_{i,k} = L_{i,k}/n_k. \qquad (B.9)$$

B.1. Grid transformation and boundary conditions

In view of the discrete pressure grid in the model, the continuity equation at each pressure level k and for each species i takes the form

$$\frac{\partial f_{i,k}}{\partial t} = H_{i,k}(f_{1,k}, f_{2,k}, \ldots, f_{I,k}; f'_{i,k}; f''_{i,k}, p_k, T_k, t), \qquad (B.10)$$

where

$$H_{i,k} = -\alpha_k f_{i,k} - w_{i,k} + u_{i,k} - v_{i,k} \qquad (B.11)$$

and

$$w_{i,k} = b_k f'_{i,k} + c_k f''_{i,k} \qquad (B.12)$$

with

$$f'_{i,k} = \frac{\partial f_i}{\partial p} \quad \text{and} \quad f''_{i,k} = \frac{\partial f_i^2}{\partial p^2}. \qquad (B.13)$$

Introducing finite differences, the two derivatives can be written as

$$f'_{i,k} = (f_{i,k+1} - f_{i,k})/sp_k, \qquad (B.14)$$

$$f''_{i,k} = g\frac{2}{sp_k}\left[\frac{f_{i,k+1} - f_{i,k}}{\Delta p_k} - \frac{f_{i,k} - f_{i,k-1}}{\Delta p_{k-1}}\right], \qquad (B.15)$$

where

$$\Delta p_k = p_{k+1} - p_k,$$

$$sp_k = \Delta p_k + \Delta p_{k+1},$$

$$g = \left[\frac{2\Delta p_k \Delta p_{k-1}}{\Delta p_k^2 + \Delta p_{k-1}^2}\right] \qquad (B.16)$$

so that $w_{i,k}$ can be expressed as

$$w_{i,k} = \alpha_k f_{i,k-1} + \beta_k f_{i,k} + \gamma_k f_{i,k+1} \qquad (B.17)$$

with

$$\alpha_k = \frac{b_k}{sp_k} + \frac{2gc_k}{\Delta p_k sp_k},$$

$$\beta_k = -\frac{2gc_k}{\Delta p_k \Delta p_{k-1}},$$

$$\gamma_k = -\frac{b_k}{sp_k} + \frac{2gc_k}{\Delta p_k sp_k}. \qquad (B.18)$$

At the boundaries the first and second derivatives in the three term approximation introduced above, include an imaginary point. For the surface we consider that the value of the mixing ratio for the imaginary point under the surface is the same with the surface value. The physical meaning of this condition is that there is no loss or gain through the surface boundary by transportation. Under this condition, the parameters of $w_{i,1}$ take the values:

$$\alpha_1 = 0, \quad \beta_1 = \frac{b_1}{2\Delta p_1} - \frac{c_k}{\Delta p_1^2}, \quad \gamma_1 = -\beta_1. \qquad (B.19)$$

At the top of the atmosphere (TOA) the adopted condition is that of a continues first derivative. Under this approximation the value of the imaginary point can be calculated from setting the second derivative to zero and the $w_{i,TOA}$ parameters take the form

$$\alpha_{TOA} = \frac{b_{TOA}}{\Delta p_{TOA}}, \quad \beta_{TOA} = -\alpha_{TOA}, \quad \gamma_{TOA} = 0 \qquad (B.20)$$

B.2. Method of solution

The continuity equation (B.10) cannot be directly integrated because the characteristic rate of change of each

species mixing ratio at each altitude, can differ by many orders of magnitude. This explains the characterization 'stiff' used for this type of equation. In order to overcome this obstacle an integration method with varying integration step (time in our case) must be used, such as the Newton–Raphson Euler iteration method (Vardavas, 1984):

$$f_{i,k}(t_{m+1}) = f_{i,k}(t_m) + \Delta t_m H_{i,k}(t_m), \qquad (B.21)$$

where Δt_m is the integration time step chosen with the criterion to be smaller than the smallest characteristic time for change in any species concentration at any altitude:

$$\Delta t_m < \tau_{ikm} = |f_{i,k,m}/(\partial f_{i,k}/\partial t)_m|. \qquad (B.22)$$

As shown in Vardavas (1984), for most cases $\Delta t_m = 0.1\tau_{ikm}$ is sufficient. As a species approaches chemical equilibrium, $\tau_{ikm} \to \infty$, the continuity equation reduces to $H_{i,k} = 0$, its steady state form. Setting $Q_{i,k} = u_{i,k} - v_{i,k}$ the H function takes the form

$$H_{i,k} = -a_{i,k}f_{i,k} - w_{i,k} + Q_{i,k} \qquad (B.23)$$

and the continuity equation for species i at level k can be written in the functional form

$$G_{i,k}(f_{1,k}, f_{2,k}, \ldots, f_{I,k}; f'_{i,k}; f''_{i,k}, p_k, T_k, t) = 0, \qquad (B.24)$$

where

$$G_{i,k}(\tau_{m+1}) = f_{i,k}(t_{m+1}) - f_{i,k}(t_m) - \Delta t_m H_{i,k}(t_m). \qquad (B.25)$$

The last equation can be solved with Newton–Raphson iteration for the mixing ratio of each species i, at a level k. If we know the mixing ratios $f_{i,k,m}$, at a time t_m, then an estimation for the mixing ratio at the next time step, $f_{i,k,m+1}$ is performed, say $f^{(1)}_{i,k,m+1}$. This estimation is accompanied with an error $\varepsilon^{(1)}_{i,k}$ for each species i at level k, which is defined by

$$\varepsilon^{(1)}_k = f^{(1)}_{i,k,m+1} - f_{i,k,m+1}$$
$$= f^{(1)}_{i,k,m+1} - f_{i,k,m} - \Delta t_m H_{i,k}(f^{(1)}_{i,k-1}; \mathbf{f}^{(1)}_k; f^{(1)}_{i,k+1}) \qquad (B.26)$$

with the vector $\mathbf{f}^{(1)}_k$ defined as

$$\mathbf{f}^{(1)}_k = (f_{1,k}, f_{2,k}, \ldots, f_{I,k}). \qquad (B.27)$$

The minimization of these errors is performed by imposing a correction $\Delta \mathbf{f}^{(1)}_k$ to the initial guess $\mathbf{f}^{(1)}_k$. The corrections are defined by Eq. (B.24), which when expanded as a Taylor series about the initial guess, takes the form

$$G^{(1)}_{i,k} + (\partial G_{i,k}/\partial f_{j,l})_{(1)} \Delta f^{(1)}_{j,l} = 0 \qquad (B.28)$$

with the j and l indices covering the total number of species and levels. Using the previous definitions, the last is reduced to the form

$$\Delta t_m \left[\alpha_k \Delta f_{i,k+1} + \beta'_k \Delta f_{i,k} + \gamma \Delta f_{i,k-1} - \sum q_{i,l,k} \Delta f_{i,k} \right] = -\varepsilon_{i,k} \qquad (B.29)$$

with

$$q_{i,l,k} = \frac{\partial Q_{i,k}}{f_{i,k}} \quad \beta'_k = 1/\Delta t_m + \alpha_k + \beta_k. \qquad (B.30)$$

The above system can be written in matrix form as

$$\begin{pmatrix} A_1 & C_1 & 0 & \cdots & \cdots & 0 \\ B_2 & C_2 & A_2 & 0 & \cdots & \vdots \\ 0 & B_3 & C_3 & A_3 & \cdots & \vdots \\ \vdots & & & \ddots & & 0 \\ \vdots & & & & \ddots & C_{K-1} \\ 0 & \cdots & \cdots & 0 & B_K & A_K \end{pmatrix} \begin{pmatrix} \Delta \mathbf{f}_1 \\ \vdots \\ \vdots \\ \vdots \\ \vdots \\ \Delta \mathbf{f}_K \end{pmatrix} = \begin{pmatrix} -\varepsilon_1 \\ \vdots \\ \vdots \\ \vdots \\ \vdots \\ -\varepsilon_K \end{pmatrix}$$

with the elements of the $I \times I$ matrices $\mathbf{A}$, $\mathbf{B}$ and $\mathbf{C}$ given by

$$a_{ilk} = -q_{ilk}\Delta t_m + \beta'_k \Delta t_m \quad \text{for } l = i$$
$$= -q_{ilk}\Delta t_m \quad \text{for } l \neq i,$$

$$b_{ilk} = \Delta t_m \gamma_k \quad \text{for } l = i$$
$$= 0 \quad \text{for } l \neq i,$$

$$c_{ilk} = \Delta t_m \alpha_k \quad \text{for } l = i$$
$$= 0 \quad \text{for } l \neq i \qquad (B.31)$$

for K levels and I species. Once the corrections $\Delta f^{(1)}_k$ are known an improved vector $\mathbf{f}^{(2)}_k$ can be calculated and the procedure is repeated until the mixing ratios converge and the errors are negligible.

Appendix C. Microphysics

The basic equation describing the evolution of size and density of an initial monomer population in 1D is provided by the Smoluchowski's description which in discrete form can be written as

$$\frac{\partial n(v_k)}{\partial t} = -\frac{1}{\mathbf{r}^2}\frac{\partial(\mathbf{r}^2 \Phi(v_k))}{\partial \mathbf{r}}$$
$$+ \frac{1}{2}\sum_{i=1}^{k-1} K(u_i, v_k - u_i)n(u_i), n(v_k - u_i)$$
$$- n(v_k)\sum_{i=1}^{\infty} K(u_i, v_k)n(u_i) + p(v_k). \qquad (C.1)$$

This is no more than a continuity equation saying that the evolution of the number density of volume v_k spherical particles is controlled by the flux of particles of this volume (here we use $\mathbf{r} = R_T + z$ to discriminate from r used as particle radius later on), $\Phi(v_k)$, the production of size v_k particles from smaller ones (first sum), the loss of size v_k particles to bigger ones (second sum) and the chemical production of this size particles (only for the monomers) and/or loss due to precipitation or other processes. K is the coagulation kernel which is considered to follow the Brownian law. The last, in terms of the coagulating particles radii r and s, is given by

$$K(r,s) = 4\pi\alpha_c(D_r + D_s)(r + s)\beta \qquad (C.2)$$

with

$$D_r = \frac{k_B T}{6\pi\eta r} G_r \qquad (C.3)$$

the diffusion coefficient. In the above, T is the local temperature, η is the atmospheric viscosity, r the radius of the particle and G_r the empirical Cunningham slip-correction factor (Fuchs, 1964):

$$G_r = (1 + 1.257 N_{Kn} + 0.4 N_{Kn} \exp[-1.1/N_{Kn}]) \qquad (C.4)$$

with N_{Kn} the Knusden number equal to the ratio of the atmospheric mean free path over the particle's radius. The last, along with term β are included in order to take into account the transition from the free molecular regime in the upper atmosphere ($N_{Kn} \gg 1$), where velocity and coagulation rate of the particles is controlled by collisions, and the continuum regime ($N_{Kn} \ll 1$) in the lower atmosphere, where the transportation of the particles approaches a 'fluid' like character (hydrodynamical).

Further,

$$\beta^{-1} = \frac{r+s}{r+s+\sqrt{\delta_r^2 + \delta_s^2}} + \frac{4(D_r + D_s)}{(r+s)\sqrt{\bar{V}_r^2 + \bar{V}_s^2}} \qquad (C.5)$$

with

$$\delta_r = \frac{(2r + \lambda_r) - (4r^2 + \lambda_r^2)^{3/2}}{6r\lambda_r} - 2r, \qquad (C.6)$$

where $\bar{V}_r$ is the particle's thermal velocity and λ_r the mean free path. In addition, we have also considered the possible enhancement of the Brownian coagulation kernel by the increased diffusion produced by eddies created in the wake of large falling particles and also the possible contribution by the gravitational coagulation, produced by the varying settling velocities among different size particles (Pruppacher and Klett, 1978). Both these processes were found to have a negligible effect on the total coagulation rate.

We consider the sticking efficiency, α_c, between particles to be constrained only by the electrostatic effects between them, which are described by (Toon et al., 1992a)

$$\alpha_c(r,s) = e^{-\tau} \qquad (C.7)$$

with

$$\tau(r,s) = \frac{(r\chi e)(s\chi e)}{(r+s)k_B T}. \qquad (C.8)$$

In the above, χ, is the particle charging rate (number of electrons per radius) which is considered to be constant with altitude and e is the unit electron charge.

The flux of particles with volume v, comprises two terms, one originating from the settling of the particles in the atmosphere and the other describing the eddy mixing of the particles:

$$\Phi(v) = -n(v)V_S(v) - Kn(v)\frac{\partial f_v}{\partial \mathbf{r}}, \qquad (C.9)$$

where K is the eddy diffusion coefficient, V_S the settling speed of particles of volume v and f_v the volume mixing

ratio of the particles with volume v. The settling speed can be calculated from:

$$V_S(v) = \frac{2\rho g r^2}{9\eta} G_r, \qquad (C.10)$$

where ρ is the mass density of the aerosols, g the acceleration due to gravity and r the radius of the particle with volume v.

The particles for each size bin are considered as another species of the photochemical model that is described by equation (B.1) but with modified parameters for expressions (B.3)

$$C_1'(p,T) = \frac{D}{k_B T} V_S(v),$$

$$C_2'(p,T) = K\frac{p^2}{k_B T H} \qquad (C.11)$$

and the production and loss rates which are defined by the coagulation rate.

References

Ackermann, L., Hippler, H., Pagsberg, P., Reihs, C., Troe, J., 1990. Pulse radiolysis flash photolysis and shock wave study of the recombination H + benzyl → toluene at 300 and 1300–1650 K. J. Phys. Chem. 94, 5247–5251.

Adachi, H., Basco, N., James, D.G.L., 1980. Mutual interaction of the methyl and methylperoxy radicals studied by flash photolysis and kinetic spectroscopy. Int. J. Chem. Kinetics 12, 949–977.

Adam, L., Hack, W., Zhu, H., Qu, Z.-W., Schinke, R., 2005. Experiment and theoretical investigation of the reaction NH($X^3\Sigma^-$)+H(^{2}S) → N(^{4}S) + H$_2$($X^1\Sigma_g^+$). J. Chem. Phys. 122, 114301–114307.

Ahmed, M., Peterka, D.S., Suits, A.G., 1999. The photodissociation of the vinyl radical (C$_2$H$_3$) at 243 nm studied by velocity map imaging. J. Chem. Phys. 110, 4248–4253.

Aleksandrov, E.N., Arutyunov, V.S., Dubrovina, I.V., Kozlov, S.N., 1980. Study of the reaction of atomic hydrogen with allene. Kinet. Catal. 21, 1323–1326.

Aleksandrov, E.N., Vedeneev, V.I., Kozlov, S.N., Obvivalneva, A.A., Pryakhin, G.A., 1990. Rate constants and mechanism of the reactions of N(^{4}S) atoms with methane and ethane. Bull. Acad. Sci. URSS, Div. Chem. Sci. 39, 625.

Aleksandrov, E.N., Basevich, V.Y., Vedeneev, V.I., 1994. Initial act of nitrogen atoms interaction with H$_2$ in gas phase. Khim. Fiz. 13, 90–93.

Allamandola, L.J., Tielens, A.G.G.M., Barker, J.R., 1989. Interstellar polycyclic aromatic hydrocarbons: the infrared emission bands, the excitation/emission mechanism, and the astrophysical implications. Astrophys. J. Suppl. 71, 733–775.

Allen, C.W., 1976. Astrophysical Quantities. The Athlone Press, University of London.

Allen, M., Pinto, J.P., Yung, Y.L., 1980. Titan: aerosol photochemistry and variations related to the sunspot cycle. Astrophys. J. 242, L125–L128.

Arrington, C.A., Ramos, C., Robinson, A.D., Zwier, T.S., 1998. Aromatic ring-forming reactions of metastable diacetylene with 1,3-Butadiene. J. Phys. Chem. A 102, 3315–3322.

Atakan, B., Wolfrum, J., 1992. Kinetic studies of the reactions of CN radicals with alkanes in the temperature range between 294 and 1260 K. Chem. Phys. Lett. 186, 547–552.

Atkinson, D.B., Hudgens, J.W., 1999. Rate coefficients for the propargyl radical self-reaction and oxygen addition reaction measured using ultraviolet cavity ring-down spectroscopy. J. Phys. Chem. 103, 4242–4252.

Back, R.A., Winkler, C.A., 1954. The reaction of active nitrogen with butanes. Can. J. Chem 32.

Backx, C., Wight, G.R., Van der Wiel, M.J., 1976. Oscillator strengths (10–70 eV) for absorption, ionization and dissociation in H_2, HD and D_2, obtained by an electron-ion coincidence method. J. Phys. B: Atom. Mol. Phys. 9, 315–331.

Balucani, N., Asvany, O., Chang, A.H.H., Lin, S.H., Lee, Y.T., Kaiser, R.I., Bettinger, H.F., Schleyer, P.v.R., Schaefer, H.F., 1999. Crossed beam reaction of cyano radicals with hydrocarbon molecules. I. Chemical dynamics of cyanobenzene (C_6H_5CN; X^1A_1) and perdeutero cyanobenzene (C_6D_5CN; X^1A_1) formation from reaction of CN ($X^2\Sigma^+$) with benzene C_6H_6 (X^1A_{1g}) and d_6-benzene C_6D_6 (X^1A_{1g}). J. Chem. Phys. 111, 7457–7471.

Balucani, N., Cartechini, L., Alagia, M., Casavecchia, P., Volpi, G.G., 2000. Observation of nitrogen-bearing organic molecules from reactions of nitrogen atoms with hydrocarbons: a crossed beam study of $N(^2D)$ + ethylene. J. Phys. Chem. 104, 5655–5659.

Balucani, N., Mebel, A.M., Lee, Y.T., Kaiser, R.I., 2001. A combined crossed molecular beam and *ab initio* study of the reactions $C_2(X^1\Sigma_g^+, a^3\Pi_u) + C_2H_4 \rightarrow n - C_4H_3(X^2A') + H(^2S_{1/2})$. J. Phys. Chem. A 105, 9813–9818.

Banks, P.M., Kockarts, G., 1973. Aeronomy. Academic Press, NY.

Bar-Nun, A., Kleinfeld, I., Ganor, E., 1988. Shape and optical properties of aerosols formed by photolysis of acetylene, ethylene and hydrogen cyanide. J. Geophys. Res. 93, 8383–8387.

Baulch, D.L., Cobbs, C.J., Cox, R.A., Esser, C., Frank, P., Just, Th., Kerr, J.A., Pilling, M.J., Troe, J., Walker, R.W., Warnatz, J., 1992. Evaluated kinetic data for combustion modeling. J. Phys. Chem. Ref. Data 21, 411–734.

Baulch, D.L., Cobbs, C.J., Cox, R.A., Esser, C., Frank, P., Just, Th., Kerr, J.A., Pilling, M.J., Troe, J., Walker, R.W., Warnatz, J., 1994. Evaluated kinetic data for combustion modeling. Supplement I. J. Phys. Chem. Ref. Data 23, 847–1033.

Bauschlicher Jr., C.W., Ricca, A., 2000. Mechanisms for polycyclic aromatic hydrocarbon (PAH) growth. Chem. Phys. Lett. 326, 283–287.

Bénilan, Y., Andrieux, D., Khlifi, M., Bruston, P., Raulin, F., Guillemin, J.-C., Cossart-Magos, C., 1996. Temperature dependence of HC_3N, C_6H_2, and C_4N_2 mid-UV absorption coefficients: application to the interpretation of Titan's atmospheric spectra. Astrophys. Space Sci. 236, 85–95.

Bénilan, Y., Smith, N., Jolly, A., Raulin, F., 2000. The long wavelength range temperature variations of the mid-UV acetylene absorption coefficient. Planet. Space Sci. 48, 463–471.

Bergmann, K., Demtröder, W., 1968. Mass-spectrometric investigation of the primary processes in the photodissociation of 1,3-butadiene. J. Chem. Phys. 48, 18–22.

Blitz, M.A., Beasley, M.S., Pilling, M.J., Robertson, S.H., 2000. Formation of the propargyl radical in the reaction of $^1CH_2$ and C_2H_2: experiment and modelling. Phys. Chem. Chem. Phys. 2, 805–812.

Bocherel, P., Herbert, L.B., Rowe, B.R., Sims, I.R., Smith, I.W.M., Travers, D., 1996. Ultralow-temperature kinetics of CH(X2II) reactions: rate coefficients for reactions with O_2 and NO (T = 13−708 K), and with NH_3(T = 23−295 K). J. Phys. Chem. 100, 3063–3069.

Böhland, T., Temps, F., Wagner, H.Gg., 1985a. The contributions of intersystem crossing and reaction in the removal of $CH_2(\tilde{a}^1A_1)$ by hydrocarbons studied with the LMR. Ber. Bunsenges. Phys. Chem. 89, 1013–1018.

Böhland, T., Temps, F., Wagner, H.Gg., 1985b. Kinetics of the reactions between $CH_2(X^3B_1)$ radicals and saturated hydrocarbons in the temperature range 296–707 K. Ber. Bunsenges. Phys. Chem. 89, 1110.

Böland, T., Temps, F., Wagner, H.Gg., 1988. Kinetics of the reactions of CH2 (X 3B1)-radicals with C_2H_2 and C_4H_2 in the temperature range 296 K < T < 700 K. Symp. Int. Combust. Proc. 21, 841–850.

Borysow, A., Frommhold, L., 1986a. Collision induced rototranslational absorption spectra of $N_2 - N_2$ pairs for temperatures from 50 to 300 K. Astrophys. J. 311, 1043–1057.

Borysow, A., Frommhold, L., 1986b. Theoretical collision induced rototranslational absorption spectra for modeling Titan's atmosphere: $H_2 - N_2$ pairs. Astrophys. J. 303, 495–510.

Borysow, A., Frommhold, L., 1986c. Theoretical collision induced rototranslational absorption spectra for the outer planets: $H_2 - CH_4$ pairs. Astrophys. J. 304, 849–865.

Borysow, A., Frommhold, L., 1987. Collision induced rototranslational absorption spectra of $CH_4 - CH_4$ pairs at temperatures from 50 to 300 K. Astrophys. J. 318, 940–943.

Borysow, A., Tang, C., 1993. Far infrared CIA spectra of $N_2 - CH_4$ pairs for modeling of Titan's atmosphere. Icarus 105, 175–183.

Boudon, V., Champion, J.-P., Gabard, T., Loëte, M., Michelot, F., Pierre, G., Rotger, M., Wenger, Ch., Rey, M., 2004. Symmetry-adapted tensorial formalism to model rovibrational and rovibronic spectra of molecules pertaining to various point groups. J. Mol. Spectrosc. 228, 620–634.

Braun, W., McNesby, J.R., Bass, A.N., 1967. Flash photolysis of methane in the vacuum ultraviolet. II. Absolute rate constants for reactions of CH with methane, hydrogen and nitrogen. J. Chem. Phys. 46, 2071–2080.

Brown, R.L., 1973. A measurement of the rate of the reaction $N + H + M \rightarrow NH + M$. Int. J. Chem. Kinet. 5, 663–668.

Brownsword, R.A., Gatenby, S.D., Herbert, L.B., Smith, I.W.M., Stewart, D.W.A., Symonds, A.C., 1996. Kinetics of reactions between neutral free radicals Rate constants for the reaction of CH radicals with N atoms between 216 and 584 K. J. Chem. Soc. Faraday Trans. 92, 723–727.

Brownsword, R.A., Canosa, A., Rowe, B.R., Sims, I.R., Smith, I.W.M., Stewart, D.W.A., Symonds, A.C., Travers, D., 1997. Kinetics over a wide range of temperature (13–744 K): rate constants for the reactions of CH(n = 0) with H_2 and D_2 and for the removal of CH(n = 1) by H_2 and D_2. J. Chem. Phys. 106, 7662–7677.

Burton, G.R., Chan, W.F., Cooper, G., Brion, C.E., 1993. The electronic absorption spectrum of NH_3 in the valence shell discrete and continuum regions. Absolute oscillator-strengths for photoabsorption (5–200 eV). Chem. Phys. 177, 217–231.

Butler, J.E., Fleming, J.W., Goss, L.P., Lin, M.C., 1981. Kinetics of CH radical reactions with selected molecules at room temperature. Chem. Phys. 56, 355–365.

Butterfield, M.T., Yu, T., Lin, M.C., 1993. Kinetics of CN reactions with allene, butadiene, propylene and acrylonitrile. Chem. Phys. 169, 129–134.

Canosa, A., Sims, I.R., Travers, D., Smith, I.W.M., Rowe, B.R., 1997. Reactions of the methylidiyne radical with $CH_4, C_2H_2, C_2H_4, C_2H_6$, and but-1-ene studied between 23 and 295 K with a CRESU apparatus. Astron. Astrophys. 323, 644–651.

Capone, L.A., Dubach, J., Prasad, S.S., Whitten, R.C., 1983. Galactic cosmic rays and N_2 dissociation on Titan. Icarus 55, 73–82.

Carty, D., Le Page, V., Sims, I.R., Smith, I.W.M., 2001. Low temperature rate coefficients for the reactions of CN and C_2H radicals with allene ($CH_2 = C = CH_2$) and methylacetylene ($CH_3C = CH$). Chem. Phys. Lett. 344, 310–316.

Chan, W.F., Cooper, G., Sodhi, R.N.S., Brion, C.E., 1993. Absolute optical oscillator strengths for discrete and continuum photoabsorption of molecular nitrogen (11–200 eV). Chem. Phys. 170, 81–97.

Chang, A.H.H., Mebel, A.M., Yang, X.M., Lin, S.H., Lee, Y.T., 1998. Ab initio/RRKM approach toward the understanding of ethylene photodissociation. J. Chem. Phys. 109, 2748–2761.

Chang, Y.W., Wang, N.S., 1994. Rates of the reactions $CN + H_2CO$ and $NCO + H_2CO$ in the temperature range 294–769 K. Chem. Phys. 200, 431–437.

Chassefiere, E., Cabane, M., 1995. Two formation regions for Titan's hazes: indirect clues and possible synthesis mechanism. Planet. Space Sci. 43, 91–103.

Chastaing, D., James, P.L., Sims, I.R., Smith, I.W.M., 1998. Neutral-neutral reactions at the temperatures of interstellar clouds. Rate coefficients for reactions of C_2H radicals with O_2, C_2H_2, C_2H_4 and C_3H_6 down to 15 K. Faraday Disc. 109, 165–181.

Chastaing, D., Le Picard, S.D., Sims, I.R., Smith, I.W.M., 2001. Rate coefficients for the reactions of $C(^3P_J)$ atoms with C_2H_2, C_2H_4, CH_3C_2H and CH_2CCH_2 at temperatures down to 15 K. Astron. Astrophys. 365, 241–247.

Chen, F.Z., Wu, C.Y.R., 2004. Temperature-dependent photoabsorption cross sections in the VUV-UV region. I. Methane and ethane. J. Quant. Spectrosc. Radiat. Transfer 85, 195–209.

Chen, F.Z., Judge, D.L., Wu, C.Y.R., Caldwell, J., 1999. Low and room temperature photoabsorption cross sections of NH_3 in the UV region. Planet. Space Sci. 47, 261–266.

Chen, F.Z., Judge, D.L., Wu, C.Y.R., 2000. Temperature dependent photoabsorption cross sections of allene and methylacetylene in the VUV-UV region. Chem. Phys. 260, 215–223.

Clarke, D.W., Ferris, J.P., 1995. Photodissociation of cyanoacetylene: application to the atmospheric chemistry of Titan. Icarus 115, 119–125.

Clarke, D.W., Ferris, J.P., 1997. Titan haze: structure and properties of the cyanoacetylene and cyanoacetylene-acetylene photopolymers. Icarus 127, 158–172.

Clyne, M.A.A., Stedman, D.H., 1967. Rate of recombination of nitrogen atoms. J. Phys. Chem. 71, 3071–3073.

Cody, R.J., Romani, P.N., Nesbitt, F.L., Iannone, M.A., Tardy, D.C., Stief, L.J., 2003. Rate constant for the reaction $CH_3 + CH_3 \rightarrow C_2H_6$ at T = 155 K and model calculation of the CH_3 abundance in the atmospheres of Saturn and Neptune. J. Geophys. Res. 108, doi: 10.1029/2002JE002037.

Coll, P., Coscia, D., Gazeau, M.-C., de Vanssay, E., Guillemin, J.C., Raulin, F., 1995. Organic chemistry in Titan's atmosphere: new data from laboratory simulations at low temperature. Adv. Space Res. 16, 93–103.

Coll, P., Coscia, D., Gazeau, M.-C., Guez, L., Raulin, F., 1998. Review and latest results of laboratory investigations of Titan's aerosols. Origins Life Evol. Biosphere 28, 195–213.

Coll, P., Coscia, D., Smith, N., Gazeau, M.-C., Ramirez, S.I., Cernogora, G., Israël, G., Raulin, F., 1999. Experimental laboratory simulation of Titan's atmosphere: aerosols and gas phase. Planet. Space Sci. 47, 1331–1340.

Collin, G.J., 1988. Photochemistry of simple olefines: Chemistry of electronically excited states or hot ground state? Adv. Photochem. 14, 135–176.

Connors, R.E., Roebber, J.L., Weiss, K., 1974. Vacuum ultraviolet spectroscopy of cyanogen and cyanoacetylenes. J. Chem. Phys. 60, 5011–5024.

Cooper, G., Burton, G.R., Brion, C.E., 1995a. Absolute UV and soft X-ray photoabsorption of acetylene by high resolution dipole (e,e) spectroscopy. J. Electron. Spectrosc. 73, 139–148.

Cooper, G., Olney, T.N., Brion, C.E., 1995b. Absolute UV and soft X-ray photoabsorption of ethylene by high resolution dipole (e,e) spectroscopy. Chem. Phys. 194, 175–184.

Courtin, R., Wagener, R., McKay, C.P., Caldwell, J., Fricke, K.-H., Raulin, F., Bruston, P., 1991. UV spectroscopy of Titan's atmosphere, planetary organic chemistry and prebiological synthesis II. Interpretation of new IUE observations in the 220–335 nm range. Icarus 90, 43–56.

Coustenis, A., Bézard, B., Gautier, D., 1989. The gas composition of Titan's equatorial region. Icarus 80, 54–76.

Coustenis, A., Bézard, B., Gautier, D., Marten, A., Samuelson, R., 1991. Titan's Atmosphere from Voyager Infrared Observations. III. The vertical distributions of hydrocarbons and nitriles near Titan's north pole. Icarus 89, 152–167.

Coustenis, A., Lellouch, E., Maillard, J.P., McKay, C.P., 1995. Titan's surface: composition and variability from the near-infrared albedo. Icarus 118, 87–104.

Coustenis, A., Salama, A., Schulz, B., Ott, S., Lellouch, E., Encrenaz, Th., Gautier, D., Feuchtgruber, H., 2003. Titan's atmosphere from ISO mid-infrared spectroscopy. Icarus 161, 383–403.

Coustenis, A., and 24 co-authors, 2007. The composition of Titan's stratosphere from Cassini/CIRS mid-infrared spectra. Icarus 189 (1), 35–62.

Derecskei-Kovacs, A., North, S.W., 1999. The unimolecular dissociation of vinylcyanide: a theoretical investigation of a complex multichannel reaction. J. Chem. Phys. 110, 2862–2871.

Diau, E.W., Lin, M.C., 1994. A theoretical study of the $CH_3 + C_2H_2$ reaction. J. Chem. Phys. 101, 3923–3927.

Dimitrov, V., Bar-Nun, A., 2002. Aging of Titan's aerosols. Icarus 156, 530–538.

Dobe, S., Oehlers, C., Temps, F., Wagner, H.Gg., Ziemer, H., 1994. Observations of an H/D-isotope exchange channel in the reaction $D + H_2CO$. Ber. Bunsenges. Phys. Chem. 98, 754–757.

Dransfeld, P., Wagner, H.Gg., 1987. Investigation of the gas phase reaction $N + NH_2 \rightarrow N_2 + 2H$ at room temperature. Z. Phys. Chem. (Munich) 153.

Duràn, R.P., Amorebieta, V.T., Colussi, A.J., 1988. Is the homogeneous thermal dimerization of acetylene a free-radical chain reaction? Kinetic and thermochemical analysis. J. Phys. Chem. 92, 636–640.

Eden, S., Limão-Vieira, P., Kendall, P., Mason, N.J., Hoffmann, S.V., Spyrou, S.M., 2003. High resolution photo-absorption studies of acrylonitrile C_2H_3CN and acetonitrile CH_3CN. Eur. Phys. J. D 26, 201–210.

Ehrenfreund, P., Boon, J.J., Commandeur, J., Sagan, C., Thompson, W.R., Khare, B., 1995. Analytical pyrolysis experiments of Titan aerosol analogues in preparation for the Cassini-Huygens mission. Adv. Space Res. 15, 335–342.

Eshleman, V.R., Lindal, G.F., Tyler, G.L., 1983. Is Titan wet or dry? Science 22, 53–55.

Fagerstrom, K., Jodkowski, J.T., Lund, A., Ratajczak, E., 1995. Kinetics of the self-reaction and the reaction with OH of the amidogen radical. Chem. Phys. Lett. 236, 103–110.

Fahr, A., 2003. Ultraviolet absorption spectrum and cross-sections of ethynyl (C_2H) radicals. J. Molec. Spectr. 217, 249–254.

Fahr, A., Nayak, A.K., 1994. Temperature dependent ultraviolet absorption cross sections of 1,3-butadiene and butadiyne. Chem. Phys. 189, 725–731.

Fahr, A., Nayak, A., 1996. Temperature dependent ultraviolet absorption cross section of propylene, methylacetylene and vinylacetylene. Chem. Phys. 203, 351–358.

Fahr, A., Stein, S.E., 1989. Reactions of vinyl and phenyl radicals with ethyne, ethene, and benzene. In: 22nd International Symposium on Combustion. The Combustion Institute, Pittsburgh, p. 1023.

Fahr, A., Laufer, A., Klein, R., Braun, W., 1991. Reaction rate determinations of vinyl radical reactions with vinyl, methyl, and hydrogen atoms. J. Phys. Chem. 95, 3218–3224.

Fahr, A., Hassanzadeh, P., Laszlo, B., Huie, R.E., 1997. Ultraviolet absorption and cross sections of propargyl (C_3H_3) radicals in the 230–300 nm region. Chem. Phys. 215, 59–66.

Fahr, A., Hassanzadeh, P., Atkinson, D.B., 1998. Ultraviolet absorption spectrum and cross-sections of vinyl (C_2H_3) radical in the 225–238 nm region. Chem. Phys. 236, 43–51.

Fennelly, J.A., Torr, D.G., 1992. Photoionization and photoabsorption cross sections of O, N_2, O_2, and N for aeronomic calculations. Atom. D. Nucl. D. Tables 51, 321–363.

Flasar, F.M., 44 co-authors, 2005. Titan's atmospheric temperatures winds and composition. Science 308, 975–978.

Frederick, J.E., Rusch, D.W., 1977. On the chemistry of metastable atomic nitrogen in the F region deducted from simultaneous satellite measurements of the 5200 Å airglow and atmospheric composition. J. Geophys. Res. 82, 3509–3517.

Fuchs, N.A., 1964. The Mechanics of Aerosols. Pergamon Press, Oxford.

Fulcignoni, M., 42 coworkers, 2005. In situ measurements of the physical characteristics of Titan's environment. Nature, doi:10.1038/nature04314.

Fulle, D., Hippler, H., 1996. The high-pressure range of the reaction of $CH(^2\Pi)$ with N_2. J. Chem. Phys. 105, 5423–5430.

Fulle, D., Hippler, H., 1997. The temperature and pressure dependence of the reactions $CH + H_2 \Leftrightarrow CH_3 \Leftrightarrow CH_2 + H$. J. Chem. Phys. 106, 8691–8698.

Gardner, E.P., McNesby, J.R., 1982. Vacuum-ultraviolet photolysis of methylamine. J. Phys. Chem. 86, 2646–2651.

Garland, L.J., Bayes, K.D., 1990. Rate constants for some radical-radical cross sections and the geometric rule. J. Phys. Chem. 94, 4941–4945.

Garrett, B.C., Koszykowski, M.L., Melius, C.F., Page, M., 1990. Theoretical calculations of the thermal rate constants for the gas-phase chemical reactions $H + NH_3 \rightarrow H_2 + NH_2$ and $D + ND_3 \rightarrow D_2 + ND_2$. J. Phys. Chem. 94, 7096–7106.

Ge, S.-H., Cheng, X.-L., Yang, X.-D., Liu, Z.-J., Wang, W., 2006. Calculations of the thermochemistry of six reactions leading to ammonia formation in Titan's atmosphere. Icarus 183, 153–158.

von Gehring, M., Hoyermann, K., Wagner, H.Gg., Wolfrum, J., 1971. Die reaktion von atomaren wasserstoff mit hydrazin. Ber. Bunsenges. Phys. Chem. 75.

Gladstone, G.R., Allen, M., Yung, Y.L., 1996. Hydrocarbon photochemistry in the upper atmosphere of Jupiter. Icarus 119, 1–52.

Glicker, S., Okabe, H., 1987. Photochemistry of diacetylene. J. Phys. Chem. 91, 437–440.

Gueymard, C.A., 2004. The sun's total and spectral irradiance for solar energy applications and solar radiation models. Solar Energy 76, 423–453.

Hack, W., Wagner, H.Gg., Zaspypkin, A., 1994. Elementary reactions of $NH(a^1\Delta)$ and $NH(X^3\Sigma)$ with N, O and NO. Bunsenges. Phys. Chem. 98, 156–164.

Haider, N., Husain, D., 1993. Absolute rate data for the reactions of ground-state atomic carbon, C[2p2(3PJ)], with alkenes investigated by time-resolved atomic resonance absorption spectroscopy in the vacuum ultraviolet. J. Chem. Soc. Faraday Trans. 89, 7–14.

Halberstadt, M.L., Crump, J., 1973. Insertion of methylene into the carbonhydrogen bonds of the C_1 to C_4 alkanes. J. Photochem. 1, 295.

Halpern, J.B., Miller, G.E., Okabe, H., 1989. The reaction of CN radicals with cyanoacetylene. Chem. Phys. Lett. 155, 347–350.

Hampson, R.F., McNesby, J.R., 1965. Vacuum-ultraviolet photolysis of ethane at high temperature. J. Chem. Phys. 42, 2200–2208.

Hanning-Lee, M.A., Pilling, M.J., 1992. Kinetics of the reaction between H atoms and allyl radicals. Int. J. Chem. Kinetics 24, 271–278.

Harding, L.B., Guadagnini, R., Schatz, G.C., 1993. Theoretical studies of the reactions $H + CH \rightarrow C + H_2$ and $C + H_2 \rightarrow CH_2$ using an ab initio global ground-state potential surface for CH_2. J. Phys. Chem. 97, 5472–5481.

Harding, L.B., Georgievskii, Y., Klippenstein, S.J., 2005. Predictive theory for hydrogen atom—hydrocarbon radical association kinetics. J. Phys. Chem. A. 109, 4646–4656.

Hartmann, J-M., Boulet, C., Brodbeck, C., van Thanh, N., Fouchet, T., Drossart, P., 2002. A far wing lineshape for H_2 broadened CH_4 infrared transitions. J. Quant. Spectrosc. Radiat. Transfer 72, 117–122.

Hatzianastassiou, N., Fotiadi, A., Matsoukas, C., Drakakis, E., Pavlakis, K.G., Hatzidimitriou, D., Vardavas, I.M., 2004. Long-term global distribution of Earth's shortwave radiation budget at the top of the atmosphere. Atmos. Chem. Phys. 4, 1217–1235.

Hatzianastassiou, N., Matsoukas, C., Fotiadi, A., Pavlakis, K.G., Drakakis, E., Hatzidimitriou, D., Vardavas, I.M., 2005. Global distribution of Earth's surface shortwave radiation budget. Atmos. Chem. Phys. 5, 2847–2867.

Heckmann, E., Hippler, H., Troe, J., 1996. High-temperature reactions and thermodynamic properties of phenyl radicals. Symp. Int. Combust. Proc. 26, 543–550.

Herron, J.T., 1999. Evaluated chemical kinetics data for reactions of $N(^2D)$, $N(^2P)$, and $N_2(A^3\Sigma_u^+)$ in the gas phase. J. Phys. Chem. Ref. Data 28, 1453–1483.

Hess, W.P., Durant Jr., J.L., Tully, F.P., 1989. Kinetic study of the reactions of CN with ethane and propane. J. Phys. Chem. 93, 6402–6407.

Ho, G.H., Lin, M.S., Wang, Y.L., Chang, T.W., 1998. Photoabsorption and photoionization of propyne. J. Chem. Phys. 109, 5868–5879.

Holland, D.M.P., Shaw, D.A., Hayes, M.A., Shpinkova, L.G., Rennie, E.E., Karlsson, L., Baltzer, P., Wannberg, B., 1997. A photoabsorption, photodissociation and photoelectron spectroscopy study of C_2H_4 and C_2D_4. Chem. Phys. 219, 91–116.

Hoobler, R.J., Leone, S.R., 1997. Rate coefficients for reactions of ethynyl radical (C_2H) with HCN and CH_3CN: implications for the formation of complex nitriles on Titan. J. Geophys. Res. 102, 28717–28723.

Hoobler, R.J., Leone, S.R., 1999. Low temperature rate coefficients for reactions of the ethynyl radical (C_2H) with C_3H_4 isomers methylacetylene and allene. J. Phys. Chem. 103, 1342–1346.

Hoobler, R.J., Opansky, B.J., Leone, S.R., 1997. Low-temperature rate coefficients for the reactions of ethynyl radical (C_2H) with propane, isobutane, n-Butane, and neopentane. J. Phys. Chem. A 101, 1338–1342.

Horne, D.G., Norrish, R.G.W., 1970. The photolysis of acyclic azines and the electronic spectra of R_1R_2CN radicals. Proc. R. Soc. London A 315.

Huang, C.S., Zhu, Z.Q., Xin, Y., Pei, L.S., Chen, C.X., Chen, Y., 2004. Kinetics of $C_2(a^3\Pi_u)$ radical reactions with alkanes by LIF. J. Chem. Phys. 120, 2225–2229.

Huang, L.C.L., Lee, Y.T., Kaiser, R.I., 1999. Crossed beam reaction of the cyanogen radical, $CN(X^2\Sigma^+)$, with acetylene, $C_2H_2(X^1\Sigma_g^+)$: observation of cyanoacetylene, $HCCCN(X^1\Sigma^+)$. J. Chem. Phys. 110, 7119–7122.

Hubin-Franskin, M.-J., Delwiche, J., Giuliani, A., Ska, M.-P., Motte-Tollet, F., Walker, I.C., Mason, N.J., Gingell, J.M., Jones, N.C., 2002. Electronic excitation and optical cross sections of methylamine and ethylamine in the UV-VUV spectral region. J. Chem. Phys. 116, 9261–9268.

Hudgins, D.M., Bauschlicher, C.W., Allamandola, L.J., 2005. Variation in the peak position of the 6.2 μm interstellar emission future: a tracer of N in the interstellar polycyclic aromatic hydrocarbon population. Astrophys. J. 632, 316–332.

Hudson, R.D., 1971. Critical review of ultraviolet photoabsorption cross sections for molecules of astrophysical and aeronomic interest. Rev. Geophys. Space Phys. 9, 305–406.

Husain, D., Ioannou, A.X., 1997. Reactions of atomic carbon, C[2p2(3PJ)], with dienes and diynes investigated by time-resolved atomic resonance absorption spectroscopy in the vacuum ultraviolet. J. Chem. Soc. Faraday Trans. 93, 3625–3629.

Husain, D., Kirsch, L.J., 1971. Reactions of atomic carbon by kinetic absorption spectroscopy in the vacuum ultraviolet. Trans. Faraday Soc. 67, 2025.

Husain, D., Young, A.N., 1975. Kinetic investigation of ground-state carbon atoms. J. Chem. Soc. Faraday Trans. 71, 525.

Imanaka, H., Khare, B.N., Elsila, J.E., Bakes, E.L.O., McKay, C.P., Cruikshank, D.P., Sugita, S., Matsui, T., Zare, R.N., 2004. Laboratory experiments of Titan tholin formed in cold plasma at various pressures: implications for nitrogen-containing polycyclic aromatic compounds in Titan haze. Icarus 168, 344–366.

Irwin, P.G.J., Sromovsky, L.A., Strong, E.K., Sihra, K., Teanby, N.A., Bowles, Calcutt, S.B., Remedios, J.J., 2005. Improved near-infrared methane band models and k-distribution parameters from 2000 to $9500\,cm^{-1}$ and implications for the interpretations of outer planet spectra. Icarus 181, 309–319.

Israël, G., and 21 coworkers, 2005. Complex organic matter in Titan's atmospheric aerosols from in situ pyrolysis and analysis. Nature, doi: 10.1038/nature04349.

Jackson, W.M., Anex, D.S., Continetti, R.E., Balko, B.A., Lee, Y.T., 1991. Molecular beam studies of the photolysis of allene and the secondary photodissociation of the C_3H_x fragments. J. Chem. Phys. 95, 7327–7336.

Jacobs, T.A., Giedt, R.R., Cohen, N., 1965. Kinetics of decomposition of HF in shock waves. J. Chem. Phys. 43.

Jamieson, J.W.S., Brown, G.R., Tanner, J.S., 1970. The reaction of atomic hydrogen with methyl cyanide. Can. J. Chem. 48, 3619–3622.

Jodkowski, J.T., Ratajczak, E., Fagerstrom, K., Lund, A., Stothard, N.D., Humpfer, R., Grotheer, H.-H., 1995. Kinetics of the cross reaction between amidogen and methyl radicals. Chem. Phys. Lett. 240, 63–71.

Joseph, J.H., Wiscombe, W.J., Weinman, J.A., 1976. The Delta–Eddington approximation or radiative flux transfer. J. Atmos. Sci. 33, 2452–2459.

Kameta, K., Machida, S., Kitajima, M., Ukai, M., Kouchi, N., Hatano, Y., Ito, K., 1996. Photoabsorption, photoionization, and neutral-dissociation cross sections of C_2H_6 and C_3H_8 in the extreme-uv region. J. Electron. Spectrosc. 79, 391–393.

Kameta, K., Kouchi, N., Ukai, M., Hatano, Y., 2002. Photoabsorption, photoionization and neutral-dissociation cross sections of simple hydrocarbons in the vacuum ultraviolet range. J. Quant. Spectrosc. Radiat. Transfer 123, 225–238.

Karkoschka, E., 1994. Spectrophotometry of the Jovian planets and Titan at 300 to 1000 nm wavelength: the methane spectrum. Icarus 111, 174–192.

Kassner, Ch., Stuhl, F., 1994. The VUV photodissociation $CH_3 \rightarrow CH(A^2\Delta$ and $B^2\Sigma^-) + H_2$. Chem. Phys. Lett. 222, 425–430.

Keller, C.N., Cravens, T.E., Gan, L., 1992. A model of the ionosphere of Titan. J. Geophys. Res. 97, 12117–12135.

Kerr, J.A., Parsonage, M.J., 1972. Evaluated Kinetic Data on Gas-phase Addition Reactions: Reactions of Atoms and Radicals with Alkenes, Alkynes, and Aromatic Compounds. Butterworth, London.

Khare, B.N., Sagan, C., Arakawa, E.T., Suits, F., Calcott, T.A., Williams, M.W., 1984a. Optical constants of organic tholins produced in a simulated Titanian atmosphere: from soft X-ray to microwave frequencies. Icarus 60, 127–137.

Khare, B.N., Sagan, C., Thompson, W.R., Arakawa, E.T., Suits, F., Callcott, T.A., Williams, M.W., Shrader, S., Ogino, H., Willingham, T.O., Nagy, B., 1984b. The organic aerosols of Titan. Adv. Space Res. 4, 59–68.

Khare, B.N., Sagan, C., Thompson, W.R., Arakawa, E.T., Meese, C., Tuminello, P.S., 1994. Optical properties of poly-HCN and their astronomical applications. Can. J. Chem. 72, 678–694.

Khare, B.N., Bakes, E.L.O., Imanaka, H., McKay, C.P., Cruikshank, D.P., Arakawa, E.T., 2002. Analysis of the time-dependent chemical evolution of Titan haze tholin. Icarus 160, 172–182.

Kinsman, A.C., Roscoe, J.M., 1994. A kinetic analysis of the photolysis of mixtures of acetone and propylene. Int. J. Chem. Kinetics 26, 191–200.

Kley, D., Washida, N., Groth, W., 1974. Mechanism of CN* production in flames of active nitrogen with cyanogen. Ber. Bunsenges. Phys. Chem. 78, 205.

Kloster-Jensen, E., Haink, H.-J., Christen, H., 1974. The electronic spectra of unsubstituted mono- to penta- acetylene in the gas phase and in solution in the range 1100 to 4000 Å. Helvetica Chimica Acta 57, 1731–1744.

Koizumi, H., Yoshimi, T., Shinsaka, K., Ukai, M., Morita, M., Hatano, Y., Yagishita, A., Ito, K., 1985. VUV-optical oscillator strength distributions of C_3H_6 and C_4H_8 isomers. J. Chem. Phys. 82, 4856–4861.

Knyazev, V.D., Slagle, I.R., 1996. Unimolecular decomposition of n-C4H9 and iso-C4H9 radicals. J. Phys. Chem. 100, 5318–5328.

Knyazev, V.D., Slagle, I.R., 2001a. Kinetics of the reaction of allyl and propargyl radicals with CH_3. J. Phys. Chem. A 105, 3196–3204.

Knyazev, V.D., Slagle, I.R., 2001b. Kinetics for the reactions of n-alkyl (C_2H_5, n-C_3H_7, and n-C_4H_9) radicals with CH_3. J. Phys. Chem. A 105, 6490–6498.

Knyazev, V.D., Bencsura, A., Stoliarov, S.I., Slagle, I.R., 1996. Kinetics of the $C_2H_3 + H_2 \leftrightarrows H + C_2H_4$ and $CH_3 + H_2 \leftrightarrows H + CH_4$ reactions. J. Phys. Chem. 100, 11346–11354.

Kraus, H., Oehlers, C., Temps, F., Wagner, H.Gg., Wolf, M., 1993. Rate constants for the reactions of $CH_2(X^3B_1)$ with selected alkenes at temperatures between 296 and 728 K. Ber. Bunsenges. Phys. Chem. 97, 545–553.

Kuiper, G.P., 1944. Titan: a satellite with an atmosphere. Astrophys. J. 100, 378–383.

Langford, A.O., Petek, H., Moore, C.B., 1983. Collisional removal of $CH_2(^1A_1)$: absolute rate constants for atomic and molecular collisional partners at 295 K. J. Chem. Phys. 78, 6650–6659.

Lara, L.M., Lellouch, E., Lopez-Moreno, J., Rodrigo, R., 1996. Vertical distribution of Titan's atmospheric neutral constituents. J. Geophys. Res. 101, 23261–23283.

Laufer, A.H., Fahr, A., 2004. Reactions and kinetics of unsaturated C_2 hydrocarbon radicals. Chem. Rev. 104, 2813–2832.

Laufer, A.H., Gardner, E.P., Kwok, T.L., Yung, Y.L., 1983. Computations and estimates of rate coefficients for hydrocarbon reactions of interest to the atmospheres of the outer solar system. Icarus 56, 560–567.

Lebonnois, S., 2005. Benzene and aerosol production in Titan and Jupiter's atmospheres: a sensitivity study. Planet. Space Sci. 53, 486–497.

Lebonnois, S., Toublanc, D., Hourdin, F., Rannou, P., 2001. Seasonal variations of Titan's atmospheric composition. Icarus 152, 384–406.

Lebonnois, S., Bakes, E.L.O., McKay, C.P., 2002. Transition from gaseous compounds to aerosols in Titan's atmosphere. Icarus 159, 505–517.

Lee, A.Y.T., Yung, Y.L., Cheng, B., Bahou, M., Chung, C., Lee, Y., 2001. Enhancement of deuterated ethane on Jupiter. Astrophys. J. 551, 93–96.

Lee, L.C., 1980. CN($A^2\Pi_i \rightarrow X^2\Sigma^+$) and CN($B^2\Sigma^+ \rightarrow X^2\Sigma^+$) yields from HCN photodissociation. J. Chem. Phys. 72, 6414–6421.

Lee, S.-H., Lee, Y.T., Yang, X., 2004. Dynamics of photodissociation of ethylene and its isotopomers at 157 nm: branching ratios and kinetic-energy distributions. J. Chem. Phys. 120, 10983–10991.

Lellouch, E., Coustenis, A., Gautier, D., Raulin, F., Dubouloz, N., Frere, C., 1989. Titan's atmosphere and hypothesized ocean–a reanalysis of the Voyager 1 radio-occultation and IRIS 7.7 μm data. Icarus 79, 328–349.

Lellouch, E., Romani, P.N., Posenqvist, J., 1994. The vertical distribution and origin of HCN in Neptune's atmosphere. Icarus 108, 112–136.

Lemaire, P., Emerich, C., Vial, J.-C., Curdt, W., Schühle, U., Wilhelm, K., 2005. Variation of the full sun hydrogen lyman profiles through solar cycle 23. Adv. Space Res. 35, 384–387.

Lias, S.G., Collin, G.J., Rebbert, R.E., Ausloos, P., 1970. Photolysis of ethane at 116–118 eV. J. Chem. Phys. 52, 1841–1851.

Lindal, G.F., Wood, G.E., Hotz, H.B., Sweetnam, D.N., Eshleman, V.R., Tyler, G.L., 1983. The atmosphere of Titan: an analysis of the Voyager 1 radio occultation measurements. Icarus 53, 348–363.

Lungard, R., Heicklen, J., 1984. Pyrolysis of vinylacetylene between 300 and 450 °C. Int. J. Chem. Kinetics 16, 125–148.

Manabe, S., Wetherland, R.T., 1967. Thermal equilibrium of the atmosphere with a given distribution of relative humidity. J. Atmos. Sci. 24, 241–259.

Mantei, K.A., Bair, E.J., 1968. Reactions of nitrogen-hydrogen radicals. III. Formation and disappearance of NH radicals in the photolysis of ammonia. J. Chem. Phys. 49, 3248–3256.

Marston, G., Nesbitt, F.L., Stief, L.J., 1989. Branching ratios in the N + CH_3 reaction: formation of the methylene amidogen (H_2CN) radical. J. Chem. Phys. 91, 3483–3491.

Martinotti, F.F., Welch, M.J., Wolf, A.P., 1968. The reactivity of thermal carbon atoms in the gas phase. Chem. Commun. 3, 115.

Mason, E.A., Marreno, T.R., 1970. The diffusion of atoms and molecules. In: Bates, D.R., Esterman, I. (Eds.), Advances in Atomic and Molecular Physics. Academic, San Diego, Calif., pp. 155–232.

McDonald, G.D., Thompson, W.R., Heinrich, M., Khare, B.N., Sagan, C., 1994. Chemical investigation of Titan and Triton tholins. Icarus 108, 137–145.

McEwan, M.J., Phillips, L.F., 1975. Chemistry of the Atmosphere. Edward Arnold ISBN: 0713124776.

McKay, C.P., 1996. Elemental composition, solubility and optical properties of Titan's organic haze. Planet. Space Sci. 44, 741–747.

McKay, C.P., Pollack, J.B., Courtin, R., 1989. The thermal structure of Titan's atmosphere. Icarus 80, 23–53.

McKay, C.P., Pollack, J.B., Courtin, R., 1991. The greenhouse and antigreenhouse effects on Titan. Science 253, 1118–1121.

McKay, C.P., Coustenis, A., Samuelson, R.E., Lemmon, M.T., Lorenz, R.D., Cabane, M., Rannou, P., Drossart, P., 2001. Physical properties of the organic aerosols and clouds on Titan. Planet. Space Sci. 49, 79–99.

McKellar, A.R.W., 1989. The spectrum of gaseous methane at 77 K in the 1.1–2.6 μm region: A benchmark for planetary astronomy. 1–2.6 μm region: A benchmark for planetary astronomy. Can. J. Phys. 67, 1027–1035.

Mebel, A.M., Lin, M.C., 1999. Prediction of absolute rate constant for the reaction of NH_2 with alkanes from ab initio G2M/TST calculations. J. Phys. Chem. A 103, 2088–2096.

Mebel, A.M., Lin, M.C., Yu, T., Morokuma, K., 1997. Theoretical study of potential energy surface and thermal rate constants for the C_6H_5 + H_2 and C_6H_6 + H reactions. J. Phys. Chem. A 101, 3189–3196.

Mebel, A.M., Hayashi, M., Jackson, W.M., Wrobel, J., Green, M., Xu, D., Lin, S.H., 2001. Branching ratios of C_2 products in the photodissociation of C_2H at 193 nm. J. Chem. Phys. 114, 9821–9831.

Monks, P.S., Romani, P.N., Nesbitt, F.L., Scanlon, M., Stief, L.J., 1993. The kinetics of the formation of nitrile compounds in the atmosphere of Titan and Neptune. J. Geophys. Res. 98, 17115–17122.

Monks, P.S., Nesbitt, F.L., Payne, W.A., Scanlon, M., Stief, L.J., Shallcross, D.E., 1995. Absolute rate constants and product branching ratios for the reaction between H and C_2H_3 at T = 213 and 298 K. J. Phys. Chem. 99, 17151–17159.

Mordaunt, D.H., Lambert, I.R., Morley, G.P., Ashfold, N.R., Dixon, R.N., Western, C.M., Schnieder, L., Welge, K.H., 1993. Primary product channels in the photodissociation of methane at 121.6 nm. J. Chem. Phys. 98, 2054–2065.

Morter, C.L., Farhat, S.K., Adamson, J.D., Glass, G.P., Curl, R.F., 1994. Rate constant measurement of the recombination reaction C_3H_3 + C_3H_3. J. Phys. Chem. 98, 7029–7035.

Moses, J.I., Bézard, B., Lellouch, E., Gladstone, G.R., Feuchtgruber, H., Allen, M., 2000. Photochemistry of Saturn's Atmosphere: I. Hydrocarbon Chemistry and Comparisons with ISO Observations. Icarus 143, 244–298.

Moses, J.I., Fouchet, T., Bézard, B., Gladstone, G.R., Lellouch, E., Feuchtgruber, H., 2005. J. Geophys. Res. 110, E08001, doi: 10.1029/2005JE002411.

Mullen, C., Smith, M.A., 2005. Low temperature H radical reactions with NO, saturated and unsaturated hydrocarbons studied in a pulsed supersonic Laval nozzle flow reactor between 53 and 188 K. J. Phys. Chem. 109, 1391–1399.

Munk, J., Pagsberg, P., Ratajczak, E., Sillesen, A., 1986a. Spectrokinetic studies of ethyl and ethylperoxy radicals. J. Phys. Chem. 90, 2752–2757.

Munk, J., Pagsberg, P., Ratajczak, E., Sillesen, A., 1986b. Spectrokinetic studies of i-C_3H_7 and i-$C_3H_7O_2$ radicals. Chem. Phys. Lett. 132.

Münzel, N., Schweig, A., 1988. UV/VIS absorption spectrum, geometry and electronic structure of transient o-Benzyne. Chem. Phys. Lett. 147, 192–194.

Murhpy, J.E., Vakhtin, A.B., Leone, S.R., 2003. Laboratory kinetics of C_2H radical reactions with ethane propane and n-butane at T = 96–296 K: implications for Titan. Icarus 163, 175–181.

Nakayama, T., Watanabe, K., 1964. Absorption and photoionization coefficients of acetylene, propyne and 1-butyne. J. Chem. Phys. 40, 558–561.

Nava, D.F., Mitchell, M.B., Stief, L.J., 1986. The reaction H + C_4H_2: Absolute rate constant measurement and implication for atmospheric modeling of Titan. J. Geophys. Res. 91, 4585–4589.

Nesbitt, F.L., Marston, G., Stief, L.J., 1990. Kinetic studies of the reactions of H_2CN and D_2CN radicals with N and H. J. Phys. Chem. 94, 4946–4951.

Nguyen, M.T., Sengupta, D., Ha, T.-K., 1996. Another look at the decomposition of methyl azide and methanimine: how is HCN formed? J. Phys. Chem. 100, 6499–6503.

Nicholas, J.E., Spiers, A.I., Matin, N.A., 1986. Kinetics and mechanism in the decomposition of NH_3 in a radio-frequency pulse discharge. Plasma Chem. Plasma Process. 6.

Nicolas, C., Alcaraz, C., Thissen, R., Vervloet, M., Dutuit, O., 2003. Dissociative photoionization of N_2 in the 24–32 eV photon energy range. J. Phys. B: At. Mol. Phys. 36, 2239–2251.

Niemann, H.B., and 17 co-authors, 2005. The abundance of constituents of Titan's atmosphere from the GCMS instrument on the Huygens probe. Nature doi:10.1038/nature04122.

Nizamov, B., Dagdigian, P.J., 2003. Spectroscopic and kinetic investigation of methylene amidogen by cavity ring-down spectroscopy. J. Phys. Chem. A 107, 2256–2263.

Nizamov, B., Leone, S.R., 2004. Kinetics of C_2H reactions with hydrocarbons and nitriles in the 104–296 K temperature range. J. Phys. Chem. A. 108, 1746–1752.

Nuth, J.A., Glicker, S., 1982. The vacuum ultraviolet spectra of HCN, C_2N_2, and CH_3CN. J. Quant. Spectrosc. Radiat. Transfer 28, 223–231.

Obi, K., Akimoto, H., Ogata, Y., Tanaka, I., 1971. Photolyses of propane, n-Butane, and Cyclobutane at Xe and Kr resonance lines. J. Chem. Phys. 55, 3822–3828.

Okabe, H., 1978. Photochemistry of small molecules. Wiley, New York.

Okabe, H., 1981. Photochemistry of acetylene at 1470 A. J. Chem. Phys. 75, 2772–2778.

Okabe, H., 1983. Photochemistry of acetylene. Can. J. Chem. 61, 850–855.

Okabe, H., Becker, D.A., 1963. Vacuum ultraviolet photochemistry. VII. J. Chem. Phys. 39, 2549–2555.

Onyszchuk, M., Breitman, L., Winkler, C.A., 1953. The reaction of active nitrogen with propane. Can. J. Chem. 32.

Opansky, B.J., Leone, S.R., 1996a. Low-temperature rate coefficients of C_2H with CH_4 and CD_4 from 154 to 359 K. J. Phys. Chem. 100, 4888–4892.

Opansky, B.J., Leone, S.R., 1996b. Rate coefficients of C_2H with C_2H_4, C_2H_6, and H_2 from 150 to 359 K. J. Phys. Chem. 100, 19904–19910.

Pagsberg, P.B., Eriksen, J., Christensen, H.C., 1979. Pulse radiolysis of gaseous ammonia-oxygen mixtures. J. Phys. Chem. 83, 582–590.

Park, J., Burova, S., Rodgets, A.S., Lin, M.C., 1999. Experimental and theoretical studies of the C_6H_5 + C_6H_6 reaction. J. Phys. Chem. 103, 9036–9041.

Parker, J.K., Payne, W.A., Cody, R.J., Stief, L.J., 2004. Kinetics of the reaction of atomic hydrogen with cyanoacetylene from T = 200 to 298 K. J. Phys. Chem A 108, 1938–1945.

Pavlakis, K.G., Hatzidimitriou, D., Matsoukas, C., Drakakis, E., Hatzianastassiou, N., Vardavas, I.M., 2004. Ten-year global distribution of down-welling longwave radiation. Atmos. Chem. Phys. 4, 127–142.

Payne, W.A., Monks, P.S., Nesbitt, F.L., Stief, L.J., 1996. The reaction between N(^{4}S) and C_2H_3: rate constant and primary reaction channels. J. Chem. Phys. 104, 9808–9815.

Peeters, J., Boullart, W., Langhans, I., 1994. Branching ratio of the C_2H_2 + O reaction at 290 K from kinetic modelling of relative methylene concentration versus time profiles in C_2H_2/O/H systems. Int. J. Chem. Kinet. 26, 869–886.

Petrie, S., Osamura, Y., 2004. NCCN and NCCCCN formation in Titan's atmosphere: 2. HNC as a viable precursor. J. Phys. Chem. A 108, 3623–3631.

Petrishchev, V.A., Sapozhkov, A.Yu., 1981. Rate constant of the N + H_2 reaction. Kinetics Catal. 22.

Pilling, M.J., Bass, A.M., Braun, W., 1971. Oscillator strengths of CH_2 and CH_3 in the vacuum ultraviolet. Chem. Phys. Lett. 9, 147–148.

Pitts, W.M., Pasternack, L., McDonald, J.R., 1982. Temperature dependence of the $C_2(X^1S_g^+$ and a $^3\Pi_u$ equilibrated states) with O_2. Chem. Phys. 68, 417–422.

Pruppacher, H.R., Klett, J.D., 1978. Microphysics of clouds and precipitation. Reidel Publishing Company, Dordrecht.

Ramanathan, V., Coakley, J.A., 1978. Climate modeling through radiative-convective models. Rev. Geophys. Space Phys. 16, 465–490.

Ramirez, S.I., Coll, P., da Silva, A., Navarro-Gonzalez, R., Lafait, J., Raulin, F., 2002. Complex refractive index of Titan's aerosol analogues in the 200–900 nm domain. Icarus 156, 515–529.

Rannou, P., Cabane, M., Chassefiere, E., Botet, R., McKay, C.P., Courtin, R., 1995. Titan's geometric albedo: role of the fractal structure of the aerosols. Icarus 118, 355–372.

Rannou, P., Cabane, M., Botet, R., Chassefiere, E., 1997. A new interpretation of scattered light measurements at Titan's limb. J. Geophys. Res. 102, 10997–11014.

Rannou, P., McKay, C.P., Lorenz, R.D., 2003. A model of Titan's haze of fractal aerosols constrained by multiple observations. Planet. Space Sci. 51, 963–976.

Rages, K., Pollack, J.B., 1980. Titan aerosols: optical properties and vertical distribution. Icarus 41, 119–130.

Rages, K., Pollack, J.B., Smith, P.H., 1983. Size estimate of Titan's aerosols based on Voyager high-phase-angle images. J. Geophys. Res. 88, 8721–8728.

Redondo, P., Pauzat, F., Ellinger, Y., 2006. Theoretical survey of the $NH + CH_3$ potential energy surface in relation to Titan atmospheric chemistry. Planet. Space Sci. 54, 181–187.

Reisler, H., Mangir, M.S., Wittig, C., 1980. Kinetics of free radicals generated by IR laser photolysis. IV. Intersystem crossings and reactions of $C_2(X^1\Sigma_g^+)$ and $C_2(a^3\Pi_u)$ in the gaseous phase. J. Chem. Phys. 73, 2280–2286.

Rennie, E.E., Johnson, C.A.F., Parker, J.E., Holland, D.M.P., Shaw, D.A., Hayes, M.A., 1998. A photoabsorption, photodissociation and photoelectron spectroscopy study of C_6H_6 and C_6D_6. Chem. Phys. 229, 107–123.

Rettig, T.W., Tegler, S.C., Pasto, D.J., Mumma, M.J., 1992. Comet outbursts and polymers of HCN. Astrophys. J. 398, 293–298.

Ricca, A., Bauschlicher Jr., C.W., Bakes, E.L.O., 2001. A computational study of the mechanisms for the incorporation of a nitrogen atom into polycyclic aromatic hydrocarbons in the Titan haze. Icarus 154, 516–521.

Richter, H., Howard, J.B., 2000. Formation of polycyclic aromatic hydrocarbons and their growth to soot- a review of chemical reaction pathways. Prog. Energy Combust. Sci. 26, 565–608.

Romani, P.N., 1996. Recent rate constant and product measurements of the reactions $C_2H_3 + H_2$ and $C_2H_3 + H$–Importance for the photochemical modeling of hydrocarbons on Jupiter. Icarus 122, 233–241.

Romanzin, C., and 8 co-authors, 2005. Methane photochemistry: a brief review in the frame of a new experimental program of Titan's atmosphere simulations. Adv. Space Research 36, 258–267.

Sagan, C., Khare, B.N., 1979. Tholins: organic chemistry of interstellar grains and gas. Nature 277, 102–107.

Sagan, C., Thompson, W.R., 1984. Production and condensation of organic gases in the atmosphere of Titan. Icarus 59, 133–161.

Samson, J.A.R., Marmo, F.F., Watanabe, K., 1962. Absorption and photoionization coefficients of propylene and butene-1 in the vacuum ultraviolet. J. Chem. Phys. 36, 783–786.

Samson, J.A.R., Haddad, G.N., Masuoka, T., Pareek, P.N., Kilcoyne, D.A.L., 1989. Ionization yields total absorption and dissociative photoionization cross sections of CH_4 from 110 to 950 Å. J. Chem. Phys. 90, 6925–6932.

Samuelson, R.E., 1983. Radiative equilibrium model of Titan's atmosphere. Icarus 53, 364–387.

Samuelson, R.E., Mayo, L.A., Knuckles, M.A., Khanna, R.J., 1997. C_4N_2 ice in Titan's north polar stratosphere. Planet. Space Sci. 45, 941–948.

Sato, K., Misawa, K., Kobayashi, Y., Matsui, M., Tsunashima, S., Kurosaki, Y., Takayanagi, T., 1999. Measurements of thermal rate constants for the reactions of $N(^2D, {}^2P)$ with C_2H_4 and C_2D_4 between 225 and 292 K. J. Phys. Chem. A 103, 8650–8656.

Scala, A.A., Salomon, D., 1976. The gas phase photolysis and γ radiolysis of ethylenimine. J. Chem. Phys. 65, 4455–4461.

Scattergood, T.W., Lau, E.Y., Stone, B.M., 1992. Titan's aerosols. I. Laboratory investigations of shapes, size distributions, and aggregation of particles produced by UV photolysis of model Titan atmospheres. Icarus 99, 98–105.

Scherzer, K., Claus, P., Karwath, M., 1985. Untersuchungen sur kinetik und zum mechanismus der addition von methylradicalen an vinylacetylen. Z. Chem. Phys. (Leipzig) 266, 321.

Schiavello, M., Volpi, G.G., 1962. Reaction of hydrogen atoms with hydrazine, ammonia and nitrous oxide. J. Chem. Phys. 37, 1510–1513.

Schofield, K., 1973. Evaluated chemical kinetic rate constants for various gas phase reactions. J. Phys. Chem. Ref. Data 2, 25–84.

Schwanebeck, W., Warnatz, J., 1975. Reaktionen des butadiins. I. Die reaction mit wasserstoffatomen. Ber. Bunsenges. Phys. Chem. 79, 530–535.

Seki, K., Okabe, H., 1992. Photodissociation of methylacetylene at 193 nm. J. Phys. Chem. 96, 3345–3349.

Seki, K., Okabe, H., 1993. Photochemistry of acetylene at 1933 nm. J. Phys. Chem. 97, 5284–5290.

Seki, K., Nakashima, N., Nishi, N., Kinoshita, M., 1986. Photochemistry of acetylene at 193 nm: two pathways for diacetylene formation. J. Chem. Phys. 85, 274–279.

Seki, K., Yagi, M., He, M.Q., Halpern, J.B., Okabe, H., 1996. Reaction rates of the CN radical with diacetylene and dicyanoacetylene. Chem. Phys. Lett. 258, 657–662.

Shindo, F., Benilan, Y., Guillemin, J.-C., Chaquin, P., Jolly, A., Raulin, F., 2005. Ultraviolet and infrared spectrum of C_6H_2 revisited and vapor pressure curve in Titan's atmosphere. Planet. Space Sci. 51, 9–17.

Sillesen, A., Ratajczak, E., Pagsberg, P., 1993. Kinetics of the reaction $H + C_2H_4 \rightarrow C_2H_5$, $H + C_2H_5 \rightarrow 2CH_3$, $CH_3 + C_2H_5 \rightarrow$ products studied by pulse radiolysis combined with infrared diode lase spectroscopy. Chem. Phys. Lett. 201, 171–177.

Sims, I.R., Queffelec, J.-L., Travers, D., Rowe, B., Herbert, L.B., Karthäuser, J., Smith, I.W.M., 1993. Rate constants for the reactions of CN with hydrocarbons at low and ultra-low temperatures. Chem. Phys. Lett. 211, 461–468.

Sims, I.R., Queffelec, J.L., Defrance, A., Rebrion-Rowe, C., Travers, D., Bocherel, P., Rowe, B.R., Smith, I.W.M., 1994. Ultralow temperature kinetics of neutral-neutral reactions. The technique and results for the reactions $CN + O_2$ down to 13 K and $CN + NH_3$ down to 25 K. J. Chem. Phys. 100, 4229–4241.

Slack, M.W., 1976. Kinetics and thermodynamics of the CN molecule. III. Shock tube measurement of CN dissociation rates. J. Chem. Phys. 64, 228–236.

Smith, N.S., Raulin, F., 1999. Modeling of methane photolysis in the reducing atmospheres of the outer solar system. J. Geophys. Res. 104, 1873–1876.

Smith, N.S., Bénilan, Y., Bruston, P., 1998. The temperature dependent absorption cross-sections of C_4H_2 at mid ultraviolet wavelengths. Planet. Space Sci. 46, 1215–1220.

Smith, P.L., Yoshino, K., Parkinson, W.H., 1991. High-resolution VUV (147–201 nm) photoabsorption cross sections for C_2H_2 at 195 and 195 K. J. Geophys. Res. 96, 17529–17533.

Sromovsky, L.A., Irwin, P.G.J., Fry, P.M., 2006. Near-IR methane absorption in the outer planet atmospheres: improved models of temperature dependence and implications for Uranus cloud structure. Icarus 182, 577–593.

Stewart, P.H., Larson, C.W., Golden, D.M., 1989. Pressure and temperature dependence of reactions proceeding via a bound complex. II. Application to $2 CH_3?C_2H_5CH$. Combust. Flame 75, 25.

Stief, L.J., 1970. Ratio of disproportionation to combination of N_2H_3 radicals. J. Chem. Phys. 52, 4841–4845.

Stief, L.J., Nesbitt, F.L., Payne, W.A., Kuo, S.C., Tao, W., Klemm, R.B., 1995. Rate constant and reaction channels for the reaction of atomic nitrogen with the ethyl radical. J. Chem. Phys. 102, 5309–5316.

Strobel, D.F., 1974. The photochemistry of hydrocarbons in the atmosphere of Titan. Icarus 21, 466–470.

Strong, K., Taylor, F.W., Calcutt, S.B., Remedios, J.J., Ballard, J., 1993. Spectral parameters for self- and hydrogen-broadened methane from 2000 to 9500 cm^{-1} for remote sounding of the atmosphere of Jupiter. J. Quant. Spectrosc. Radiat. Transfer 50, 363–429.

Sun, Q., Yang, D.L., Wang, N.S., Bowman, J.M., Lin, M.C., 1990. Experimental and reduced dimensionality quantum rate coefficients for $H_2(D_2) + CN \rightarrow H(D)CN + H(D)$. J. Chem. Phys. 93, 4730–4739.

Sun, W., Yokoyama, K., Robinson, J.C., Suits, A.G., Neumark, D.M., 1999. Discrimination of products isomers in the photodissociation of propyne and allene at 193 nm. J. Chem. Phys. 110, 4363–4368.

Suto, M., Wang, X., Lee, L.C., 1985. Fluorescence from VUV excitation of formaldehyde. J. Chem. Phys. 85, 4228–4233.

Suto, M., Wang, X., Shan, J., Lee, L.C., 1992. Quantitative photoabsorption and fluorescence spectroscopy of benzene, naphthalene and some derivatives at 106–295 nm. J. Quant. Spectrosc. Radiat. Transfer 48, 79–89.

Takahashi, S., Miyazaki, S., 1977. The reactions of the nitrogen atom with ethylene and ethylene-d4. Bull. Chem. Soc. Jpn. 50, 1627–1628.

Teng, L., Jones, W.E., 1972. Kinetics of the reactions of hydrogen atoms with ethylene and vinyl fluoride. J. Chem. Soc. Faraday Trans. 68, 1267–1277.

Teslja, A., Nizamov, B., Dagdigian, P.J., 2004. The electronic spectrum of methyleneimine. J. Phys. Chem. 108, 4433–4439.

Thompson, W.R., Sagan, C., 1989. Atmospheric formation of organic heteropolymers from $N_2 + CH_4$: structural suggestions for amino acid and oligomer precursors. Origins of Life 19, 503–504.

Tomasko, M.G., Smith, P.H., 1982. Photometry and polarimetry of Titan: pioneer 11 observations and their implications for aerosols properties. Icarus 51, 65–95.

Tomasko, M.G., Lemmon, M., Roose, L.R., Smith, P.H., Eibl, A., West, R.A., 1997. Models of the penetration of sunlight into the atmosphere of Titan. ESASP-1177, 345–358.

Tomasko, M.G., and 39 co-authors, 2005. Rain, winds, and haze during the Huygens probe's descent to Titan's surface. Nature, doi:10.1038/nature04126.

Toon, O.B., Turco, R.P., Pollack, J.B., 1992a. A physical model of Titan's clouds. Icarus 43, 260–282.

Toon, O.B., McKay, C.P., Griffith, C.A., Turco, R.P., 1992b. A physical model of Titan's aerosols. Icarus 95, 24–53.

Toublanc, D., Parisot, J.P., Brillet, J., Gautier, D., Raulin, F., McKay, C.P., 1995. Photochemical modeling of Titan's atmosphere. Icarus 113, 2–26.

Tran, B.N., Joseph, J.C., Ferris, J.P., Persans, P.D., Chera, J.J., 2003. Simulation of Titan haze formation using a photochemical flow reactor: the optical constants of the polymer. Icarus 165, 379–390.

Tsang, W., 1988. Chemical kinetic data base for combustion chemistry. III. Propane. J. Phys. Chem. Ref. Data 17, 887–951.

Tsang, W., 1990. Chemical kinetic data base for combustion chemistry. IV. Isobutane. J. Phys. Chem. Ref. Data 17, 887–951.

Tsang, W., 1991. Chemical kinetic data base for combustion chemistry. V. Propene. J. Phys. Chem. Ref. Data 20, 221–274.

Tsang, W., 1992. Chemical kinetic data base for propellant combustion. II. Reactions involving CN, NCO, and HNCO. J. Phys. Chem. Ref. Data 21, 753.

Tsang, W., Hampson, R.F., 1986. Chemical kinetic data base for combustion chemistry. Part 1. Methane and related compounds. J. Phys. Chem. Ref. Data 15, 1087–1279.

Tsang, W., Herron, J.T., 1991. Chemical kinetic data base for propellant combustion. I. Reactions involving NO, NO_2, HNO, HNO_2, HCN and N_2O 20. J. Phys. Chem. Ref. Data 20, 609–663.

Vaghjiani, G.L., 1993. Ultraviolet absorption cross section for N_2H_4 vapor between 191–291 nm and $H(^2S)$ quantum yield in 248 nm photodissociation at 296 K. J. Chem. Phys. 98, 2123–2132.

Vaghjiani, G.L., 1995. Laser photolysis studies of hydrazine vapor: 193 and 222-nm H-atom primary quantum yields at 296 K, and the kinetics of $H + N_2H_4$ reaction over the temperature range 222–657 K. Int. J. Chem. Kinet. 27, 777–790.

Vakhtin, A.B., Heard, D.E., Smith, I.W.M., Leone, S.R., 2001a. Kinetics of reactions of C_2H radical with acetylene, O_2, methylacetylene, and allene in a pulsed Laval nozzle apparatus at $T = 103$ K. Chem. Phys. Lett. 344, 317–324.

Vakhtin, A.B., Heard, D.E., Smith, I.W.M., Leone, S.R., 2001b. Kinetics of C_2H radical reactions with ethene, propene and l-butene measured in a pulsed Laval nozzle apparatus at $T = 103$ and 296 K. Chem. Phys. Lett. 348, 21–26.

Vardavas, I.M., 1984. Modelling reactive gas flows within shock tunnels. Aust. J. Phys. 37, 157–177.

Vardavas, I.M., Carver, J.H., 1984a. Comments on the Newton–Raphson method for obtaining temperature profiles from radiative-convective models. Planet. Spac. Sci. 32, 803–807.

Vardavas, I.M., Carver, J.H., 1984b. Solar and terrestrial parameterizations for radiative-convective models. Planet. Spac. Sci. 32, 1307–1325.

Vargaftik, N.B., 1975. Tables on the Thermophysical Properties of Liquids and Gases in Normal and Dissociated States. Wiley, NY.

Vuitton, V., Gée, C., Raulin, F., Bénilana, Y., Crépin, C., Gazeau, M.-C., 2003. Intrinsic lifetime of metastable excited C_4H_2: implications for the photochemistry of C_4H_2 in Titan's atmosphere. Planet. Space Sci. 51, 847–852.

Vuitton, V., Yelle, R.V., Anicich, V.G., 2006a. The nitrogen chemistry of Titan's upper atmosphere revealed. Astrophys. J. 647, L175–L178.

Vuitton, V., Doussin, J.-F., Bènilan, Y., Raulin, F., Gazeau, M.-C., 2006b. Experimental and theoretical study of hydrocarbon photochemistry applied to Titan stratosphere. Icarus 185, 287–300.

Wakeham, W.A., Slater, D.H., 1973. Diffusion coefficients for *n*-alkanes in binary gaseous mixtures with nitrogen. J. Phys. B Atom. Molec. Phys. 6, 886–896.

Wang, B., Hou, H., Gu, Y., 2000. Mechanism and rate constant of the reaction of atomic hydrogen with propyne. J. Chem. Phys. 112, 8458–8465.

Wang, H., Frenklach, M., 1994. Calculations of rate coefficients for the chemically activated reactions of acetylene with vinylic and aromatic radicals. J. Phys. Chem. 98, 1465–1489.

Wang, H., Frenklach, M., 1997. A detailed kinetic modeling study of aromatics formation in laminar premixed acetylene and ethylene flames. Combust. Flame 110, 173–221.

Wang, J.-H., Liu, K., 1998. VUV photochemistry of CH_4 and isotopomers. I. Dynamics and dissociation pathway of the H/D-atom elimination channel. J. Chem. Phys. 109, 7105–7112.

Wang, J.-H., Liu, K., Min, Z., Su, H., Bersohn, R., Preses, J., Larese, Z., 2000. Vacuum ultraviolet photochemistry of CH_4 and isotopomers. II. Product channel fields and absorption spectra. J. Chem. Phys. 113, 4146–4152.

Warnatz, J., 1984. Rate coefficients in the C/H/O system. In: Gardiner, Jr., W.C. (Ed.), Combustion Chemistry. Springer, Berlin.

Weissman, M.A., Benson, S.W., 1988. Rate parameters for the reactions of C_2H_3 and C_4H_5 with H_2 and C_2H_2. J. Phys. Chem. 92, 4080–4084.

West, R.A., Smith, P.H., 1991. Evidence for aggregate particles in the atmospheres of Titan and Jupiter. Icarus 90, 330–333.

West, R.A., Lane, A.L., Hart, H., Simmons, K.E., Hord, C.W., Coffeen, D.L., Esposito, L.W., Sato, M., Pomphrey, R.B., 1983. Voyager 2 photopolarimeter observations of Titan. J. Geophys. Res. 88, 8699–8708.

Westmoreland, P.R., Dean, A.M., Howard, J.B., Longwell, J.P., 1989. Forming benzene in flames by chemically activated isomerization. J. Phys. Chem. 93, 8171–8180.

Whyte, A.R., Phillips, L.F., 1983. Rate of reaction of N with CN($v = 0, 1$). Chem. Phys. Lett. 98, 590–593.

Wilson, E.H., Atreya, S.K., 2000. Sensitivity studies of methane photolysis and its impact on hydrocarbon chemistry in the atmosphere of Titan. J. Geophys. Res. 105, 20263–20273.

Wilson, E.H., Atreya, S.K., 2003. Chemical sources of haze formation in Titan's atmosphere. Planet. Space Sci. 51, 1017–1033.

Wilson, E.H., Atreya, S.K., 2004. Current state of modeling the photochemistry of Titan's mutually dependent atmosphere and ionosphere. J. Geophys. Res. 109, doi: 10.1029/2003JE001896.

Wilson, E.H., Atreya, S.K., Coustenis, A., 2003. Mechanisms for the formation of benzene in the atmosphere of Titan. J. Geophys. Res. 108, doi: 10.1029/2002JE002181.

Wilson, S.H.S., Howe, J.D., Rosser, K.N., Ashfold, M.N.R., Dixon, R.N., 1994. A reinvestigation of the near-ultraviolet photodissociation dynamics of the methyl radical. Chem. Phys. Lett. 227, 456–460.

Woods, T.N., Rottman, G.J., 2002. Solar ultraviolet variability over time periods of aeronomic interest. In: Mendillo, M., et al. (Eds.), Comparative Aeronomy in the Solar System. American Geophysical Union Monograph.

Xu, Z.-F., Fang, D.-C., Fu, X.-Y., 1998. Ab initio study on the reaction $2NH_2 \rightarrow NH + NH_3$. Int. J. Quantum Chem. 70, 321–329.

Xu, Z.-F., Li, S.-M., Yu, Y.-X., Li, Z.-S., Sun, C.-C., 1999. Theoretical studies on the reaction path dynamics and variational transition-state theory rate constants of the hydrogen-abstraction reactions of the $NH(X^3\Sigma^-)$ radical with methane and ethane. J. Phys. Chem. A 103, 4910–4917.

Yang, D.L., Yu, T., Lin, M.C., Melius, C.F., 1992a. CN radical reactions with hydrogen cyanide and cyanogen: comparison of theory and experiment. J. Chem. Phys. 97, 222–226.

Yang, D.L., Yu, T., Wang, N.S., Lin, M.C., 1992b. Temperature dependence of cyanogen radical reactions with selected alkanes: CN reactivities towards primary, secondary and tertiary C–H bonds. Chem. Phys. 160, 307–315.

Yelle, R.V., 1991. Non-LTE models of Titan's upper atmosphere. Astrophys. J. 383, 380–400.

Yelle, R.V., Strobel, D.F., Lellouch, E., Gautier, D., 1997. Engineering models for Titan's atmosphere, ESA SP-1177. European Space Agency, Noordwijk, 243–256.

Yelle, R.V., Borggren, N., de la Haye, V., Kasprzal, W.T., Niemann, H.B., Müller-Wodarg, I., Waite, J.H., 2006. The vertical structure of Titan's upper atmosphere from the Cassini ion neutral mass spectrometer measurements. Icarus 182, 567–576.

Yokoyama, A., Zhao, X., Hintsa, E.J., Continetti, R.E., Lee, Y.T., 1990. Molecular beam studies of the photodissociation of benzene at 193 and 248 nm. J. Chem. Phys. 92, 4222–4233.

Young, E.F., Rannou, P., McKay, C.P., Griffith, C.A., Noll, K., 2002. A three dimensional map of Titan's tropospheric haze distribution based on HST imaging. Astron. J. 123, 3473–3486.

Yu, T., Lin, M.C., Melius, C.F., 1994. Absolute rate constant for the reaction of phenyl radical with acetylene. Int. J. Chem. Kin. 26, 1095–1104.

Yung, Y.L., 1987. An update of nitrile photochemistry on Titan. Icarus 72, 468–472.

Yung, Y.L., Allen, M., Pinto, J.P., 1984. Photochemistry of the atmosphere of Titan: comparison between model and observations. Astrophys. J. Suppl. 55, 465–506.

Zabarnick, S., Lin, M.C., 1989. Kinetics of $CN(X^2\Sigma^+)$ radical reactions with HCN, BrCN, and CH_3CN. Chem. Phys. 134, 185–191.

Zabarnick, S., Fleming, J.W., Lin, M.C., 1988. Kinetics of $CH(X^2\pi)$ radical reactions with cyclopropane, cyclopentane, and cyclohexane. J. Chem. Phys. 88.

Zabarnick, S., Fleming, J.W., Lin, M.C., 1991. Direct measurement of rate constants for the reactions of CH and CD with HCN and DCN. Chem. Phys. 150, 109–115.

Zelikoff, M., Watanabe, K., 1953. Absorption coefficients of ethylene in the vacuum ultraviolet. J. Opt. Soc. Am. 43, 756–759.

Zetzsch, C., Stuhl, F., 1981. Formation and fate of $NH(X^3\Sigma^-)$ in the pulsed vacuum UV photolysis of NH_3. Ber. Bunsenges. Phys. Chem. 85.

Zhu, R.S., Xu, Z.F., Lin, M.C., 2004. *Ab initio* studies of alkyl radical reactions: Combination and disproportionation reactions of CH_3 with C_2H_5, and the decomposition of chemically activated C_3H_8. J. Chem. Phys. 120, 6566–6573.

Zhu, Z., Zhang, Z., Huang, C., Pei, L., Chen, C., Chen, Y., 2003. Kinetics of CCN radical reactions with a series of normal alkanes. J. Phys. Chem. A 107, 10288–10291.

Zu, Z.-F., Fang, D.-C., Fu, X.-Y., 1997. Ab initio study on the reaction $2NH(X^2\Sigma^-) \rightarrow NH_2(X^2B_1) + N(^4S)$. Chem. Phys. Lett. 275, 386–391.

Zwier, T.S., Allen, M., 1996. Metastable diacetylene reactions as routes to large hydrocarbons in Titan's atmosphere. Icarus 123, 578–583.